Motor property of mammalian myosin 10

A Dissertation Presented

By

Kazuaki Homma

Submitted to the Faculty of the

University of Massachusetts Graduate School of Biomedical Sciences, Worcester

In partial fulfillment of the requirements for the degree of

DOCTOR OF PHILOSOPHY

July 31th 2007.

Program in Cellular and Molecular Physiology

Parts of this dissertation have appeared in:

Homma, K., and M. Ikebe. 2005. Myosin X is a high duty ratio motor. *J Biol Chem*. 280:29381-91.

Homma, K., J. Saito, R. Ikebe, and M. Ikebe. 2001. Motor function and regulation of myosin X. *J Biol Chem*. 276:34348-54.

Homma, K., M. Yoshimura, J. Saito, R. Ikebe, and M. Ikebe. 2001. The core of the motor domain determines the direction of myosin movement. *Nature*. 412:831-4.

MOTOR PROPERTY OF MAMMALIAN MYOSIN 10

A Dissertation Presented

By

Kazuaki Homma

Approved as to style and content by:

James G. Dobson, Ph.D., Chair of Committee

Jack L. Leonard, Ph.D., Member of Committee

Chih-Lueh Albert Wang, Ph.D., Member of Committee

Yu-Li Wang, Ph.D., Member of Committee

George B. Witman, Ph.D., Member of Committee

Mitsuo Ikebe, Ph.D., Dissertation Mentor

Anthony Carruthers, Ph.D.,
Dean of Graduate School of Biomedical Sciences

July 31th 2007

ACKNOWLEDGEMENTS

I would like to thank Dr. Mitsuo Ikebe for the opportunity to work in his lab, for his belief in my success on projects, and for helping me reach this first milestone in my scientific career.

I would like to thank members of Ikebe lab, current and former, for sharing research experience, for support, and for fruitful discussion.

I would like to thank my committee members, Dr. James Dobson, Dr. Jack Leonard, Dr. Yu-Li Wang, Dr. George Witman, and Dr. Albert Wang, for their guidance and faithful service.

I would like to thank people of Yanagida lab (Osaka Univ.), White lab (EVMS), and Goldman lab (UPenn) for generous sharing of their expertise when I visited them. Especially, I would like to thank Dr. Yoshiyuki Arai (Osaka Univ.) for his helping me to setup a TIRFM in Ikebe lab.

I would like to thank Dr. Katsuhide Mabuchi (BBRI) and Dr. Hyun Suk Jung (UMass) for taking EM pictures of myosin samples.

I would like to thank people in the Physiology Department, current and former, especially, Pat (Morrison), Pat (Keith), Cheryl, Donna, Eileen, Janice, Lynn, and Missy. Things always run smoothly because of their supports.

I would like to thank my family and my lifelong friends, Nobuyasu and Takehiko, for encouraging me all the time from the other side of this planet.

Lastly, I would like to thank Satoe. I did not think I could meet such a wonderful person like her. Satoe- thank you very much for being with me. You have made my life much happier.

ABSTRACT

Myosin 10 is a vertebrate specific actin-based motor protein that is expressed in a variety of cell types. Cell biological evidences suggest that myosin 10 plays a role in cargo transport and filopodia extension. In order to fully appreciate these physiological processes, it is crucial to understand the motor property of myosin 10. However, little is known about its mechanoenzymatic characteristics. In vitro biochemical characterization of myosin 10 has been hindered by the low expression level of the protein in most tissues. In this study, we succeeded in obtaining sufficient amount of recombinant mammalian myosin 10 using the baculovirus expression system. The movement directionality of the heterologously expressed myosin 10 was determined to be plus end-directed by the in vitro motility assay with polarity-marked actin filament we developed. The result is consistent with the proposed physiological function of myosin 10 as a plus end-directed transporter inside filopodia. The duty ratio of myosin 10 was determined to be 0.6~0.7 by the enzyme kinetic analysis, suggesting that myosin 10 is a processive motor. Unexpectedly, we were unable to confirm the processive movement of dimeric myosin 10 along actin filaments in a single molecule study. The result does not support the proposed function of myosin 10 as a transporter. One possible explanation for this discrepancy is that the apparent nonprocessive nature of myosin 10 is important for generating sufficient force required for the intrafilopodial transport by working in concert with numbers of other myosin 10 molecules while not interfering with each other.

Altogether, the present study provided qualitative and quantitative biochemical evidences for the better understanding of the motor property of myosin 10 and of the biological processes in which it is involved.

Finally, a general molecular mechanism of myosin motors behind the movement directionality and the processivity is discussed based on our results together with the currently available experimental evidences. The validity of the widely accepted 'lever-arm hypothesis' is reexamined.

TABLE OF CONTENTS

LIST OF FIGURES

CHAPTER II

CHAPTER III

CHAPTER IV

CHAPTER VI

APPENDIX A

APPENDIX F

LIST OF TABLES

CHAPTER II

CHAPTER III

APPENDIX F

LIST OF SCHEMES

CHAPTER III

LIST OF ABBREVIATIONS

CC	coiled-coil
PEST	proline-, glutamate-, serine-, and threonine-rich
PH	pleckstrin homology
MyTH4	myosin tail homology 4
FERM	band 4.1 ezrin radixin moesin
CaM	calmodulin
CLP	calmodulin-like protein
SAH	stable alpha helix
MDCC	7-diethylamino-3-((((2-maleimidyl)ethyl)amino)carbonyl)coumarin
PBP	phosphate binding protein
Mant	(2'-(or-3')-*O*-(*N*-methylanthraniloyl)
Ni-NTA	Nickel-nitrilotriacetic acid agarose
PNPase	Purine nucleoside phosphorylase
MEG	7-methylguanosine
PI(3)K	phosphoinositide 3-kinase
NEM	*N*-ethylmaleimide
TIRFM	total internal reflection microscope

CHAPTER I

GENERAL INTRODUCTION

Molecular motors – keys to understanding how life works

Life is maintained by biological molecules comprised of organic compounds such as nucleic acids, lipids, carbohydrates, and amino acids, etc. Like machines invented by humans such as computers and automobiles, biological events are driven by the input of energy. Recent molecular biological studies have identified numerous molecular players that are responsible for a variety of biological processes. In most cases, those are protein molecules, and many of them use energy to execute their physiological tasks. They are often referred to as 'molecular machines', however, these machines are very unique compared to our artificial machines. In general, proteins are not very solid entities. For most proteins, the free energy difference between the native state and the denatured state is usually 2 ~10 $x10^{-20}$ J (5 ~ 25 k_BT), which is not so different from the thermal noise energy (~4 x 10^{-21} J ≅1 k_BT) (Chen et al., 2007; Howard, 2001). The low rigidity confers structural dynamics to proteins, and is important for their physiological functions. This is completely different from the artificial machines, whose structural stabilities are far greater than the thermal noise. This may be a key to understanding the uniqueness of life. How do those molecular machines actually work under such conditions?

Motor proteins such as myosin, kinesin, and dynein are good examples of biological molecular machines. They carry out mechanical work using energy from ATP hydrolysis to control cellular structures, properly position cellular organelles, or transport

cellular components to specific locations in cells (Kalhammer and Bahler, 2000; Sellers, 2000). Dynein and myosin are essential components of flagella, cilia, and muscles, and their motor activities are the fundamental bases of the movement of living organisms.

How do these molecular motors convert the chemical energy of ATP into mechanical work? When compared to artificial machines such as electric devices and automobiles, we can easily find two very unique features of the biological molecular motors other than the flexibility of the structure mentioned above. First, input energy of the molecular motors given by ATP hydrolysis is not very high compared to the thermal noise. Although ATP is often regarded as a high energy compound, its free energy released by the hydrolysis under a typical physiological condition is merely ~9 x 10^{-20} J (~20 k_BT), which is not so different from the thermal noise energy of ~4 x 10^{-21} J (~1 k_BT) (Howard, 2001). This is contrary to the artificial machines operated by the significant energy input of electric voltage or gasoline explosion, which is far greater than the thermal noise to make the machines work precisely and quickly. Second, energy conversion efficiency of the biological molecular motors is high. The work done by these molecular motors is 5.6~7.9 x 10^{-20} J / ATP (Altman et al., 2004; Howard, 2001; Tanaka et al., 2002; Taniguchi et al., 2005). Thus, the energy conversion efficiency is 60~90 %, which is far greater than that of the latest energy efficient automobiles (~30%).

Not only for those molecular motors, ATP is a commonly used energy source that drives many biological processes throughout living organisms. Thus, understanding how the biological molecular motors work would eventually help us understand how life operates so robustly and efficiently.

Myosin motors

Myosin is a generic term used to refer to a diverse family of molecular motors capable of translocating actin filaments or of transporting cargos along actin filaments by hydrolyzing ATP. The myosin superfamily is comprised of 24 distinct classes of proteins based on sequence homology of the N-terminal motor domain (Foth et al., 2006). The N-terminal globular motor domain contains an ATP hydrolysis site and actin interacting sites, and is well conserved within the superfamily. The crystal structures of the motor domains from different myosins solved so far have shown remarkable overall structural similarities (Coureux et al., 2004; Dominguez et al., 1998; Houdusse et al., 1999; Menetrey et al., 2005; Rayment et al., 1993), suggesting that myosins share the common molecular mechanism by which chemical energy of ATP is converted into the mechanical work. The C-terminal tail portions of myosins are highly variable among the superfamily, implying their distinct physiological roles in a cell.

One promising strategy for unraveling the molecular mechanism of the myosin motors is to compare different myosins with different motor properties to obtain structure–function information. Despite the overall structural similarity of the motor domain within the myosin superfamily, each myosin has distinct motor properties. Since the differences in motor properties are attributed to differences in the amino acid sequences, it is possible to identify the regions responsible for deciding the motor property by comparing myosins with different motor properties. Also, since it is very likely that these motor properties of myosins are specifically tuned for their physiological

functions in cells, understanding of these motor properties of myosins can help us appreciate the biological processes where those myosins are involved.

In this study, we have mainly focused on biochemical and biophysical characterization of class 10 myosin. There are two main objectives for characterizing this myosin. The first objective is to obtain underlying biochemical properties of myosin 10 to explain its physiological function in a cell. Quite a few cell biological studies have been done on myosin 10, however, little is known about its motor property. The second objective is to obtain an additional example of the structure-function relationship of myosin motors to understand the molecular mechanism of myosin motors as a whole. Recent biochemical and biophysical characterizations of myosins from different classes have been beneficial for providing detailed pictures of how the unique motor property is determined, and characterization of yet to be analyzed myosins will contribute to a better understanding of how myosin motors work.

Class 10 myosin

Myosin 10 is a vertebrate-specific, ubiquitously expressed myosin (Berg et al., 2000). Like other myosins, the overall structure can be divided into three distinct regions: head, neck, and tail (Fig. II-1). The N-terminal globular motor domain is often called 'head' because of its globular head-like structure. This domain contains ATP hydrolysis site and actin interaction sites, and is responsible for the motor activity. The neck region is comprised of three consecutive IQ motifs (IQXXXRGXXXR) to which calmodulins or calmodulin-like proteins bind (Homma et al., 2001; Rogers and Strehler,

2001), and thought to be a target of Ca^{2+}-dependent regulation. The tail region contains a predicted coiled-coil region, three PEST (proline-, glutamate-, serine-, and threonine-rich) regions, three PH (pleckstrin homology) domains, a MyTH4 (myosin tail homology 4) domain, and a FERM (band 4.1 ezrin radixin moesin) domain (Fig. II-1). The predicted coiled-coil region suggests that myosin 10 can be dimerized. The PEST regions are susceptible to cleavage by Ca^{2+}-dependent protease calpain, and suggested to be important for protein turnover (Berg et al., 2000). Of the three PH domains, the second PH domain has been reported to bind PtdIns(3,4,5)P_3 (Isakoff et al., 1998; Mashanov et al., 2004), suggesting that myosin 10 is a downstream effector of PI(3)K (phosphoinositide 3-kinase). In fact, Cox *et al*. recently showed that myosin 10 is required for Fc-mediated phagocytosis in macrophages, and its localization to the phagocytic cup (pseudopods of macrophages) is PI(3)K-dependent (Cox et al., 2002). The MyTH4 domain is found in five classes of myosins (class 4, 7, 10, 12 and 15), and the MyTH4 domain of *Xenopus* myosin 10 has recently been reported to bind to microtubules, which gives myosin 10 an ability to function as a motorized link between actin and microtubules (Weber et al., 2004). The tail of myosin 10 ends with a FERM domain. FERM domain is found in a number of cytoskeleton-associated proteins that are localized at the interface between the plasma membrane and the cytoskeleton. The FERM domain of myosin 10 binds to the cytoplasmic domain of β_1-, β_3- or β_5-integrin, suggesting that myosin 10 functions as a motorized clutch to link cell adhesion molecules to the actin cytoskeleton (Zhang et al., 2004).

One of the most interesting features of myosin 10 is its intrafilopodial motility. Myosin 10 localizes at the tips of filopodia (Berg and Cheney, 2002; Berg et al., 2000). Filopodium is a highly dynamic protrusion structure of a cell, and it has been thought to act as a sensor that explores the environment for growth cone guidance (Davenport et al., 1993), angiogenesis (Gerhardt et al., 2003), and cell migration (Rorth, 2003). Bundled actin filaments form the core of the filopodia with their barbed (plus) end at the tip of the filopodium and their pointed (minus) ends towards the cell body (Svitkina et al., 2003). The structural dynamics of filopodia is controlled by the balance of actin polymerization (at the barbed ends) and depolymerization (at the pointed ends) (Mallavarapu and Mitchison, 1999). Overexpression of myosin 10 induces filopodia formation (Berg and Cheney, 2002), suggesting that myosin 10 has an ability to promote actin polymerization inside filopodia. Tokuo *et al*. have recently shown that myosin 10 colocalizes with VASP, and moves together inside the filopodia (Tokuo and Ikebe, 2004). VASP is an actin binding protein that localizes to actin stress fiber, filopodia, and the leading edge of lamellipodia (Bear et al., 2002). VASP has been reported to facilitate actin polymerization by directly binding to the barbed (plus) end of actin and competing with actin capping proteins that block the actin polymerization (Bear et al., 2002). These evidences strongly suggest that myosin 10 indirectly induces and maintains filopodia by carrying an anti-capping protein (VASP) to the barbed end tip, thereby countering to the continuous retraction of actin filaments. Also, the ability of myosin 10 to bind β-integrins makes it an attractive candidate for the formation of the adhesive structures at the tips of filopodia. The tips of filopodia are recognized as specialized sites of adhesion

(Tsui et al., 1985), which exert a pulling force of ~100 pN on the substrate (Bridgman et al., 2001).

In addition to the role in the formation/maintenance of filopodia, myosin 10 is also involved in phagocytosis (Cox et al., 2002), spindle formation (Weber et al., 2004), nerve regrowth (Tanabe et al., 2003), axomal path finding (Zhu et al., 2007), some forms of acute lymphoblastic leukemia (Ross et al., 2003), and cell-cell adhesion (Yonezawa et al., 2003). These findings strongly indicate that myosin 10 is a multi-functional protein. In this study, we particularly focused on the intrafilopodial motility of myosin 10.

CHAPTER II

MOVEMENT DIRECTIONALITY OF MYOSIN 10

Introduction

Since actin filaments have polarity, movement directionality on actin filaments is one of the most important features of myosins that determines its distinct physiological function in a cell. For examples, the barbed end-directed motility of muscle myosins (type 2 myosins) is essential for the muscle cells to contract, while the pointed end-directed motility of myosin 6 is crucial for its role in endocytosis (Aschenbrenner et al., 2004; Buss et al., 2001; Hasson, 2003) and for the maintenance of the stereocilia structure in hair cells (Frank et al., 2004; Self et al., 1999). Myosin 10 is involved in intrafilopodial motility, and shows bidirectional movements inside filopodia (Berg and Cheney, 2002). The speed of the rearward movement (towards the cell body) is approximately 10 nm/sec, which can be explained by the rate of the continuous retrograde flow of actin filaments in filopodia (Mallavarapu and Mitchison, 1999), whereas the forward movement (towards the tip) is approximately 100 nm/sec. Since overexpression of myosin 10 increases the number and the length of filopodia (Berg and Cheney, 2002), it is likely that the forward movement is driven by myosin 10. However, it is still possible that myosin 10 functions as a retrograde transport (such as dynein in intraflagellar transport). *In vitro* biochemical study provides direct evidence for this issue.

The motor activity of myosins is easily assessed by an *in vitro* motility assay in which we simply observe movement of fluorescently labeled actin filaments on a glass surface coated with myosin molecules (Kron and Spudich, 1986). The velocity can be determined by analyzing the rate of actin filament movement, and the movement directionality can be determined if the actin filaments are polarity-marked with different fluorescent probes or with different fluorescence intensities. However, the procedure for specifically labeling either end of actin filaments has not been established. Conventionally, the movement directionality of myosins was determined by the *Nitella*-based *in vitro* motility assay (Sheetz and Spudich, 1983). In this assay, myosin-coated polystyrene beads move over a fixed substratum of well-organized polar arrays of actin filaments derived from dissection of *Nitella axillaris*, a giant fresh water alga. Although this assay has provided reproducible qualitative data on the movement directionalities of myosins (Cheney et al., 1993; Sheetz and Spudich, 1983), the system is not ideal because it depends on the biochemically undefined actin cables of *Nitella*, where unknown endogenous factors might affect the motor property of myosin.

For studies of microtubule-dependent motors, a polarity-marked microtubule has been established with a bright seed at the minus end and a dim elongated segment only on the plus end (Walker et al., 1990). The selective elongation towards the plus end is achieved by inclusion of NEM (*N*-ethylmaleimide)–treated tubulin, a competitive inhibitor of minus end polymerization. Although such chemical modification that specifically inhibits elongation at either end of the actin filament is not known, it seems

possible to allow an actin filament to elongate only (or predominantly) at plus end because of the relatively low dissociation rate constant in the presence of ATP (Fig. II-3). In the current study, we developed a method to produce polarity-marked actin filament. An alternative protocol using gelsolin that specifically binds to the plus end of an actin filament has also been developed by others (Herm-Gotz et al., 2002). These protocols have enabled us to determine movement directionality of myosins by performing simple *in vitro* motility assays.

Materials and methods

Materials - Restriction enzymes were purchased from New England Biolabs (Beverly, MA). Actin was prepared from rabbit skeletal muscle. Silicone-coating reagent (SIGMACOTE), bovine serum albumin, pyruvate kinase, phosphoenolpyruvate, anti-FLAG M2 affinity gel, and FLAG peptide (DYKDDDDK) were purchased from Sigma (St. Louis, Mo). Phalloidin, tetramethylrhodamin-5-(or-6-)maleimide, fluorescein phalloidin, and Alexa Fluor 488 phalloidin were purchased from Invitrogen (Carlsbad,CA). Recombinant human calmodulin was expressed in E. coli, and purified as described previously (Ikebe et al., 1998).

Recombinant myosin 10 full-length construct - Three cDNA clones of bovine myosin 10, *i.e.* clones 17 (nucleotides 1-1564), 27 (nucleotides 976-2653), and 5-2-1 (nucleotides 2030-7769), were kindly provided by Dr. David P Corey at Harvard Medical School.

These clones were joined by introducing *Eco*RI site and *Xba*I site at nucleotide positions 1240 and 2517, respectively, and the ORF region was subcloned in pFastBac vector with *Sal*I site and *Xba*I site at 5'-side and 3'-side, respectively. The introduction of the *Xba*I site at 2517 changed the amino acid sequence whereas the *Eco*RI site did not. The *Xba*I site was fixed by site-directed mutagenesis after subcloned in the pFast vector. The pFastBac vector (for baculovirus expression system) was modified to put an N-terminal FLAG epitope tag or an N-terminal GFP to a protein to be expressed.

Recombinant calmodulin - Human testis total RNA was purchased from Clontech (Mountain View, CA), and cDNA library was obtained by reverse transcription with random oligonucleotides. Human calmodulin ORF was subcloned in pFastBac vector with *Spe*I site and *Xho*I site at 5'-side and 3'-side, respectively. For expression in *E.coli*, the ORF was subcloned in pET30 with *Nhe*I site and *Xho*I site at 5'-side and 3'-side, respectively.

Baculovirus preparation - Baculoviruses used to express recombinant myosin 10 (full-length) and recombinant calmodulin were prepared by following the instruction provided by Invitrogen (Carlsbad,CA).

Protein expression and purification - To express the full-length recombinant myosin 10, Sf9 cells (approximately 2 x 10^8 cells) were co-infected with two viruses expressing the myosin 10 heavy chain and calmodulin. The infected cells were harvested after culturing

for three days at 28°C, and washed with a buffer containing 150 mM NaCl, 30 mM Tris-HCl, pH 7.5, and 5 mM EGTA. The cells were then lysed by sonication in 10 ml of lysis buffer (100 mM NaCL, 50 mM Tris-HCl, pH 7.5, 2 mM $MgCl_2$, 3 mM EGTA, 1 mM ATP, 1 mM phenylmethyl sulfonyl fluoride, 0.1 mg/ml trypsin inhibitor, 10 µg/ml leupeptin, 1 mM 2-mercaptoethanol). After centrifugation at 300,000 ×g for 10 min at 4°C, the supernatant was incubated with 500 µl of anti-FLAG M2 affinity gel in a 14-ml conical tube on a rotation wheel for 30 min at 4°C. The resin suspension was then loaded on a column (1 x 10 cm) and washed with 10 ml of buffer A (150 mM NaCl, 50 mM Tris-HCl, pH 7.5, and 0.1 mM EGTA). Protein was eluted with buffer A containing 0.1 mg/ml FLAG peptide. Freshly prepared DTT (1 mM final concentration) was added to the eluted fraction, and stored on ice.

Polarity-marked actin filaments - F-actin was freshly prepared according to the method by Spudich and Watt (Spudich and Watt, 1971). To produce minus end seeds, F-actin (1.3 mg/ml) was labeled with 5-fold molar excess of tetramethylrhodamin-5-(or-6)maleimide in the presence of 20 µM phalloidin in buffer S (25 mM KCl, 25 mM HEPES-KOH, pH 7.5, 5 mM $MgCl_2$, 1 mM EGTA) in the dark at 4°C for 30 min. The reaction was terminated by 10 mM DTT, and the fluorescently labeled F-actin was obtained by centrifugation (300,000 ×g for 7 min at 4°C). To wash away the unbound fluorescent dye, the pellet was resuspended in buffer W (buffer S plus 10 µM phalloidin and 5 mM DTT), and pelleted again (300,000 ×g for 7 min at 4°C). The pellet was homogenized and diluted with buffer W (F-actin concentration was approximately 0.03

mg/ml), and subjected to brief sonication. Fragmentation of the labeled F-actin was visually confirmed with a fluorescence microscope. The fragmentated F-actins serve as the minus end seed of the polarity-marked actin filaments. G-actin was freshly extracted from approximately 50 mg of rabbit back muscle acetone powder with 2 ml of buffer E (1 mM ATP, 0.5 mM DTT, 1.5 mM $CaCl_2$. To adjust pH at 7.5 ~ 8.0, 0.8 mM Tris-base was added.) on ice for 30 min. To minimize ADP, ATP stock solution (~0.1 M) was also freshly prepared from powder by dissolving 18 mg of ATP in 300 µl of 150 mM Tris-base. The extract was then centrifuged (300,000 ×g, 10 min at 4^{o}C), and the supernatant was saved. The concentration of G-actin was determined by measuring OD at 280 nm (ε_{280} = 1.1 ml mg^{-1} cm^{-1}). The G-actin (1 µM) was added to the fluorescently labeled minus end seeds (~3 µg/ml) in the presence of 20 units/ml pyruvate kinase, 1 mM phosphoenolpyruvate, and 10 units/ml fluorescein phalloidin (or Alexa Fluor 488 phalloidin) in buffer S. The elongation of actin filaments was carried out overnight in the dark at 4^{o}C.

In vitro motility assay - A coverslip was first coated with silicon, and then coated with purified myosin 10. The residual glass surface was blocked by bovine serum albumin to prevent polarity-marked actin filament from directly binding to the glass surface. The movement of polarity-marked actin filaments was observed at 25^{o}C in buffer S containing 2 mM ATP, 4.5 mg/ml glucose, 36 µg/ml catalase, 216 µg/ml glucose oxidase, and 143 mM 2-mercaptoethanol. Visualization of the polarity-marked actin filaments was performed with an IX71 microscope platform (Olympus) with SensiCam^{QE}

CCD camera (Cooke). A dichroic mirror (51004v2bs, Chroma) and a fluorescence emission filter (51004v2m, Chroma) were set in the fluorescence mirror unit cassette of the IX71 platform, and two separate excitation filters (s555/25x and s484/15x, Chroma) were set in an external filter wheel unit (ProScan^{TM} II, PRIOR scientific). The position of the excitation filters was controlled by computer software (IPLab, Scanalytics), and two distinct sequential images were captured (One for TRITC, the other for FITC). Sequential images of polarity-marked actin filaments were obtained by merging the two sequential images from the two filters. The movement speed of polarity-marked actin filaments was analyzes by collecting ≥100 data points obtained from ≥10 different actin filaments. The error bar indicates the standard deviation of the data.

Results

Purification of recombinant myosin 10

Although myosin 10 is ubiquitously expressed in a variety of cell types, the expression level of the protein is relatively low – just hundreds or a few thousand copies per cell (Berg et al., 2000). To obtain sufficient amount of the protein with high purity required for our biochemical experiments, we decided to employ the baculovirus expression system with cDNA of full-length bovine myosin 10 (Fig. II-1). This expression system has been used successfully in expressing a sufficient amount of functional myosin molecules. (Bacteria do not express functional myosins probably due to the folding or the post-translational modification problem.) The baculovirus system

also allows co-expression of several different proteins with different amounts. Since most myosins require calmodulins or other light chains for the functions, and the endogenous calmodulin expressed in the host cell (sf9) is not sufficient in most cases, it is advantageous to be able to control the expression level of different protein components by simply changing the baculovirus dose. A FLAG-epitope tag was attached to the N-terminal end of myosin 10 to facilitate the purification. We successfully expressed and purified the full-length myosin 10 (Fig. II-2). Reasonable amount of calmodulin was also co-purified with the heavy chain that is consistent with the primary structure of myosin 10 with three IQ motifs (Fig. II-1).

Polarity-marked actin filaments

We first prepared F-actin, and labeled it extensively at Cys-374 with tetramethylrhodamine maleimide. The filament was fragmentated by brief sonication to make minus end nuclei of polarity-marked filaments. Unlabeled G-actin was added at ~1μM concentration together with comparable concentration of fluorescein phalloidin to label the elongated filaments. We tested the quality of the polarity-marked filament in an *in vitro* motility assay with myosin 5a, a well-known plus end-directed myosin. In most preparations, we observed many polarity-marked actins having rhodamine-labeled nuclei at minus end as expected. However, in some preparations, we observed significant numbers of actin filaments having the rhodamine-labeled nuclei at plus end or in the middle of actin filaments. This could be explained by the polymerization–depolymerization kinetics of an actin filament (Fig. II-3). Although the second-order

association rate constant of G-actin at the plus end is five times higher than that at the minus end in the presence of ATP, the overall affinities at plus end and minus end are not very different (0.2μM at plus end vs. 0.5μM at minus end). Furthermore, in the presence of ADP (or when the bound ATP is hydrolyzed), the affinity becomes higher at the minus end (K_D vales are 6 μM at plus end and 2 μM at minus end). In any case, the possibility of generating false-polarity-marked actin filaments impairs the accuracy of directionality determination of myosins with unknown movement directionality.

In order to minimize falsely marked actin filaments, we paid particular attention to the following points in developing an improved method. First, ADP-bound G-actin has lower affinity towards the plus end (6μM) than that towards the minus end (2μM). Thus, the use of stored (frozen) G-actin was avoided because the bound ATP will be hydrolyzed during storage. Second, Ca^{2+}ATP-bound G-actin has a high critical concentration (100 ~ 200μM), and Mg^{2+}/Ca^{2+} exchange rate is very low. Thus, if G-actin is prepared in the presence of Ca^{2+}ATP instead of Mg^{2+}ATP, and Mg^{2+} is added only when polymerization takes place, we should be able to facilitate actin filament elongation predominantly at the plus end by minimizing the actual concentration of Mg^{2+}ATP-bound G-actin in the polymerization solution. Third, ATP regeneration would also increase the probability of actin filament elongation only at the plus end by minimizing the population of ADP-bound G-actin. A new protocol is established based on these considerations, and is described in 'Materials and Methods' in more detail. The polarity-marked actin filament produced by this method is phenomenal. Almost all double-stained actin

filaments have their rhodamine-labeled seeds properly positioned at the minus end. (Appendix A).

Movement directionality of full-length myosin 10

By using the polarity-marked actin filaments, we performed *in vitro* motility assay on the full-length myosin 10. Polarity-marked actin filaments moved with the rhodamine-labeled minus end leading the movement, which unambiguously demonstrates that myosin 10 is a plus end-directed motor (Fig. II-4). The conclusion is consistent with the proposed physiological role of myosin 10 as a transporter in filopodia, which carries VASP to the tip to facilitate filopodia elongation or maintenance by opposing the continuous retraction of actin filaments. In addition, the speed of actin filament translocation observed in the *in vitro* motility assay (0.12 ± 0.04 μm/sec) was consistent with the speed of plus end-directed movement of GFP-labeled myosin 10 observed in a living cell (~0.1 μm/sec). Since myosin 10 has to counteract the continuous retraction of actin cables (~0.01 μm/sec), it is reasonable that the speed observed *in vitro* was slightly faster than that observed in filopodia in a living cell.

Effect of Calmodulin-like protein on the movement directionality of myosin 10

In addition to calmodulin, calmodulin-like protein (CLP) has been reported to bind to the third IQ domain of myosin 10 (Rogers and Strehler, 2001). CLP retains ~85% amino acid sequence homology to calmodulin, and is only expressed in the epithelial cells. Since the expression of myosin 10 is ubiquitous, CLP does not seem to be the

universal light chain of myosin 10. However, it is possible that the binding of CLP may affect the movement directionality of myosin 10. To test this possibility, we co-infected Sf9 cells with full-length myosin 10 heavy chain expressing virus, calmodulin expressing virus, and CLP expressing virus. The expressed myosin 10 heavy chain was co-purified with calmodulin and CLP (Fig. II-5). To ensure complete binding of CLP to the heavy chain, the *in vitro* motility assay was performed with excess amount of exogenous CLP (1 mg/ml). As expected, the plus end-directed motility was not affected by the binding of CLP.

Effect of N-terminal GFP-tag and truncation on the directionality

Several cell biological studies have been done using myosin 10 constructs with N-terminal GFP tag (Berg and Cheney, 2002; Bohil et al., 2006; Tokuo and Ikebe, 2004; Zhang et al., 2004). We also generated several myosin 10 constructs with N-terminal GFP tag for the single molecule experiment described in Chapter IV. For enzyme kinetics study described in Chapter III, we used truncated myosin 10 construct that contains the motor domain and the first IQ motif (M10IQ1). Although N-terminal GFP-tagged myosin constructs and truncated myosin constructs have been widely used for myosin research, those modifications might affect the inherent movement directionality of myosin 10. Therefore, we checked the movement directionalities of the GFP-tagged full-length myosin 10 construct and the truncated myosin 10 construct (M10IQ1). Both of them showed plus end-directed motility with similar actin translocating velocities as

observed for full-length myosin 10 (Table II-1), suggesting that the directionality is not affected by the N-terminal GFP or the truncation at the neck region.

Discussion

Implication of the plus end directionality of myosin 10 in intrafilopodial motility

We succeeded in expressing and purifying the full-length mammalian myosin 10 using the baculovirus system. Using the recombinant myosin 10, the movement directionality was unambiguously determined to be plus end-directed by the in vitro motility assay using the polarity-marked actin filaments we developed. The directionality is consistent with the proposed physiological role of myosin 10 as a plus end-directed cargo transporter. The actin translocating velocity determined by the in vitro motility assay is also consistent with the velocity of myosin 10 observed in filopodia of living cells. The retrograde movement of myosin 10 towards the cell body can be reasonably explained by the rate of the continuous retrograde flow of actin filaments in filopodia (Mallavarapu and Mitchison, 1999). It is possible that myosin 10 takes advantage of the retrograde flow of the actin filament to recycle itself for another round of transport.

Implication of processivity

Processivity is the ability of a myosin molecule to successively move along actin track for a long distance without dissociating from the track, and it is thought that a processive myosin motor is suitable for cargo transport. The processivity of myosin 10

inferred from the observation in the in vitro motility assay is discussed, although the processivity of myosin 10 is vigorously tested in Chapter IV

Methylcellulose is sometimes added to the buffer solution for *in vitro* motility assay. This highly elongated polymer prevents actin filaments from diffusing in a direction perpendicular to the long axis. Thus, inclusion of methylcellulose (~0.5%) in the motility assay buffer greatly aids actin translocation by highly nonprocessive myosins or myosins at very low density on the glass surface, by simply slowing down the diffusion of actin filaments away from the glass surface during brief moments when no myosin molecule is bound to actin. In our experience, for highly processive myosins such as myosin 5a, methylcellulose is not necessary because at least one of the two heads of a myosin 5a molecule (double-head structure) holds actin filament due to its highly processive nature. For nonprocessive myosins such as smooth muscle myosins, however, we always needed to add methylcellulose to the assay buffer even if the loading concentration of myosin was very high (~2μM). In the case of myosin 10, we were able to visualize movement of actin filaments easily without adding methylcellulose despite the relatively low loading concentration (typically < 0.4 μM), suggesting that myosin 10 is processive, or at least more processive than smooth muscle myosin. The relatively high processivity of myosin 10 was actually confirmed by performing motor density dependent *in vitro* motility assay where 0.5% methylcellulose was used to successfully observe the actin translocations by smooth muscle myosin (Fig. II-6). It should be noted that this experiment merely shows relative degree of processivity, rather than the actual processivity. Also, since faster actin translocating velocities tend to be obtained on

myosin 10 with methylcellulose, the velocity of myosin 10 determined in this experiment will not be discussed.

Another indication of processivity is severing of actin filaments observed in the in vitro motility assay. In the case of processive myosins, simultaneous interaction of numerous myosin heads to actin filaments causes severing of the filaments, and this is conspicuous for myosin 5a at a loading concentration of ~0.5 μM. We have not seen severing of actin filaments for smooth muscle myosin at a high loading concentration (2~4 μM) with methylcellulose. For myosin 10, we observed severing of actin filaments during the *in vitro* motility assay at a loading concentration of ~0.4 μM, suggesting again that myosin 10 is a processive motor.

Other findings

Nitrocellulose-coated coverslip is usually used for *in vitro* motility assay of myosins, however, for the myosin 10 full-length construct, silicone-coated coverslips were used because full-length myosin 10 did not seem to bind to the nitrocellulose-coated glass surface. Because the silicone coating provides a hydrophobic surface on the coverslip, the result may suggest a hydrophobic nature of the C-terminal tail of myosin 10. This may induce clustering of molecules through hydrophobic interaction, and might be important for the stable dimer formation because the predicted coiled-coil region of myosin 10 does not form stable coiled-coil (Knight et al., 2005). However, at least we did not see any sign of the clustering in our single molecule experiments described in Chapter IV.

Table II-1. Directionality and velocity of the myosin 10 constructs

constructs	directionality	velocity [μm/sec]
full-length myosin 10	plus	0.12 ± 0.04
full-length GFP-myosin 10	plus	0.11 ± 0.04
M10IQ1 (Chapter III)	plus	0.17 ± 0.03

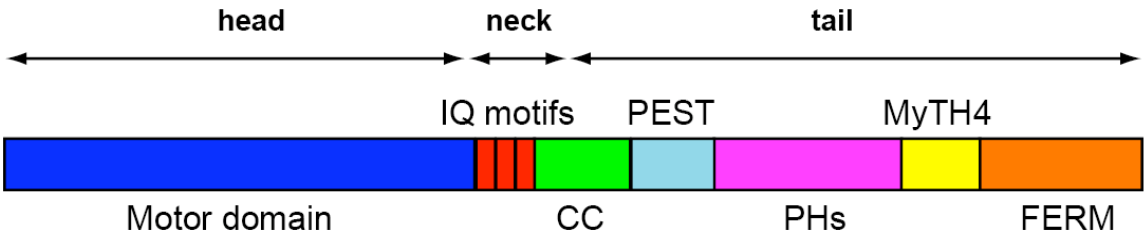

Figure II-1. Schematic representation of myosin 10. *CC*, the predicted coiled-coil; *PEST*, proline-, glutamate-, serine-, and threonine-rich region; *PH*, pleckstrin homology domain; *MyTH4*, myosin tail homology 4 domain; *FERM*, band 4.1 ezrin radixin moesin domain.

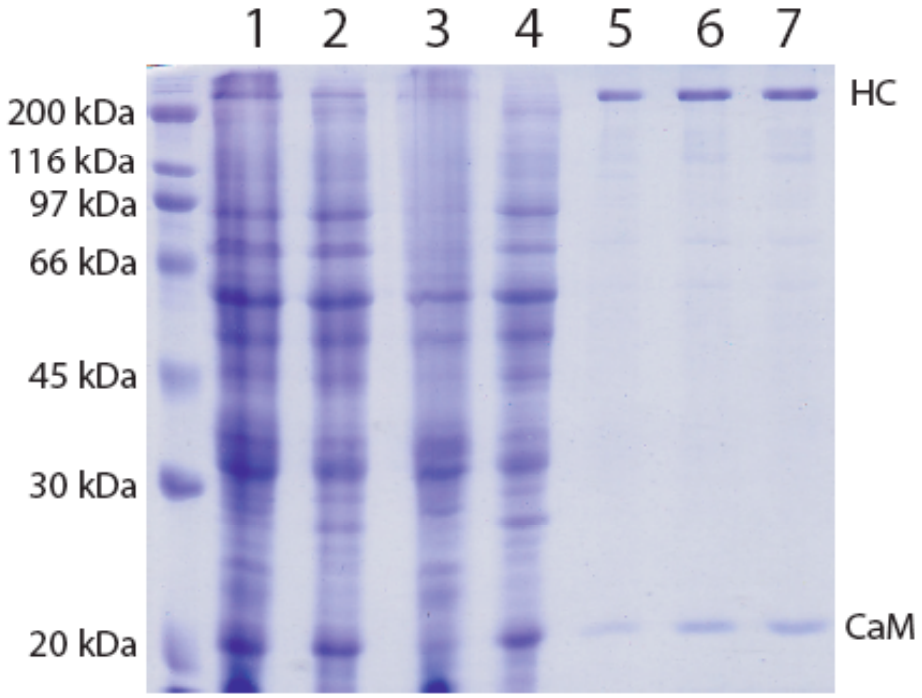

Figure II-2. Expression and purification of myosin 10 full-length construct. The sample of each purification step was examined by SDS-PAGE and stained with Coomassie Brilliant Blue. *Lane 1*, total cell lysate; *Lane 2*, 300,000 × g supernatant; *Lane 3*, 300,000 × g pellet; *Lane 4*, unbound fraction from the FLAG M2 affinity gel; *Lane 5-7*, elutes from the affinity column with 0.1mg/ml FLAG peptide. *HC*, heavy chain of myosin 10 full-length; *CaM*, calmodulin.

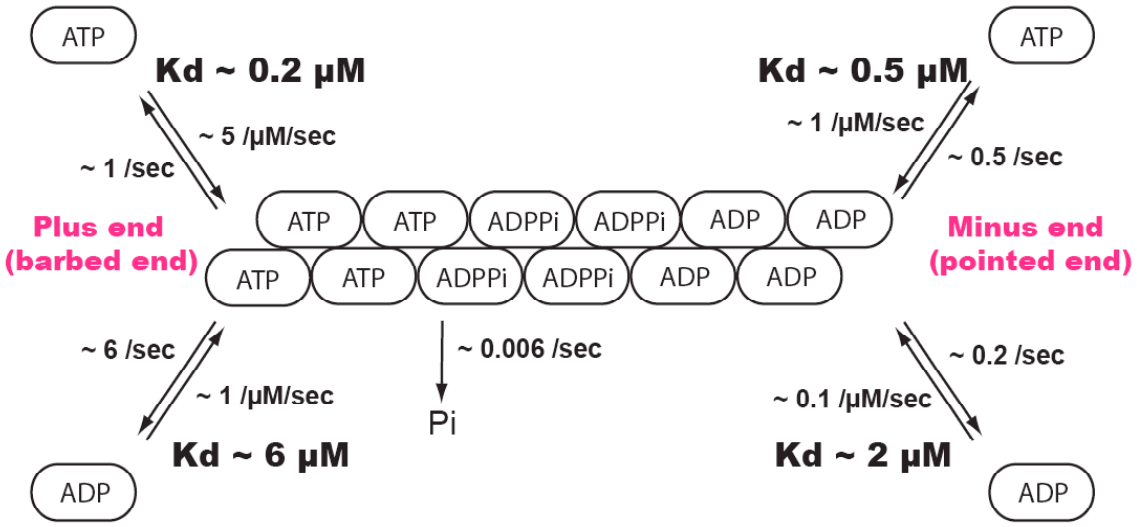

Figure II-3. Assembly and disassembly of actin.

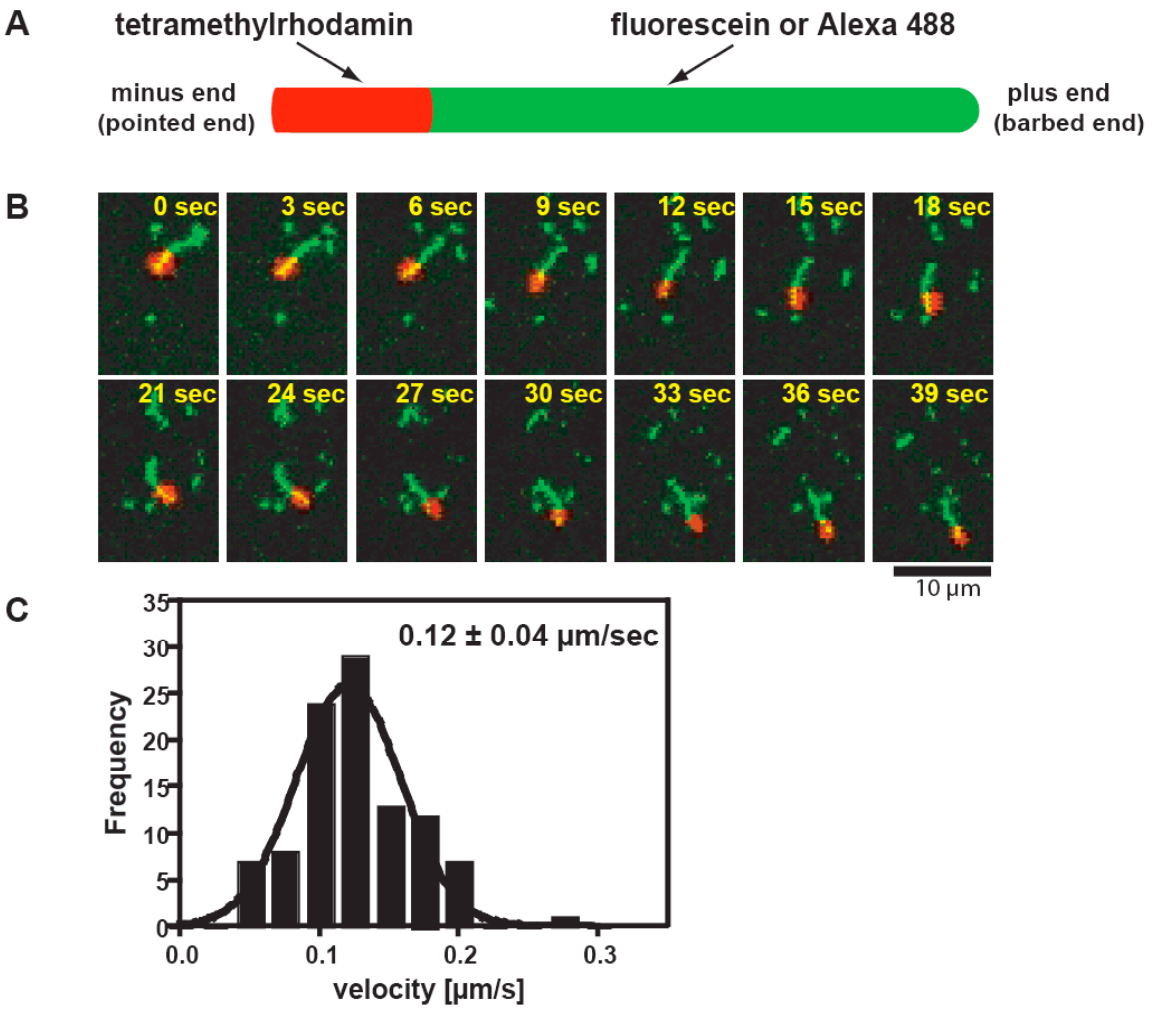

Figure II-4. Ensemble in vitro surface assay with polarity-marked actin. A, Schematic representation of the polarity-marked actin filament. **B**, Sequential images of the movement of polarity-marked actin filaments by myosin 10 full-length construct. **C**, Histogram of the velocity of the actin filaments driven by myosin 10.

Figure II-5. Copurification of calmodulin-like protein with the heavy chain of full-length myosin 10. The eluate from the FLAG affinity column was analyzed by SDS-PAGE and stained with Coomassie Brilliant Blue. *HC*, heavy chain; *CaM*, calmodulin; *CLP*, calmodulin-like protein.

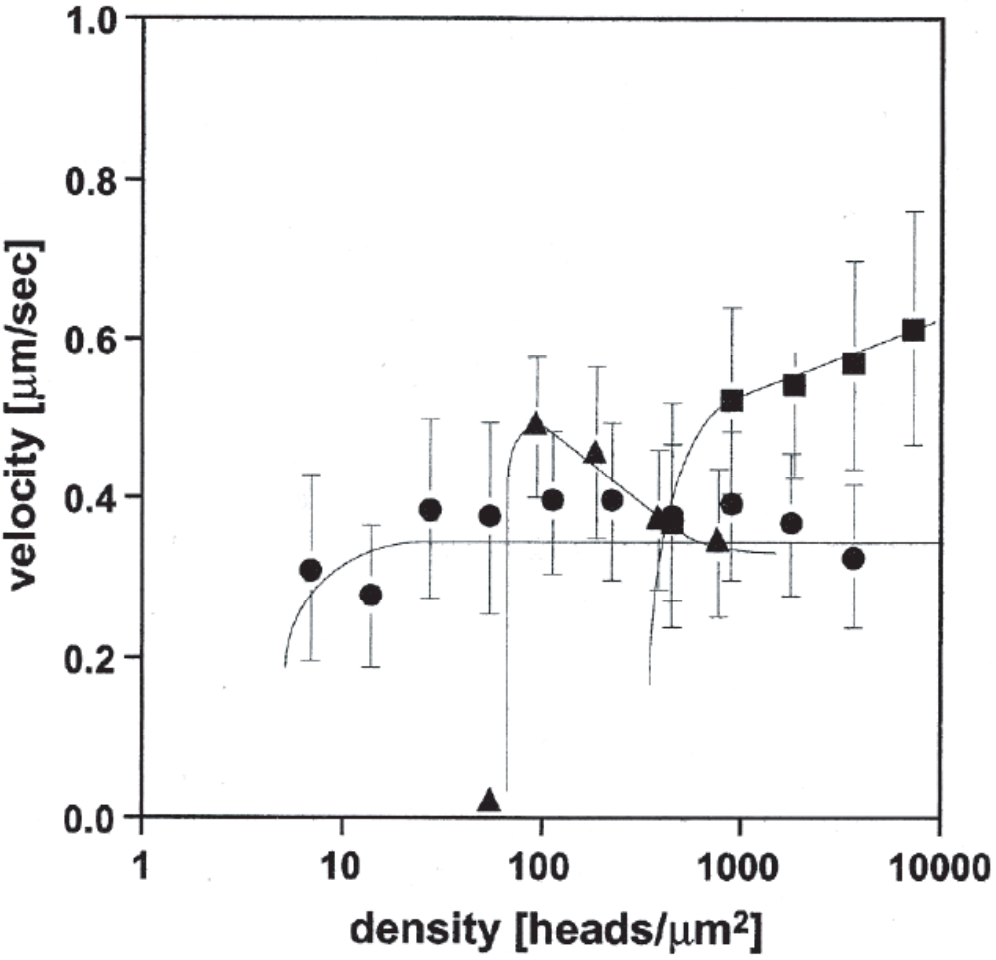

Figure II-6. Actin filament velocity as a function of myosin surface density. The surface density was calculated by the myosin concentration times the flow cell volume divided by the area of both flow cell faces, assuming all the myosins molecules added were attached on the glass surface. This would provide the upper limit of the number of molecules per unit area. Unlike all the other *in vitro* motility assays described throughout this thesis, 0.5% methylcellulose was used. ●, myosin 5a heavy meromyosin; ■, smooth muscle myosin (phosphorylated); ▲, myosin 10 (truncated at the end of the predicted coiled-coil region).

CHAPTER III

THE DUTY RATIO OF MYOSIN 10

Introduction

Myosins translocate (or move along) actin filaments by hydrolyzing the common energy source, ATP, and by releasing the common reaction products, ADP and phosphate (Pi). However, the detailed enzyme kinetic mechanism of the ATPase reaction is different among the members of the myosin superfamily, and the characteristic ATPase reaction mechanism determines the duty ratio – a quantitative indicator that is thought to be closely related to the processivity of myosin motors. Processivity, together with the movement directionality, determines the distinct physiological functions of individual myosin motors in a cell. The term "processivity" is defined as the ability of an enzyme to repetitively continue its catalytic function without dissociating from its substrate. In the case of myosin motors, the processivity is defined as the ability to repetitively translocate an actin filament without dissociating from the actin filament. It is called nonprocessive if a myosin motor translocates an actin filament only once per diffusional encounter with the filament.

The duty ratio of myosin is defined as the fraction of the time that a motor domain spends attached to an actin filament during an ATPase cycle. Myosins with high duty ratios can maintain continuous attachment to an actin filament and can move along the filament on their own (thus processive), whereas myosins with low duty ratios usually

oligomerize into a large assembly in order to produce continuous motility (the individual molecules are nonprocessive). Myosin 5a is the best-characterized processive myosin with a very high duty ratio (>0.7). The molecule has a double-headed structure (homodimer) (Cheney et al., 1993), and moves along actin filaments preocessively by hand-over-hand mechanism (Warshaw et al., 2005; Yildiz et al., 2003). For the processive movement by hand-over-hand mechanism, at least one of the two heads (the lead head) has to stay on an actin filament until the other head (the trail head) binds to the forward binding site on the actin filament. Thus the duty ratio of >0.5 is a prerequisite for making a double-headed myosin molecule processive by hand-over-hand mechanism as seen in myosin 5a. Muscle myosins such as skeletal muscle myosins are typical low duty ratio motors. Although these myosins have double-headed structure, they do not move processively along actin filaments by themselves due to their extremely low duty ratios (0.01~0.02). Muscle myosins form thick filaments, and together with actin filament, they form a lattice structure called sarcomere where numerous myosin heads simultaneously interact with actin filaments to produce quick movement and force as a whole. In this circumstance, it is advantageous to have a low duty ratio so that the binding of one head does not interfere with the translocations of actin by other heads. Thus, the very low duty ratio of muscle myosins is important for the physiological functions of muscles. By knowing the duty ratio, we can estimate the degree of processivity of a myosin molecule, and therefore, we can infer the physiological process where the myosin molecule is involved.

In this chapter, the duty ratio of myosin 10 is determined by performing transient enzyme kinetics.

Materials and methods

Materials - Nickel-nitrilotriacetic acid agarose (Ni-NTA) was purchased from Qiagen (Hilden, Germany). (2'-(or-3')-*O*-(*N*-methylanthraniloyl)adenosine 5'-triphosphate (mant-ATP) and (2'-(or-3')-*O*-(*N*-methylanthraniloyl)adenosine 5'-diphosphate (mant-ADP) were purchased from Invitrogen (Carlsbad,CA). Purine nucleoside phosphorylase (PNPase), 7-methylguanosine (MEG), phosphoenolpyruvate and pyruvate kinase were obtained from Sigma (St. Louis, MO). Pyrene-actin was prepared as previously described (Kouyama and Mihashi, 1981). 7-diethylamino-3-((((2-maleimidyl)ethyl)amino)carbonyl)coumarin-labeled phosphate binding protein (MDCC-PBP) was prepared as described (Brune et al., 1994; White et al., 1997). For other materials, see "Materials and methods" in Chapter II.

Recombinant truncated myosin 10 construct - A partial ORF of bovine myosin 10 (Met 1 – Gln 773) with the hexahistidine tag sequence at the 3'-end was subcloned in pFastBac vector (for baculovirus expression system) with *Kpn*I sites. This construct is named M10IQ1.

Baculovirus preparation - See "Materials and methods" in Chapter II.

Protein expression and purification - To express the recombinant myosin 10 (M10IQ1), Sf9 cells (approximately 4 x 10^8 cells) were co-infected with two viruses expressing the M10IQ1 heavy chain and calmodulin. Infected cells were harvested after culturing for three days at 28^{o}C, and washed with a buffer containing 150 mM NaCl, 30 mM Tris-HCl, pH 7.5, and 5 mM EGTA. The cells were then lysed by sonication in 20 ml of lysis buffer (25 mM KCl, 30 mM HEPES-KOH, pH 7.5, 2 mM $MgCl_2$, 0.2 mM EGTA, 1 mM ATP, 1 mM phenylmethyl sulfonyl fluoride, 0.1 mg/ml trypsin inhibitor, 10 μg/ml leupeptin, 1 mM 2-mercaptoethanol). After centrifugation at 300,000 ×g for 10 min at 4^{o}C, the supernatant was incubated with 300 μl of Ni-NTA resin in a 14-ml plastic tube on a rotation wheel for 10 min at 4^{o}C. The resin suspension was then loaded on a column (1 x 10 cm) and washed with 10 ml of wash buffer (50 mM KCl, 20 mM HEPES-KOH/10 mM Imidazole-HCl, pH 7.5, 0.1 mM EGTA, 5 μg/ml leupeptin, and 1 mM 2-mercaptoethanol). M10IQ1 was eluted with the wash buffer containing 200 mM Imidazole-HCl, pH 7.5. The purified M10IQ1 was dialyzed against a dialysis buffer B (25 mM KCl, 25 mM HEPES-KOH (pH 7.5), 5 mM $MgCl_2$, 1 mM EGTA). The protein was stored on ice and used within 2 days. Typically, 1~1.5 mg of M10IQ1/CaM was obtained. Protein concentration was determined by Bradford method using BSA as a control and corrected by the purity of the sample determined by densitometry analysis, assuming degradation of the protein is negligible. [2,8-^{3}H]ADP/VO_4 was used to determine the concentration of active M10IQ1. The active motor concentration was typically 70~80% of that estimated by the Bradford method. This is primarily due to the

overestimation of the M10IQ1 concentration using BSA as a control, and also minor fraction of nonfunctional M10IQ1 during the purification.

ATPase assay - The steady-state ATPase activity of M10IQ1 was measured at 25°C in the presence of 2 mM ATP with an ATP regeneration system (40 units/ml pyruvate kinase and 2 mM phosphoenolpyruvate). The reaction was carried out in buffer B with 0.2 mg/ml calmodulin at 25°C. The liberated pyruvate was determined as described (Reynard et al., 1961). Error bars show standard error from three different preparations.

Polarity-marked actin filaments - See "Materials and methods" in Chapter II.

In vitro motility assay - See "Materials and methods" in Chapter II.

Actin-cosedimentation assay - The binding of M10IQ1 with actin in the presence of ADP was determined using 1 μM M10IQ1 and 5 μM F-actin in buffer B with 0.2 mg/ml calmodulin and 0.1 mM ADP, and centrifuged at 300,000xg at 25°C for 10min. The pellet was dissolved with 8 M urea, and both supernatant and the pellet were analyzed by an SDS-PAGE with Coomassie Brilliant Blue staining.

Quenched-flow measurement - Quenched-flow measurement was performed in buffer B ith 0.2 mg/ml calmodulin at 25°C by a KinTek RQF-3 apparatus (KinTek Co., Clarence,

PA) (Kambara et al., 1999). Error bars show standard error from three independent experiments.

Stopped-flow experiments - Kinetic measurements were performed in buffer B with 0.2 mg/ml calmodulin at 25°C using a KinTek SF-2001 apparatus (KinTek Co., Clarence, PA) with a 75-watt xenon lamp. Mant-nucleotides were excited at 360 nm and the fluorescence was monitored using a 420 nm cut-off filter. Pyrene-actin was excited at 365 nm with a 365nm band-pass filter and the fluorescence was monitored using a 400 nm cut-off filter. Intrinsic tryptophan residues in M10IQ1 were excited at 295 nm and the fluorescence was monitored using 340 nm cut-off filter. MDCC-PBP was excited at 436 nm with 436 nm band pass filter and the fluorescence was monitored using 450 nm cut-off filter. 3 μM MDCC-PBP, 0.01 units/ml PNPase and 0.3 mM MEG were included in all solutions. Light scattering at 550 nm was observed to monitor dissociation of acto-M10IQ1. The volume ratio of the syringe was 1:1 in all single mixing experiments, and 1:1:1 in double mixing experiments. Curve fitting was done using the KinTek SF-2001 software. Error represents standard error from 3-10 independent experiments.

Computer simulation - Kinetic simulations were performed using STELLA v8.1.1 software (iseesystems, Lebanon, NH). See Appendix D.

Results

The truncated recombinant myosin 10 construct (M10IQ1)

The myosin 10 construct (M10IQ1) employed in this study contains the motor domain and the first IQ domain (Met1-Gln773) followed by hexahistidine tag to facilitate purification. This truncated single-headed construct was used in the present study to avoid the possible complexity arising from the formation of an oligomeric structure. The M10IQ1 was expressed using the baculovirus expression system together with calmodulin in Sf9 cells and purified with Ni^{2+}-agarose affinity column. As expected from the design of the construct, the isolated protein had an apparent molecular mass of 90 kDa co-purified with a low molecular mass protein (Fig. III-1A). The mobility of the low molecular mass peptide on an SDS-PAGE increased with Ca^{2+}, suggesting that it is calmodulin (data not shown). The amount of bound calmodulin to M10IQ1 seemed to be low, likely due to the partial loss of the bound calmodulin during the purification steps. We observed that the actin-activated ATPase of M10IQ1 increased upon addition of calmodulin, suggesting that the IQ domain of the purified M10IQ1 is not completely occupied with calmodulin (Fig. III-2). Based on this result, the apparent dissociation constants of calmodulin for M10IQ1 were estimated to be 2.7 ± 1.2 μg/ml and 1.4 ± 0.2 μg/ml, in the presence (0.1 mM) and the absence of Ca^{2+}, respectively. Therefore, we added 0.2 mg/ml calmodulin to the M10IQ1 sample in all experiments in this study. Calmodulin-like protein (CLP) has been reported to preferentially bind to the third IQ motif of myosin 10 in the presence of Ca^{2+} (Rogers and Strehler, 2001). Although it is

less likely that CLP binds to the first IQ motif of the M10IQ1 construct in our experimental condition (EGTA condition), we tested if CLP is co-purified with the M10IQ1 heavy chain. Despite the high expression level of CLP in Sf9 cell that was comparable to that of calmodulin, the co-expressed CLP was not co-purified with M10IQ1 (data not shown). The result is consistent with a previous report (Rogers and Strehler, 2001), and suggests that the affinity of CLP to the first IQ motif is very low in the absence of Ca^{2+}. Therefore, for the enzyme kinetics experiments, we focused on M10IQ1 having only calmodulin as the light chain.

Figure III-1B shows the actin-activated ATPase activity of M10IQ1 as a function of the actin concentration. The ATPase activities at various actin concentrations were fitted well with a Michaelis–Menten equation to yield V_{max} and K_{ATPase} of 13.5 ± 1.6 s^{-1} and 17.4 ± 5.2 μM, respectively. We also performed an *in vitro* motility assay on the M10IQ1 construct to see if the M10IQ1 retains the actin translocating activity. The velocity was 0.17 ± 0.03 μm/sec (Table III-1 and Fig. III-1C). The movement directionality was determined to be plus end-directed using the polarity-marked actin filament used in Chapter II (Table II-1). The results suggest that the C-terminal truncation at the neck does not impair the motor function of myosin 10. We also found that the addition of exogenous calmodulin (> 0.05 mg/ml) greatly increased the fraction of actin filament moving in the *in vitro* motility assay, suggesting that the binding of light chain to the IQ domain is essential for the motor function of myosin 10, and that the affinity of calmodulin to the first IQ domain is relatively low. This is consistent with the result of calmodulin dependent ATPase assay (Fig. III-2).

ATP binding to M10IQ1 and acto-M10IQ1

The initial step of the ATP binding is a diffusion-limited process with an association constant K_1 or K'_1 (Appendix C). After the formation of the collision complex ((MT) or (AMT)), the motor domain weakly binds to actin (weakly actin-bound state) with a rate constant k_{+2} or k'_{+2}. Figure III-3 shows the rate of mant-ATP binding to M10IQ1 as a function of mant-ATP concentration. The fluorescence intensity is sensitive to its environment (either hydrophilic or hydrophobic), and increases when the fluorophore is trapped in the active site of myosin and forms MT or AMT complex. Thus the apparent ATP biding rates become K_1k_{+2} or $K'_1k'_{+2}$ (Appendix C). The increase in the fluorescence intensity of mant-ATP followed single exponential kinetics for both M10IQ1 and acto-M10IQ1 (Fig. III-3, insets). The observed rate constants linearly increased with mant-ATP concentration to yield second order rate constants of 3.4 ± 0.3 $\mu M^{-1}s^{-1}$ and 4.7 ± 0.2 $\mu M^{-1}s^{-1}$ for acto-M10IQ1 and M10IQ1, respectively. The extrapolation of the straight lines intercepts y-axis at < 2 s^{-1}, suggesting that the rate for the reverse reaction (k_{-2} and k'_{-2}) of the ATP binding step is < 2 s^{-1}.

ATP-induced population of weakly bound acto-M10IQ1

A disadvantage of using mant-ATP is the high background fluorescence when used at high concentrations (this is also the case for other fluorescent substrates). Theoretically, k_{+2} or k'_{+2} can be determined from the maximal rates attained at saturating concentration of the substrate, however, the signal-to-noise ratio quickly plummets with

higher substrate concentrations, and the analysis usually collapses before even seeing a sign of curvature. Furthermore, mant-ATP may not properly represent regular ATP for a particular myosin, though mant-ATP has been used in many enzyme kinetics studies. An alternative way of monitoring the ATP binding and the formation of the actin weakly-bound state is to monitor the change in fluorescence of pyrene-labeled actin upon addition of ATP (myosin is premixed with the pyrene-labeled actin). Although the rates in the absence of actin cannot be determined by this method, we can determine $K'_1k'_{+2}$, k'_{+2}, and k'_{-2} by using regular ATP. The fluorescence intensity of pyrene increases upon formation of the weakly actin-bound complex (AMT) or dissociation of the motor domain from the pyrene actin, thus we can monitor the formation of AMT by simply following the pyrene fluorescence. Rapid mixing of ATP to pyrene-acto-M10IQ1 resulted in an increment of pyrene fluorescence as is observed for other unconventional myosins (De La Cruz et al., 2001; De La Cruz et al., 1999; El Mezgueldi et al., 2002). The time course of the observed fluorescence transient was best fitted to a single exponential kinetics (Fig. III-4, inset) and the apparent rate constants at various ATP concentrations showed a hyperbolic relationship against ATP concentration as expected (Fig. III-4). The binding rate constant of ATP to acto-M10IQ1 ($K'_1k'_{+2}$) can be obtained from the initial slope. The value ($2.7 \pm 0.4\ \mu M^{-1}s^{-1}$) was consistent with that obtained by using mant-ATP (Fig. III-3). The maximum rate constant estimated from the hyperbolic curve fitting (k'_{+2}) was $782 \pm 74\ s^{-1}$, which was more than 50-fold larger than the V_{max} of the steady state ATPase activity of acto-M10IQ1. Therefore, the ATP binding step and the following isomerization step (k'_{+2}) are not rate limiting for acto-M10IQ1 ATPase

cycle under physiological ATP concentrations (1~2 mM).

Dissociation of acto-M10IQ1 by ATP

The dissociation of acto-M10IQ1 was monitored by measuring the decrease in light scattering intensity upon mixing acto-M10IQ1 with ATP (Fig. III-4). The time course of the signal change was fitted with a single exponential kinetics (Fig. III-4, inset) and the apparent rate constants of acto-M10IQ1 dissociation were hyperbolically increased with ATP concentration to yield the maximum value of 885 ± 36 s^{-1}. The hyperbola was almost identical to that obtained from the change in pyrene fluorescence intensity, suggesting that the dissociation of acto-M10IQ1 (k_{+8}, k_{-8} pathway) is a rapid process.

ATP hydrolysis monitored by tryptophan fluorescence

The motor domain of myosin 10 contains a conserved tryptophan residue (W481) located at the rigid relay loop. This residue is equivalent to W510 of skeletal muscle myosin 2 that has been shown to be the largest contributor to the enhancement of the intrinsic tryptophan fluorescence associated with ATP binding and hydrolysis. The intrinsic tryptophan fluorescence intensity of M10IQ1 increased upon addition of ATP and the increase followed single exponential kinetics (Fig. III-5, inset). The apparent rate constants increased with ATP to show a hyperbolic dependence (Fig. III-5) and yielded a maximum rate constant of 395 ± 26 s^{-1}. The ATP binding rate constant obtained from the initial tangent of the hyperbola was 4.4 ± 0.6 $\mu M^{-1}s^{-1}$, which was consistent with the

value obtained from mant-ATP binding experiment (Fig. III-3). We assume that the intrinsic tryptophan fluorescence enhancement of M10IQ1 by ATP monitors predominantly the hydrolysis step ($k_{+3} + k_{-3}$, Appendix C), because the observed maximal rate constant of 300~400 s^{-1} was less than half of that of the maximal ATP binding rate (k'_{+2} ~800 s^{-1}) determined by ATP induced pyrene fluorescence change. Since the ATP binding rate constant in the absence of actin is even greater than that in the presence of actin (suggesting $k_{+2} > k'_{+2}$ if $K_1 = \sim K'_1$), if the intrinsic tryptophan fluorescece enhancement predominantly monitors the ATP binding but not the following hydrolysis step, the maximal rate should be k_{+2} which should be similar to or larger than k'_{+2} (~800 s^{-1}).

ATP hydrolysis directly measured by quenched-flow

The motor domain of a myosin forms a myosin/ADP/P ternary complex (MDP) after ATP hydrolysis. Since the protein bound phosphate is released from myosin by acid quenching of the ATPase reaction, rapid initial phosphate release is observed when the reaction is stopped by acid (Pi burst). Figure III-6 shows the time course of Pi release of M10IQ1 ATPase reaction measured by a quenched flow experiment. Single turnover experiment was carried out to determine the equilibrium of the hydrolysis step (Fig. III-6A). 1μM of [γ–^{32}P]ATP was mixed with 2 μM M10IQ1 so that all given ATP was bound to the ATP binding site of myosin 10. Pi was rapidly released from acto-M10IQ1 followed by slow Pi release. The fast phase represents the initial rapid ATP hydrolysis by M10IQ1. The slow phase (0.06 s^{-1}) corresponds to the apparent Pi release rate (k_{+4}

$_{obs}$). The presence of the slow Pi release phase suggests that a certain population of M10IQ1 is present as a prehydrolysis step (MT). From the ratio of the fraction of the fast phase to the slow phase, the Pi burst size of 0.46 ± 0.02 was obtained. The result indicates that the equilibrium of MT–MDP step is significantly shifted to the pre-hydrolyzed form. The rate of the ATP hydrolysis was also measured with higher ATP concentrations (Fig. III-6B). The initial Pi-burst rates were 65 s^{-1} and 124 s^{-1} in the presence of 10.7 μM ATP and 20.9 μM ATP, respectively. The observed rate constants were limited by ATP binding rate at a given ATP concentration, suggesting that the ATP hydrolysis rate ($k_{+3} + k_{-3}$) is greater than 120 s^{-1}.

Phosphate release rate

Fluorescently labeled phosphate binding protein (MDCC-PBP) was used to monitor the rate of phosphate release in the presence and absence of actin (Fig. III-7). The fluorescence increased upon binding of released phosphate and it followed a single exponential kinetics in the absence of actin. The observed rate, 0.06 ± 0.02 s^{-1} ($k_{+4\ obs}$), was consistent with the rate obtained from the quenched-flow experiment (Fig. III-6A). In the presence of actin, however, the fluorescence increment followed double exponential kinetics as reported recently (Kovacs et al., 2005). The fast phase was actin concentration dependent as expected from the kinetics scheme (scheme III-1). We could not see any sign of curvature within the experimentally achievable actin range tested. The slope gives us a second order rate constant for MDP–AMDP transition ($k'_{+4}/K_{9\ obs}$, Appendix C), and it was 0.71 ± 0.02 $\mu M^{-1}s^{-1}$ (Fig. III-7B). The maximum Pi release rate

in the presence of actin was estimated to be >100 s^{-1} based upon the lack of curvature up to 50μM actin. The slow phase was actin independent and fairly constant throughout the actin concentrations tested. The slow phase is not an artifact coming from the MDCC-PBP system, because we did not observe the dual phase on skeletal myosin S-1. One possible explanation for the slow phase is due to the 'attached hydrolysis (AMT–AMDP)' as reported (Kovacs et al., 2005; White et al., 1997). The other possibility is the ATP rebinding to M10IQ1 during the observation. In principle, these two possibilities can be discriminated by performing the experiment with different M10IQ1 concentrations. The rate of the slow phase is independent of M10IQ1 concentration if the former situation is the case. On the other hand, if the latter situation is the case, the rate of ATP rebinding is expected to be faster at higher M10IQ1 concentration, thus we should see faster second phase. We performed the same experiment as in Fig. III-7A as a function of M10IQ1 concentration from 0.25 to 0.67μM (in final), with fixed actin concentration (5μM in final) and ATP concentration (0.23μM in final) (Fig. III-7B, inset). The rate of the slow phase increased by increasing the M10IQ1 concentration while the fast phase remained at the same rate ~5.5 s^{-1}, suggesting the slow phase came from the ATP rebinding during the observation. With given ATP concentration (0.23 μM), the rate constant of the forward reaction is ~1 s^{-1}. The rate constant of ~1 s^{-1} for the reverse reaction (that is possible with k_{-2} = 0.2 ± 1.3, Fig. III-3) together with the equilibrium of ATP hydrolysis step (K_3 = 0.85), explains the observed ~40% contribution of the slow phase to the total phase (Fig. III-7A, inset). We think that the attached hydrolysis (AMT–AMDP) is negligible under the condition we used in this study (see

Discussion). We conclude that the phosphate release (> 100 s^{-1}) is not the rate-limiting step of acto-M10IQ1 ATPase cycle. We assume k_{-4} and k'_{-4} as ~0 s^{-1}, because mM concentrations of phosphate had little effect on the ATPase activity of M10IQ1 (Fig. III-8).

Kinetics of ADP binding and dissociation

The rate of ADP binding to acto-M10IQ1 was measured by monitoring the change in the fluorescence intensity of mant-ADP upon binding. In the absence of actin, the rate of mant-ADP binding showed a hyperbolic dependence on the mant-ADP concentration to yield the maximum rate of 1.11 ± 0.07 s^{-1} (Fig. III-9A). This result suggested that ADP binding is a two-step process as for the ATP binding. The first step is the formation of a collision complex and the second one is the conformational transition (Appendix C). The observed maximum rate constant represents the sum of the forward and backward steps, i.e., $k_5 + k_{-5}$, of the second step. The y-intercept of the mant-ADP dependence gave 0.28 ± 0.06 s^{-1}, suggesting that the rate constant of mant-ADP release is 0.28 s^{-1}. The mant-ADP release rate was directly determined by measuring the decrease in mant-ADP fluorescence intensity upon addition of 3 mM ATP to M10IQ1/mant-ADP (Fig. III-9B). The rate constant of 0.27 s^{-1} was obtained that is consistent with the value obtained from Fig. III-9A. The affinity of ADP for M10IQ1 (K_5K_6) was calculated to be 1.2 μM.

In the presence of actin, the mant-ADP binding rate increased with the mant-ADP concentration to yield the second order rate constant of 2.6 ± 1.3 $\mu M^{-1}s^{-1}$. The

dissociation rate constant of 17 ± 3.6 s^{-1} was obtained by extrapolation of the binding rate to zero mant-ADP concentration (Fig. III-10A). The rate of ADP dissociation was also directly measured by mixing acto-M10IQ1/ADP complex with excess ATP (Fig. III-10B). The rate of the change in the light scattering of acto-M10IQ1 increased with ATP, but unlike the result shown in Fig. III-4, the rate was saturated at lower ATP concentration to yield the maximum rate of 23 ± 2.0 s^{-1}. This is explained by the ADP dissociation step (k'_{+5}) from acto-M10IQ1. Fig. III-10C shows the change in pyrene-actin fluorescence intensity upon mixing pyrene-actin/M10IQ1/ADP with ATP. The time course of the fluorescence change was fitted by two exponential kinetics yielding the fast and slow rate constants of ~500 s^{-1} and 23 ± 1.5 s^{-1}, respectively. The ADP dissociation rate constants obtained from the two different experiments were in good agreement, hence assigning 23 s^{-1} for k'_{+5}. The affinity of acto-M10IQ1 for ADP as calculated from these results ($K'_5K'_6$) was 8.8 ± 4.4 μM, a value consistent with the K_{ADP} value of 6.4 μM obtained in the steady-state actin-activated ATPase measurement (Homma et al., 2001). The ADP dissociation rate was two times larger than the V_{max} of the steady state ATP hydrolysis cycle rate, indicating that this step is not the sole determinant of the ATPase cycle rate, although it contributes to the rate limitation of the ATP hydrolysis cycle to a certain extent. The rate of ADP dissociation was significantly increased by actin by approximately 100-fold.

Kinetics of actin binding and dissociation

The rate of actin binding to M10IQ1 was measured using pyrene-actin. The

fluorescence intensity of pyrene actin rapidly decreased upon the addition of M10IQ1 as a result of the binding of M10IQ1 to pyrene-actin (Fig. III-11A, inset). The binding rate constant increased linearly with actin concentration to yield a second order rate constant of 4.1 ± 0.2 $\mu M^{-1}s^{-1}$. The dissociaton rate constant of 1.4 ± 0.2 s^{-1} was obtained from the y-intercept (Fig. III-11A).

The dissociation rate constant of actin from acto-M10IQ1 was also measured by mixing an excess amount of non-labeled actin with the pyrene-acto-M10IQ1 complex. The fluorescence intensity of pyrene-actin increased upon mixing, reflecting the dissociation of pyrene-actin from acto-M10IQ1 complex (Fig. III-11B). The observed rate constant of 1.3 ± 0.1 s^{-1} agrees well with the y-intercept of Figure III-11A. Based on these results, K_d (K_{12}) of acto-M10IQ1 in the absence of nucleotides is estimated to be 0.3 μM. This value is much higher than those of other known myosins, indicating that the rigor binding of acto-myosin 10 is much weaker than those of other myosins.

The rate of actin binding to M10IQ1 was also measured in the presence of ADP using the same procedure. The time course of the change in pyrene fluorescence intensity was best fitted with double exponential kinetics (Fig. III-12A, inset). Both the fast and the slow phases showed linear actin concentration dependence. The second order rate constants of the fast and slow phases were 1.3 ± 0.1 $\mu M^{-1}s^{-1}$ and 0.13 ± 0.02 $\mu M^{-1}s^{-1}$, respectively (Fig. III-12A). From the y-intercepts of the two phases, the rate constants for actin dissociation were estimated to be 1.7 ± 0.1 s^{-1} and 0.12 ± 0.02 s^{-1} for the fast and the slow phases, respectively. The dissociation of actin from acto-M10IQ1/ADP was measured by monitoring the fluorescence change of pyrene-actin upon

mixing pyrene-acto-M10IQ1/ADP with excess non-labeled actin (Fig. III-12B). The increase in the pyrene fluorescence intensity followed single exponential kinetics and yielded the rate constant for actin dissociation of 2.1 s^{-1}. This value is consistent with the value obtained from the fast phase in Figure III-12A. The identity of the slow phase observed in Figure III-12A is unclear. Based upon these rate constants, the affinity of actin to M10IQ1/ADP was calculated to be 1.6 μM that is significantly weaker than those of other unconventional myosins such as myosin 1C (55 nM) (El Mezgueldi et al., 2002), myosin 5a (7.6 nM) (De La Cruz et al., 1999) and myosin 6 (47 nM) (De La Cruz et al., 2001). Consistently, a significant amount of M10IQ1 was recovered in the supernatant when M10IQ1(1μM) was co-precipitated with actin (5 μM) in the presence of ADP (Fig. III-12B, inset). The fraction of M10IQ1 in the supernatant and pellet was determined by densitometry to be 22 % and 78 %, respectively. These values agree well with the calculated values, i.e., 27% and 73% in the supernatant and pellets, respectively, based upon the K_d=1.6 μM estimated from the dissociation and binding rate constants.

Duty ratio of myosin 10

All rate constants and equilibrium constants obtained in the present study are summarized in Table III-1. The overall ATPase rate of myosin 10 in the absence of actin is explained by the fast equilibrium of K_3 (0.85), k_{+4} (0.13 s^{-1}) and k_{+5} (0.28 s^{-1}). The ATPase rate can be estimated to be ~0.04 s^{-1}, which agrees with the experimentally determined basal ATPase rate of 0.065 ± 0.035 s^{-1}. Likewise, in the presence of actin, the overall ATPase rate and the K_{ATPase} of acto-M10IQ1 (13.5 s^{-1} and 17.4 μM, respectively)

can be explained by the ATP hydrolysis rate ($k_{+3} + k_{-3}$ = ~400 s^{-1} ,K_3 = 0.85), the actin reassociation rate (k'_{+4}/K_9 = 1.54 $\mu M^{-1}s^{-1}$), the phosphate release rate (k'_{+4} > 100 s^{-1}) and the ADP release rate (k'_{+5} = 23 s^{-1}). The major kinetic pathway of myosin 10 is shown in bold in scheme III-1. The broken line in Figure III-1B shows computer simulation of the steady-state ATPase of M10IQ1 under saturating ATP with ATP regeneration system using the rate constants and the equilibrium constants obtained in the present study (Appendix D). Contribution of k_{+4}, [M] and [MD] to the overall ATPase rate was ignored for simplicity of the simulation. The initial values, rates and equilibrium constants employed in the simulation were as follow. $[AM]_0$ = 1 μM, $[AMT]_0 = [MT]_0 = [MDP]_0 = [AMDP]_0 = [AMD]_0$ = 0 μM, $K'_1k'_{+2}[ATP]$= 800 s^{-1}, K_8 = 100 μM (rapid equilibrium), k_{+3} = 184 s^{-1}, k_{-3} = 216 s^{-1} (K_3 = 0.85), K_9 = 65 μM (rapid equilibrium), k'_{+4}/K_9 = 1.54 $\mu M^{-1}s^{-1}$, k'_{+4} = 100 s^{-1}, k'_{+5} = 23 s^{-1}. The simultaneous differential equation was solved by Runge-Kutta 4^{th} approximation with calculation time interval of 50 μsec. A typical example of the simulation at 10 μM actin is shown in Figure III-13. Halving and doubling the time interval did not affect the result (data not shown). V_{max} and K_{ATPase} calculated by this simulation were 13.3 s^{-1} and 17.7 μM, respectively, and these values were in good agreement with the experimentally obtained values. It should be noted that K_8 value in the range of 50 μM ~ 200 μM can explain the steady-state ATPase rate (13.5 ± 1.6 s^{-1}). The duty ratio of myosin 10 at maximal actin condition was estimated to be ~0.6.

Duty ratio of myosin 10 indirectly estimated from steady-state assays

The duty ratio can be indirectly estimated by comparing a K_{ATP} value obtained from an ATPase assay at saturating actin ($K_{m\ ATPase}$) with a K_{ATP} value obtained from an ATP-dependent *in vitro* actin gliding assay ($K_{m\ motility}$). This criterion has been employed to evaluate duty ratio of other motor proteins (deCastro et al., 1999; Tominaga et al., 2003). If we define the total time taken for completion of a single ATPase cycle at saturating ATP as T_{total}, myosin spends T_{total} waiting for next ATP binding at $K_{m\ ATPase}$ where myosin takes 2 x T_{total} for each cycle (thus $K'_1k'_{+2}$ x $K_{m\ ATPase} = 1/T_{total}$). Likewise, when we define attachment time of myosin to actin during ATPase cycle at saturating ATP as T_{on}, $K_{m\ motility}$ is the ATP concentration at which a myosin spends T_{on} waiting for next ATP binding (thus $K'_1k'_{+2}$ x $K_{m\ motility} = 1/T_{on}$). Since the duty ratio is defined as T_{on}/T_{total}, the duty ratio can also be defined as $K_{m\ ATPase}/K_{m\ motility}$. We performed an ATP dependent in vitro motility assay (Fig. III-14A) and steady-state ATPase assay at various actin concentrations on M10IQ1 (Fig. III-14B). The $K_{m\ motility}$ value obtained from this experiment was 6.1 ± 0.7 μM, which is consistent with the value previously obtained for the HMM-like myosin 10 construct (5.6 μM) (Homma et al., 2001). The $K_{m\ ATPase}$ is actin dependent, and the maximal $K_{m\ ATPase}$ value was estimated to be 4.3 ± 0.5 μM. Thus the duty ratio of M10IQ1 is calculated to be 0.70 ± 0.11, which is in good agreement with the duty ratio estimated from the computer simulation using rate constants obtained in the kinetics experiment (~0.6).

Discussion

Overview

In this chapter, we analyzed the enzyme kinetic mechanism of the acto-myosin 10 ATP hydrolysis cycle. Based on the obtained results, we concluded that myosin 10 is a high duty ratio motor (the duty ratio > 0.5). We found several unique features for the acto-myosin 10 ATPase reaction. First, the strong actin binding state (AMD) of myosin 10 is much weaker than other known myosins. The dissociation constant for the binding of myosin 10/ADP (AMD) to actin is 1.6 μM, which is significantly larger than those for myosin 1C (55 nM), myosin 5a (7.6 nM) and myosin 6 (47 nM) (De La Cruz et al., 2001; De La Cruz et al., 1999; El Mezgueldi et al., 2002). The result was also confirmed by actin cosedimentation in the presence of ADP, in which a significant fraction of myosin 10 was recovered in the supernatant (Fig. III-12B, inset). Second, phosphate release step is not the rate-limiting step of acto-myosin 10 ATPase cycle despite its fast ADP release rate (2-fold larger than the V_{max}). Third, the equilibrium of ATP hydrolysis step is significantly shifted to MT and approximately equal fractions of MT and MDP are present in the ATPase cycle. This small burst size contributes to the overall ATPase rate of myosin 10 by reducing the fraction of AMDP.

Kovacs et al. (Kovacs et al., 2005) also reported kinetic mechanism of subfragment-1 like myosin 10 ATPase (Their construct is also single-headed, but it contains the whole three IQ motifs). There are several major differences between our conclusions and theirs. First, the rate of the entire ATPase cycle obtained in this study is

nearly three times larger than that reported by Kovacs *et al*. (2005). The V_{max} of HMM-like myosin 10 reported in our previous study was also smaller than the V_{max} obtained in the present study. The difference can be explained by the accuracy of the determination of protein (or active site) concentration. In the present study, we directly determined the active site concentration by measuring the radioactive ADP incorporated into M10IQ1 in the presence of vanadate (Fig. III-15). This enabled us to determine the effective protein concentration much more accurately than the routine methods such as dye binding methods or the biuret method. It should be noted that in the case of myosin 10 the conventional active site titration method using ATP or mant-ATP would not provide accurate estimation due to the presence of significant reverse reaction of the ATP binding step (k_{-2}). Second, they found a slow Pi off phase from myosin 10 in the presence of actin and argued that this was due to the attached hydrolysis. Based on our results, we think that the slow Pi off phase is not derived from the "attached hydrolysis", but due to the slow rebinding of ATP.

Attached hydrolysis pathway (AMT–AMDP)

Kovacs et al. (Kovacs et al., 2005) suggested that the slow "attached hydrolysis" plays a significant role in the acto-myosin 10 ATPase cycle. This conclusion was due to the finding of a slow Pi off phase in the Pi release kinetics of acto-myosin 10. We also measured the dual phase kinetics for phosphate release in the presence of actin, and the result was very similar (Fig. III-7). However, since the slow rate was M10IQ1 concentration dependent, we concluded that the slow phase is derived from ATP

rebinding due to the reverse reaction (k_{-2} = ~1 s^{-1}). Actually, our model explained the overall ATPase cycle very well without the slow attached hydrolysis (Fig. III-1B, broken line). Furthermore, the presence of the slow attached hydrolysis pathway in the ATPase cycle of myosin 10 is inconsistent with the results of actin gliding assay. We obtained a $K_{m\ motility}$ value of 6.1 μM for M10IQ1 (Fig. III-14A). If T_{on} is defined as the actin attached time of M10IQ1 during the ATPase cycle at a saturating ATP condition, the half velocity of M10IQ1 can be explained by adding an additional T_{on} time for ATP binding at the ATP concentration of $K_{m\ motility}$. The ATP binding rate at 6.1 μM ATP is 21 s^{-1} (3.4 $\mu M^{-1}s^{-1}$ x 6.1 μM), which is close to k'_{+5} (23 s^{-1}) for acto-M10IQ1. Since all myosins involved in the translocation of actin filaments are under a saturating actin condition in an *in vitro* motility assay, if there is a slow ~1 s^{-1} weakly actin bound ATP hydrolysis step, the T_{on} will be predominantly determined by the slow step (~1 s^{-1}). In this case, the $K_{m\ motility}$ value has to be ~0.3 μM, which is inconsistent with the experimentally determined value of 6.1 μM. Therefore, we propose that attached hydrolysis pathway (AMT–AMDP) is negligible, if any, under the condition we employed in the present study. The k_{-2} of ~1 s^{-1} would also affect the estimation of K_3 determined by the single turnover quenched-flow experiment, since the experiment also employed very low concentration of ATP. The K_3 value of 0.85 was determined by assuming k_{-2} = ~0 s^{-1}. If we assume k'_{-2} = 1 s^{-1} under the condition we measured the burst size (1μM M10IQ1 and 0.5 μM ATP, Fig. III-6A), approximately 15% of ATP remains unbound to M10IQ1. Thus, the actual K_3 value, which should be estimated from the apparent burst size of 0.46 (Fig. III-6A), will

be 1.18 instead of 0.85. However, this change does not influence our overall kinetic model.

So, is myosin 10 processive?

It has been thought that the processive movement of a two-headed myosin requires a duty ratio of greater than 0.5. For example, myosin 5a, a well-known processive myosin, has a duty ratio of >0.7. The duty ratio of myosin 10 obtained from the present study was 0.6 ~ 0.7, and it could be even higher at physiological temperature (~37^{o}C). The fraction of AMD intermediate is significantly reduced due to the unfavorable equilibrium of the hydrolysis step (K_3 = 0.85) under the experimental condition in the present study (25^{o}C). However, as pointed out previously on myosin 5a (De La Cruz et al., 2000), the hydrolysis equilibrium (K_3) may greatly increase at physiologic temperature (~37^{o}C), which increases the fraction of AMD, thus the duty ratio. Therefore, it is very likely that myosin 10 is a processive motor when it is dimerized.

All two-headed processive myosins characterized so far have high duty ratios (>0.5), however, having a high duty ratio itself does not guarantee a processive movement. In Chapter IV, we directly tested the processivity of myosin 10 with a single molecule observation assay system.

Scheme III-1. Reaction sheme of myosin 10 ATPase. Abbreviations used are as follow: A, actin; M, myosin; T, ATP; D, ADP; P, phosphate.

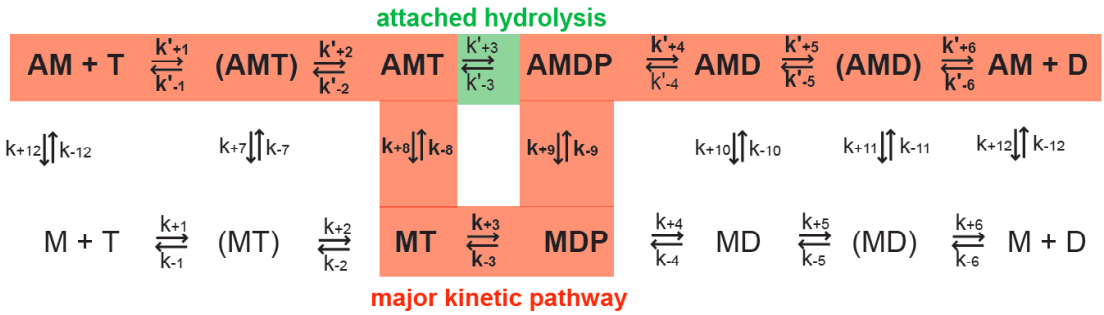

Table III-I

Kinetic parameters of M10IQ1 construct

Steady-state	
v_o (head^{-1}s^{-1})	0.065 ± 0.035
V_{max} (head^{-1}s^{-1})	13.5 ± 1.6
K_{ATPase} (μM)	17.4 ± 5.2
$K_{m\ ATPase}$ (μM)	4.3 ± 0.5
$K_{m\ motility}$ (μM)	6.1 ± 0.7
velocity $_{max}$ (μm s^{-1})	0.17 ± 0.03
duty ratio	0.70 ± 0.11 (calculated as $K_{m\ ATPase}$ / $K_{m\ motility}$)
ATP binding	
K_1k_{+2} (μM^{-1}s^{-1})	4.7 ± 0.2 (Mant-ATP)
K_1k_{+2} (μM^{-1}s^{-1})	4.4 ± 0.6 (tryptophan)
k_{-2} (s^{-1})	0.2 ± 1.3 (Mant-ATP)
$K'_1k'_{+2}$ (μM^{-1}s^{-1})	3.4 ± 0.3 (Mant-ATP)
$K'_1k'_{+2}$ (μM^{-1}s^{-1})	2.7 ± 0.4 (pyrene)
k'_{+2} (s^{-1})	782 ± 74 (pyrene)
k'_{-2} (s^{-1})	1.0 ± 1.0 (Mant-ATP)
ATP hydrolysis	
k_{+3} + k_{-3} (s^{-1})	395 ± 26 (tryptophan)
k_{+3} + k_{-3} (s^{-1})	> 100 (quenched-flow)
K_3	0.85 ± 0.05 (quenched-flow)
Phosphate release	
$k_{+4\ obs}$ (s^{-1})	0.06 ± 0.01 (quenched-flow)
$k_{+4\ obs}$ (s^{-1})	0.06 ± 0.02 (MDCC-PBP)
k_{+4} (s^{-1})	0.13 ± 0.02 (calculated as $k_{+4\ obs}(1+K_3)/K_3$)
k'_{+4} (s^{-1})	> 100 (MDCC-PBP)
ADP binding	
K_6 (μM)	3.6 ± 1.1 (Mant-ADP)
k_{+5} (s^{-1})	0.28 ± 0.06 (Mant-ADP)
k_{+5} (s^{-1})	0.27 ± 0.01 (Mant-ADP)
k_{-5} (s^{-1})	0.83 ± 0.09 (calculated as $k_{+5}+k_{-5}$=1.1s^{-1})
k_{-5}/K_6 (μM^{-1}s^{-1})	0.23 ± 0.07 (Mant-ADP)
K_5K_6 (μM)	1.2 ± 0.4 (calculated as $k_{+5}K_6/k_{-5}$)
k'_{+5} (s^{-1})	17 ± 3.6 (Mant-ADP)
k'_{+5} (s^{-1})	23 ± 2.0 (light scattering)
k'_{+5} (s^{-1})	23 ± 1.5 (pyrene)
k'_{-5} (s^{-1})	17 - 23 (pyrene)
k'_{-5}/K'_6 (μM^{-1}s^{-1})	2.6 ± 1.3 (Mant-ADP)
$K'_5K'_6$ (μM)	8.8 ± 4.4 (calculated as $k'_{+5}K'_6/k'_{-5}$)
actin binding	
k_{-12} (μM^{-1}s^{-1})	4.1 ± 0.2 (pyrene)
k_{+12} (s^{-1})	1.4 ± 0.2 (pyrene)
k_{+12} (s^{-1})	1.2 ± 0.1 (pyrene)
K_{12} (μM)	0.29 ± 0.03 (calculated as k_{+12}/k_{-12})
k_{-10} (μM^{-1}s^{-1})	1.3 ± 0.1 (pyrene)
k_{+10} (s^{-1})	1.7 ± 0.1 (pyrene)
k_{+10} (s^{-1})	2.1 ± 0.4 (pyrene)
K_{10} (μM)	1.6 ± 0.3 (calculated as k_{+10}/k_{-10})
$k'_{+4}/K_{9\ obs}$ (μM^{-1}s^{-1})	0.71 ± 0.02 (MDCC-PBP)
k'_{+4}/K_9 (μM^{-1}s^{-1})	1.54 ± 0.10 (calculated as $k'_{+4}/K_{9\ obs}$ $(1+K_3)/K_3$)
k_{+8} (s^{-1})	> ~800 s^{-1} (light scattering at 0.5μM actin)

K is defined as k_+ / k_-
Solution condition was 25mM KCl, 25mM Hepes-KOH pH7.5, 5mM $MgCl_2$, 1mM EGTA and 0.2mg/ml calmodulin at 25°C.
Error represents SE from 3~5 independent measurements.
(Error for motility velocity represents SD (n=90~150))

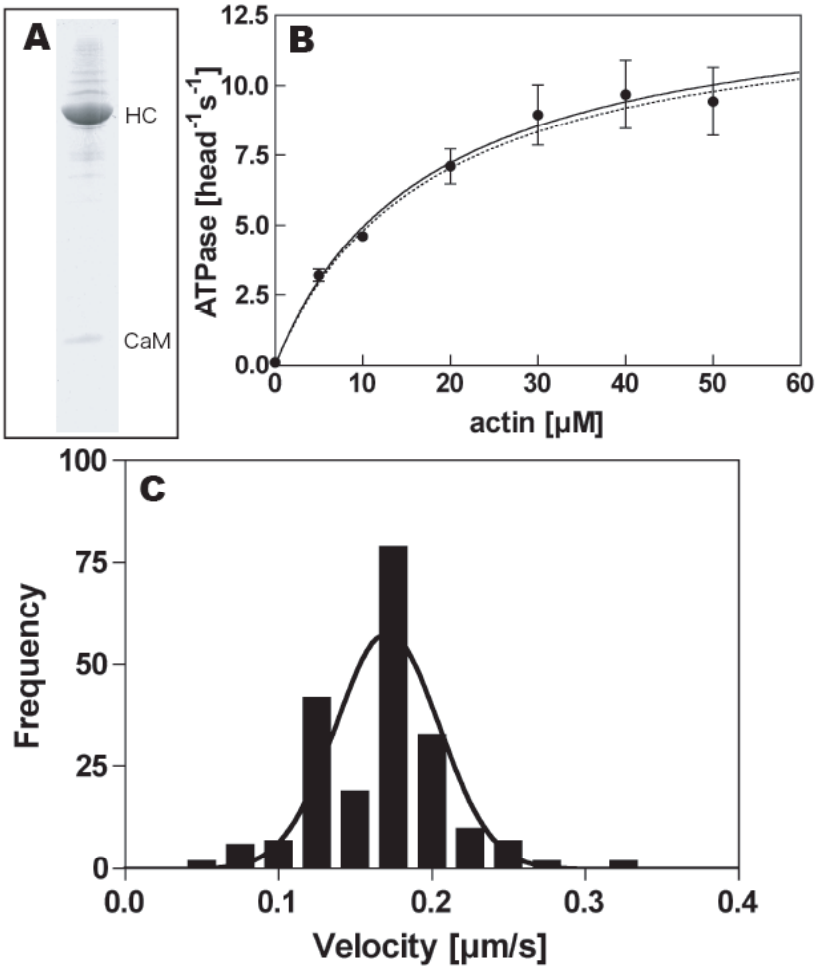

Figure III-1. Recombinant myosin 10 construct (M10IQ1). A. Purification of M10IQ1. The M10IQ1 expressed in Sf9 cells were extracted and purified as described in the text, and the purified protein was analyzed by SDS-PAGE. HC and CaM represent the heavy chain of myosin 10 construct and calmodulin, respectively. **B. Actin dependence of the Mg^{2+}ATPase activity of M10IQ1.** ATPase activity was measured as described in the text. The solid curve is the best fit to Michaelis-Menten kinetics with V_{max} and K_{ATPase} of 13.5 $head^{-1}s^{-1}$ and 17.4 μM, respectively. The broken line is simulated based on rate constants obtained in the present study (see Discussion), which gave V_{max} and K_{ATPase} of 13.3 s^{-1} and 17.7 μM, respectively. The error bars represent standard error from three independent experiments. **C. *in vitro* motility activity of M10IQ1.** *in vitro* motility assay was performed as described in the text with 0.1mM ATP. The velocity was 0.17 ± 0.03 μm s^{-1}.

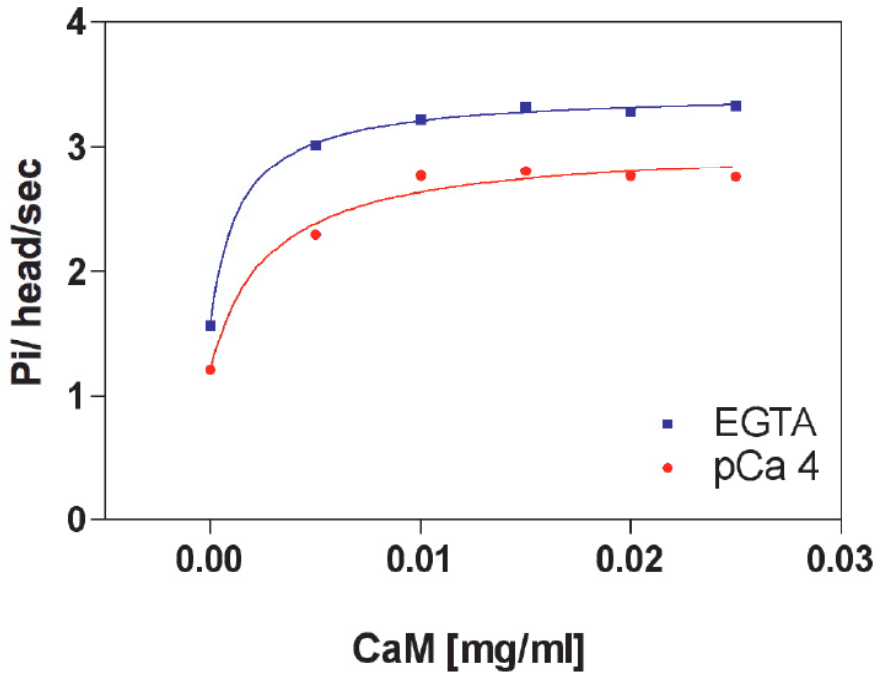

Figure III-2. Calmodulin-dependent ATPase activity of M10IQ1. The ATPase activity of M10IQ1 was measured using 50 nM M10IQ1, 50 units/ml pyruvate kinase, 1 mM phosphoenolpyruvate, 1 mM ATP, 5 µM actin, and various concentrations of calmodulin (CaM) in buffer B at 25°C. The apparent dissociation constants of calmodulin were 2.7 ± 1.2 µg/ml and 1.4 ± 0.2 µg/ml, in the presence (0.1 mM) and the absence of Ca^{2+}, respectively.

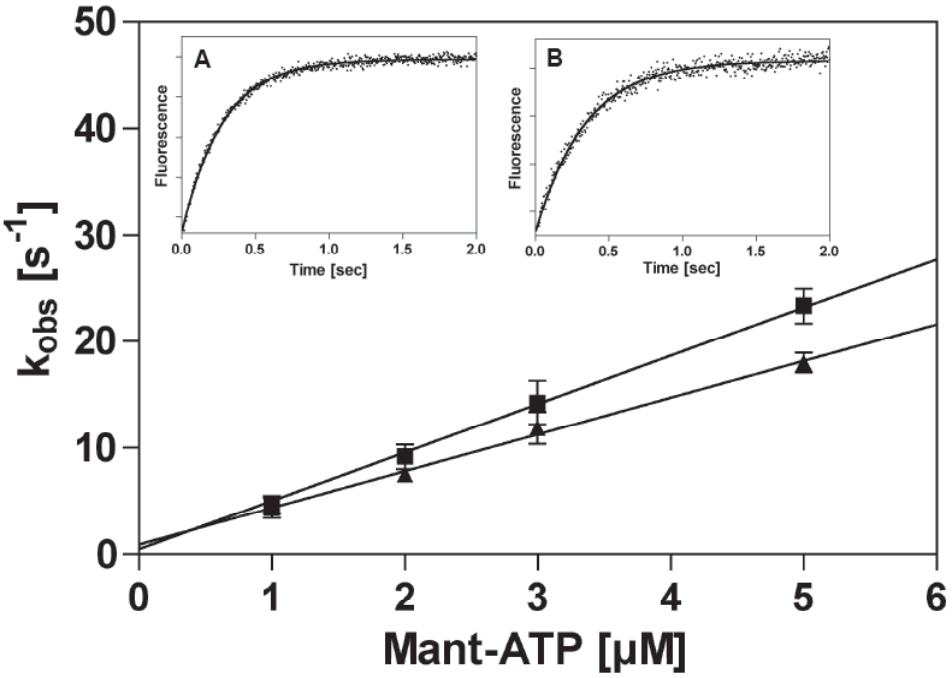

Figure III-3. Mant-ATP binding to M10IQ1 and acto-M10IQ1. The rate constants of Mant-ATP binding to M10IQ1 (square) and acto-M10IQ1 (triangle) as a function of Mant-ATP concentration are shown. The observed rate constants (k_{obs}) were obtained by fitting the time course of the change in fluorescence of Mant-ATP upon the binding to M10IQ1 at each concentration to a single exponential. The insets show typical recordings of Mant-ATP (1 μM) binding to M10IQ1 (0.25 μM) in the absence (A) and the presence of 1 μM actin (B). The concentrations indicate the final concentrations after mixing. Apparent second order binding rate constants of 4.7 $\mu M^{-1}s^{-1}$ and 3.4 $\mu M^{-1}s^{-1}$ were obtained for Mant-ATP binding to M10IQ1 and acto-M10IQ1, respectively. The solution condition was 25 mM KCl, 25mM Hepes-KOH (pH 7.5), 5mM $MgCl_2$, 1 mM EGTA and 0.2 mg/ml calmodulin at 25°C. The error bars represent the standard error from 3-6 independent experiments.

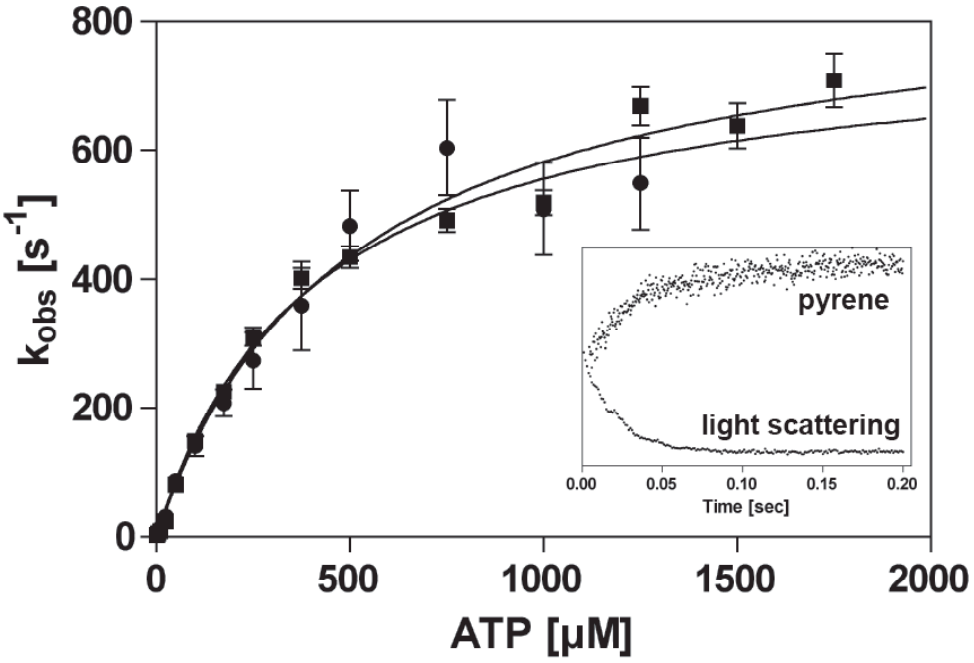

Figure III-4. ATP-induced dissociation of acto-M10IQ1 and the formation of weak actin binding form of M10IQ1. ATP-induced acto-M10IQ1 dissociation and weak actin binding formation were monitored by light scattering (square) and pyrene-actin fluorescence (circle). Inset shows the typical recordings of the time course of light scattering change (lower trace) and pyrene fluorescence change at 25 μM ATP (final). Apparent rates were obtained by single exponential fitting. At high ATP conditions, the initial signal changes were missed due to the dead time of the instrument. However, approximately 30-40% of the total signal could be monitored after the dead time even at the rate constant of $700s^{-1}$, and this was sufficient to determine the rate constant. Concentrations of M10IQ1 and actin (or pyrene-actin) after mixing were both 0.25 μM. Other conditions were the same as in Fig. III-3. The error bars represent the standard error from 3-6 independent experiments.

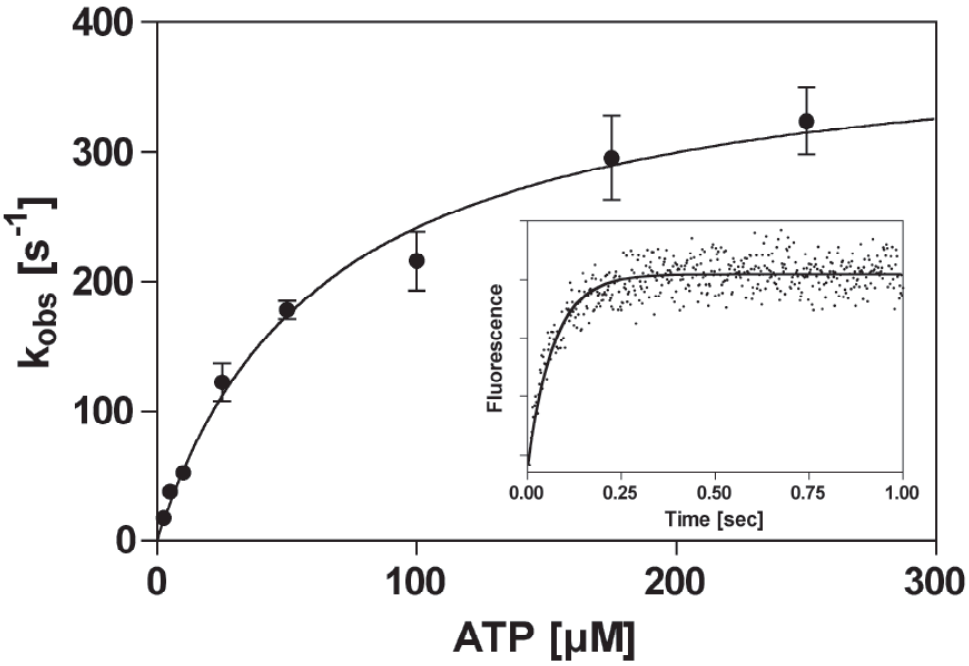

Figure III-5. ATP-induced enhancement of intrinsic tryptophan fluorescence intensity of M10IQ1. 0.5 μM (in final) M10IQ1 was mixed with various concentrations of ATP and the change in tryptophan fluorescence was monitored. Apparent rates were obtained by single exponential fitting and plotted against ATP concentration. The inset shows a typical recording of the experiment at 2.5 μM (final) ATP. The maximal rate of 395 ± 26 s^{-1} was obtained. Reaction conditions were the same as in Fig. III-3. The error bars represent the standard error from 3-5 independent experiments.

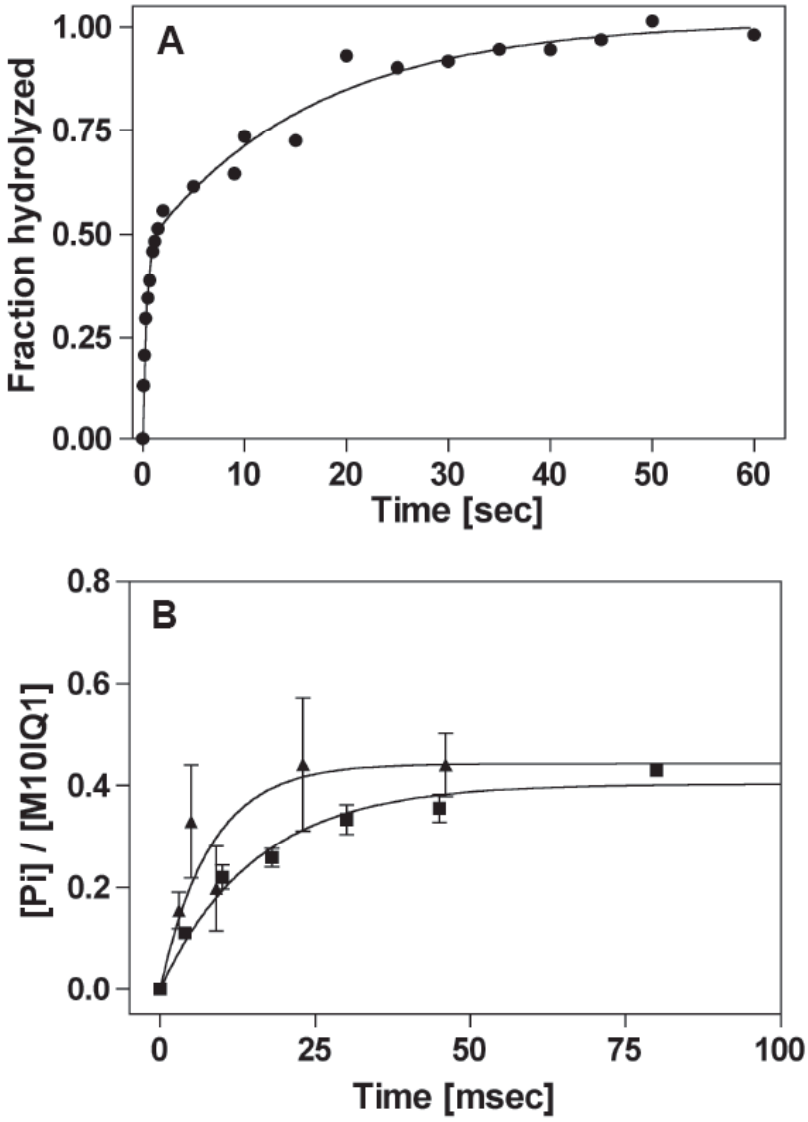

Figure III-6. ATP hydrolysis by M10IQ1. A. Single turnover experiment. 1 μM (after mixing) M10IQ1 was mixed with 0.5 μM (after mixing) [γ-^{32}P]ATP and the fraction of hydrolyzed ATP was plotted against time. The result was best fitted by double exponential kinetics. The apparent rates of the fast and slow phases were 2.7 s^{-1} and 0.06 s^{-1}, respectively. The fractional amplitude of 0.46 was obtained from the fitting. **B. Multi turn-over experiment.** 1 μM (after mixing) M10IQ1 was mixed with 10.7 μM (square) or 20.9 μM (triangle) (after mixing) [γ-^{32}P]ATP and the rate of ATP hydrolysis was measured by single exponential fitting. The apparent rate constants were 65 ± 10 s^{-1} and 124 ± 57 s^{-1}, respectively. The Pi-burst sizes estimated from the fitting were 0.40 ± 0.02 and 0.44 ± 0.07, respectively. Conditions in A and B were the same as in Fig. III-3. The error bars represent standard error from three independent experiments.

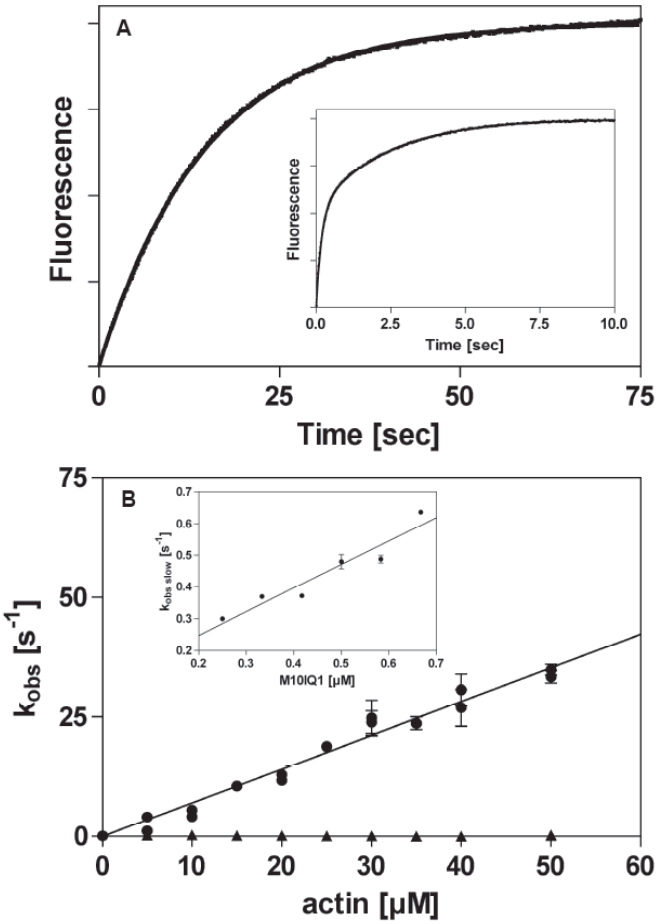

Figure III-7. Phosphate release from M10IQ1. Phosphate release from M10IQ1 was monitored through MDCC-PBP fluorescence enhancement upon binding to phosphate released from M10IQ1 by double mixing experiment. 1 μM M10IQ1 was first mixed with 0.7 μM ATP, and aged for 5 s. Then the solution was mixed with various concentration of actin (0 – 150 μM). Since the volume ratio of the syringes was 1:1:1, the final concentrations were 1/3 of the originals. **A. Typical recording of the MDCC-PBP fluorescence enhancement at 0 μM actin.** The change in fluorescence was best fitted by single exponential and the apparent rate was 0.06 s^{-1}. The inset shows MDCC-PBP fluorescence enhancement at 5 μM (in final) actin. The transient was best fitted by double exponential and the apparent rates were 5.6 s^{-1} and 0.4 s^{-1}. **B. Actin-dependence of the apparent rate constants of the fast and slow phases.** The actin concentrations indicated are the final concentration. The fast phase was actin-dependent with the apparent second order rate constant of 0.71 $\mu M^{-1}s^{-1}$, while the slow phase was actin-independent. The inset shows the apparent rate constants of the slow phase as a function of M10IQ1. The reaction condition was the same as in A except 5 μM actin (in final) and various concentrations of M10IQ1 were employed. The x-axis indicates the final concentration (after mix) of M10IQ1.
All solutions contained buffer B with 0.2 mg/ml calmodulin, 0.01 units/ml PNPase, 0.3 mM MEG and 3 μM MDCC-PBP. The error bars represent the standard error of the 3-5 independent experiments.

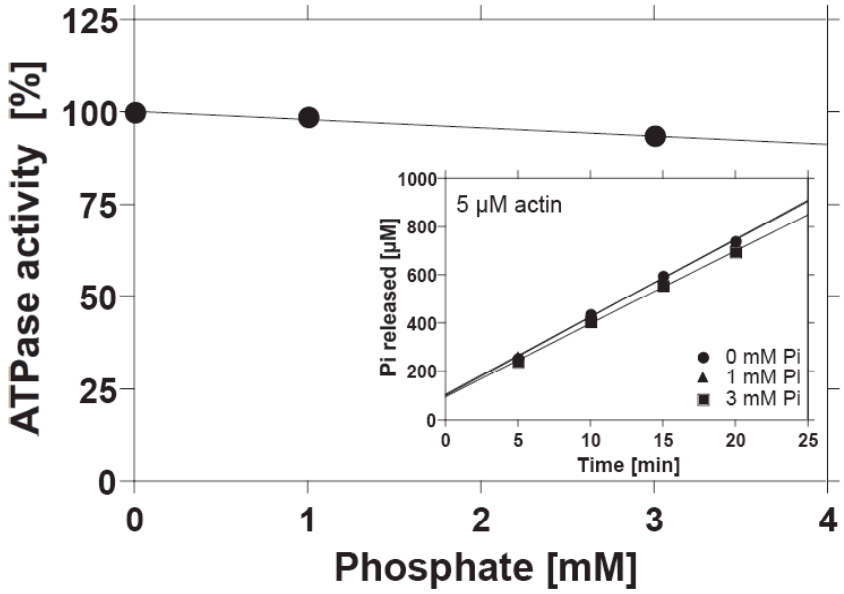

Figure III-8. Effect of phosphate on the ATPase activity of M10IQ1. The ATPase activity of M10IQ1 was measured under the condition of 0.75 μM M10IQ1, 50 units/ml pyruvate kinase, 2 mM phosphoenolpyruvate, 2 mM ATP, 5 μM actin, 0.2 mg/ml calmodulin in buffer B, and various concentrations of phosphate at 25^{o}C. Note that the actual concentration of phosphate increases as the reaction proceeds.

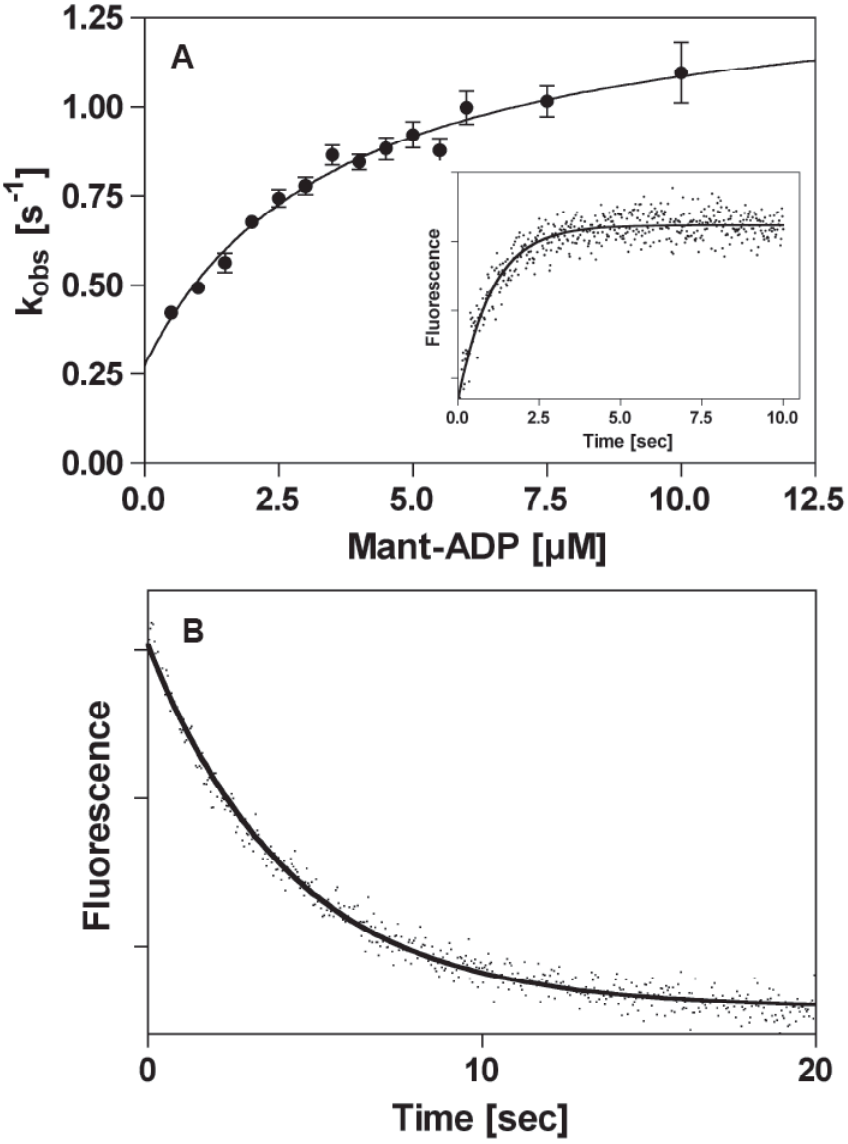

Figure III-9. The interaction of mant-ADP with M10IQ1. A. Binding of mant-ADP to M10IQ1. The rate constants of mant-ADP binding to M10IQ1 as a function of mant-ADP concentration are shown. The apparent rate constants (k_{obs}) were obtained by fitting the time course of the change in fluorescence of mant-ADP upon binding to M10IQ1 at each concentration to a single exponential. The inset shows a typical recording of the mant-ADP fluorescence change at 0.25 μM M10IQ1 and 5 μM mant-ADP (in final). The observed rate constant showed hyperbolic dependence on mant-ADP concentration to yield k_{max} of 1.11 ± 0.07 s^{-1} and K_m of 3.6 ± 1.1 μM. **B. Dissociation of mant-ADP from M10IQ1.** 3 mM ATP was added to the mixture of 1 μM M10IQ1 and 5 μM mant-ADP, and the time course of the decease in the fluorescence intensity due to mant-ADP dissociation was monitored. The time course showed a single exponential kinetics to yield a k_{obs} of 0.27 s^{-1}. Conditions were the same as in Fig. III-3. The error bars represent standard error from three independent experiments.

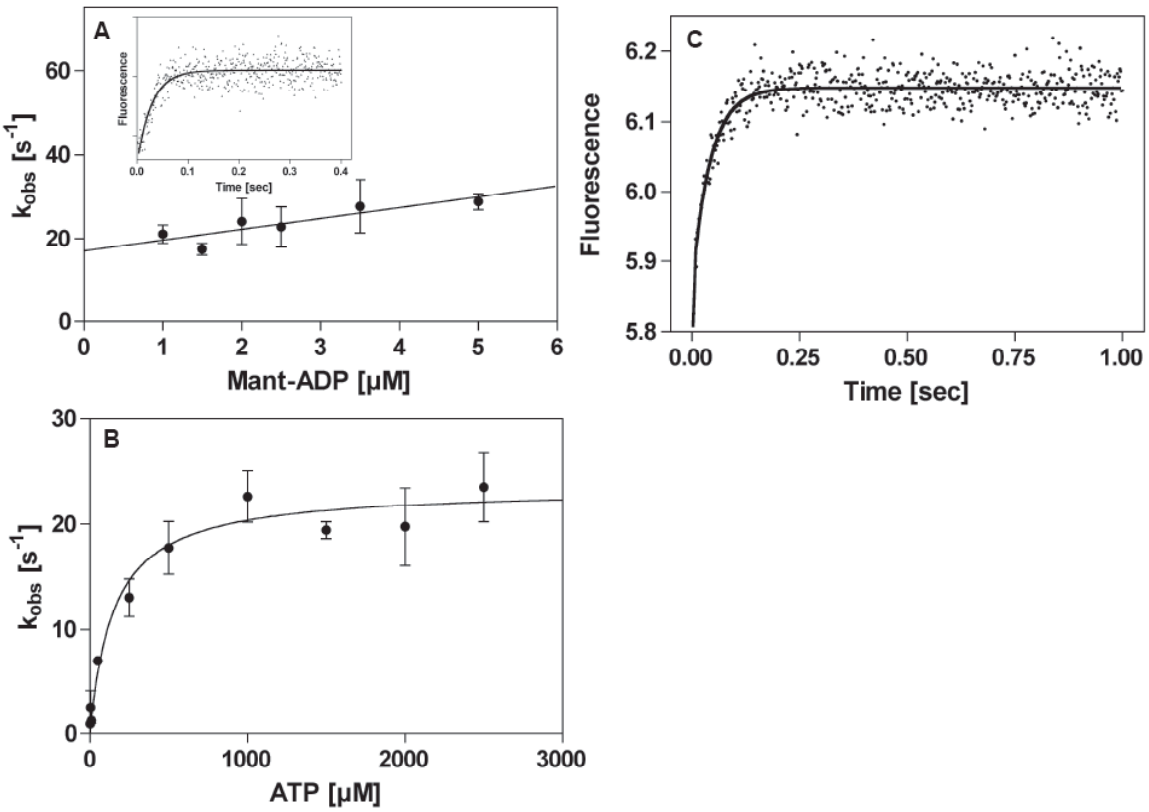

Figure III-10. The interaction of mant-ADP with acto-M10IQ1. A. Binding of mant-ADP to acto-M10IQ1. The mixture of 1 μM M10IQ1 and 2 μM actin was mixed with various concentrations of mant-ADP. The final concentrations are half of the originals. The change in the fluorescence intensity showed single exponential increase, and the apparent rates (k_{obs}) were plotted against mant-ADP concentration. The indicated mant-ADP concentrations are the final concentrations. The inset shows a typical recording of mant-ADP fluorescence change at 2μM mant-ADP (in final). **B. Dissociation of ADP from acto-M10IQ1/ADP complex.** The mixture of 0.5 μM M10IQ1, 1 μM actin and 0.1 mM ADP was mixed with various concentrations of ATP, and the dissociation rate of acto-M10IQ1 was monitored by measuring the light scattering intensity. The time course of light scattering intensity was analyzed by single exponential fitting as in Fig. III-4, and the apparent rates were plotted against ATP concentration. **C. ADP release from pyrene-acto-M10IQ1.** The mixture of 1 μM M10IQ1, 1 μM pyrene-actin and 0.2 mM ADP was mixed with 1 mM ATP (before mix), and the change in pyrene-actin fluorescence intensity was monitored. The transient showed a double exponential kinetics to yield 503 s^{-1} and 23.5 s^{-1} with approximately 1:1 amplitude ratio. Conditions were the same as in Fig. III-3. The error bars represent standard error from 3-4 independent experiments.

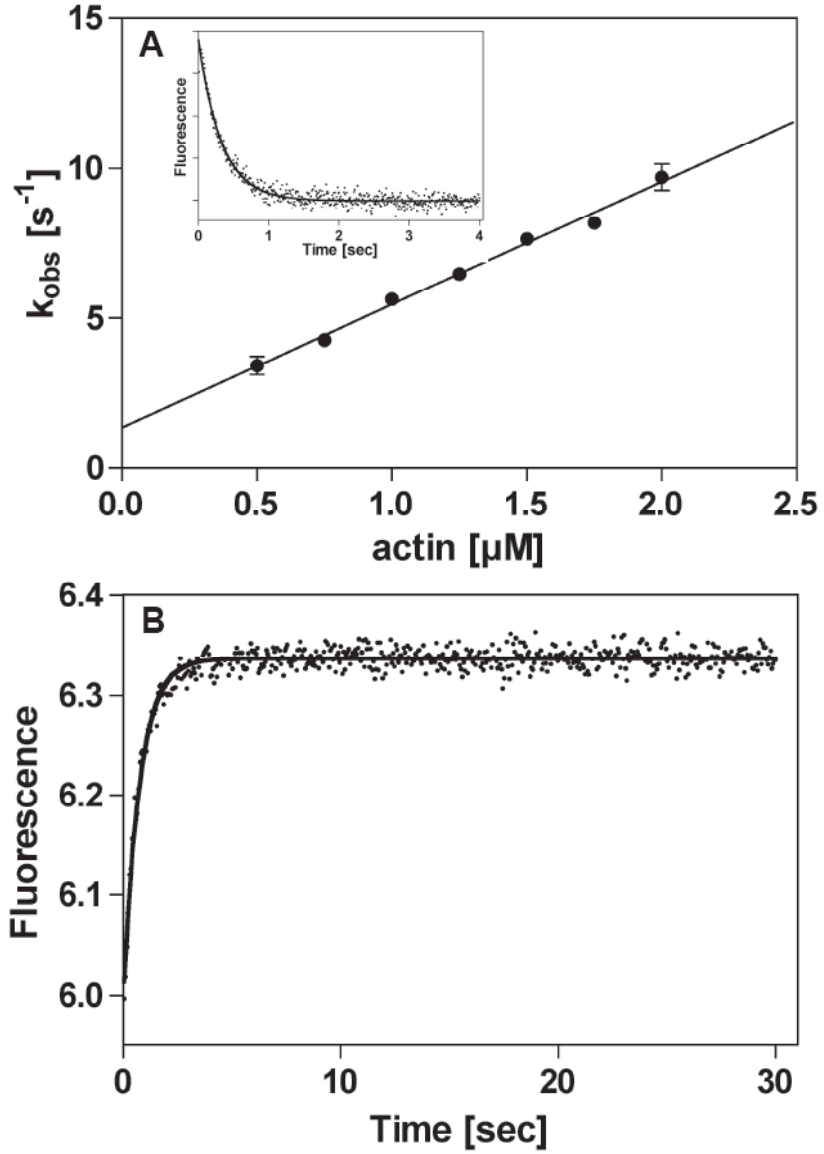

Figure III-11. Actin binding to M10IQ1 in the absence of ADP. A. Actin binding to M10IQ1. 0.25 μM M10IQ1 and various concentrations of pyrene-actin were mixed and the decrease in the fluorescence signal due to the binding of the two proteins was monitored. The inset shows a typical recording of the experiment performed at 0.5 μM actin. The transients followed single exponential kinetics and the apparent rate were plotted against pyrene-actin concentration. **B. Dissociation of actin from M10IQ1.** The mixture of 1 μM M10IQ1 and 1 μM pyrene-actin was mixed with an excess amount of non-labeled actin (40 μM before mix), and the increase in the fluorescence signal of pyrene-actin was monitored. The apparent rate of 1.3 s^{-1} was obtained from single exponential analysis. Conditions were the same as in Fig. III-3. The error bars represent standard error from three independent experiments.

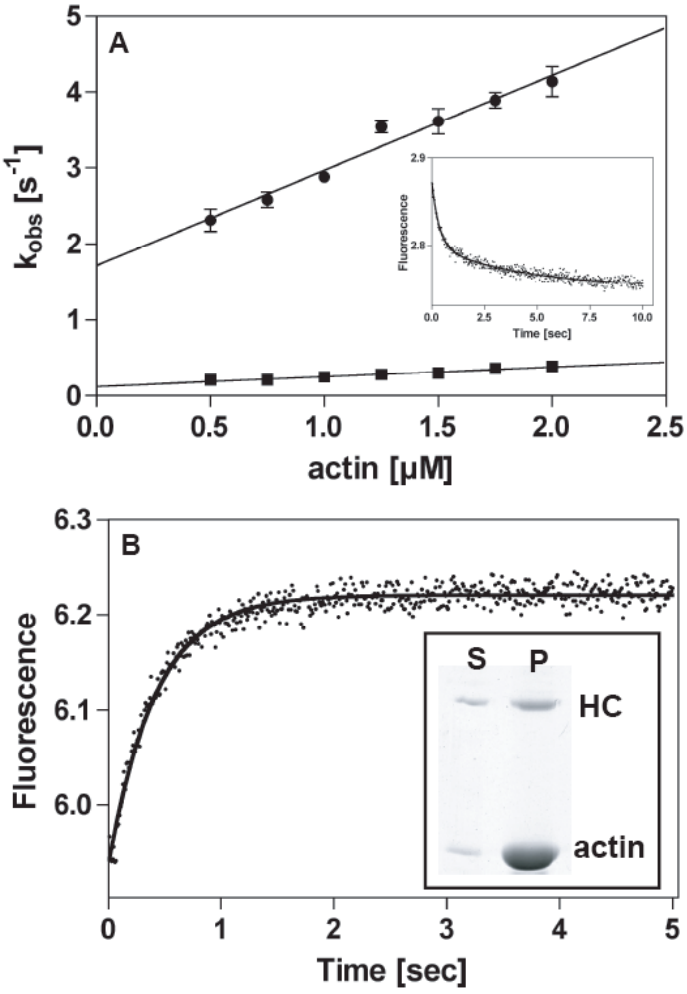

Figure III-12. Actin binding to M10IQ1 in the presence of ADP. A. Actin binding to M10IQ1. The mixture of 0.5 μM M10IQ1 and 0.2 mM ADP was mixed with various concentrations of pyrene-actin premixed with 0.2 mM ADP, and the change in pyrene-actin fluorescence intensity was monitored. The inset shows a typical example of the experiment done at 1 μM (after mix) pyrene-actin. The fluorescence transients followed double exponential kinetics and both the fast (circle) and the slow (square) apparent rates were plotted against pyrene-actin concentration. The error bars represent standard error from three independent experiments. **B. Dissociation of actin from M10IQ1.** The mixture of 1 μM M10IQ1, 1 μM pyrene-actin and 0.2 mM ADP (before mix) was mixed with excess amount of non-labeled actin (40 μM before mix) with 0.2 mM ADP, and the increase in the fluorescence signal of pyrene-actin was monitored. The apparent rate of 2.1 s^{-1} was obtained from single exponential fitting. **Inset. Co-precipitation of M10IQ1 with actin in the presence of ADP.** Mixture of 1 μM M10IQ1, 5 μM actin and 0.1 mM ADP was subjected to ultracentrifugation. The supernatant and pellets were subjected to SDS-PAGE followed by densitometry to quantitate the amount of proteins. 22% of M10IQ1 was found in the supernatant.
Experimental conditions were the same as in Fig. III-3.

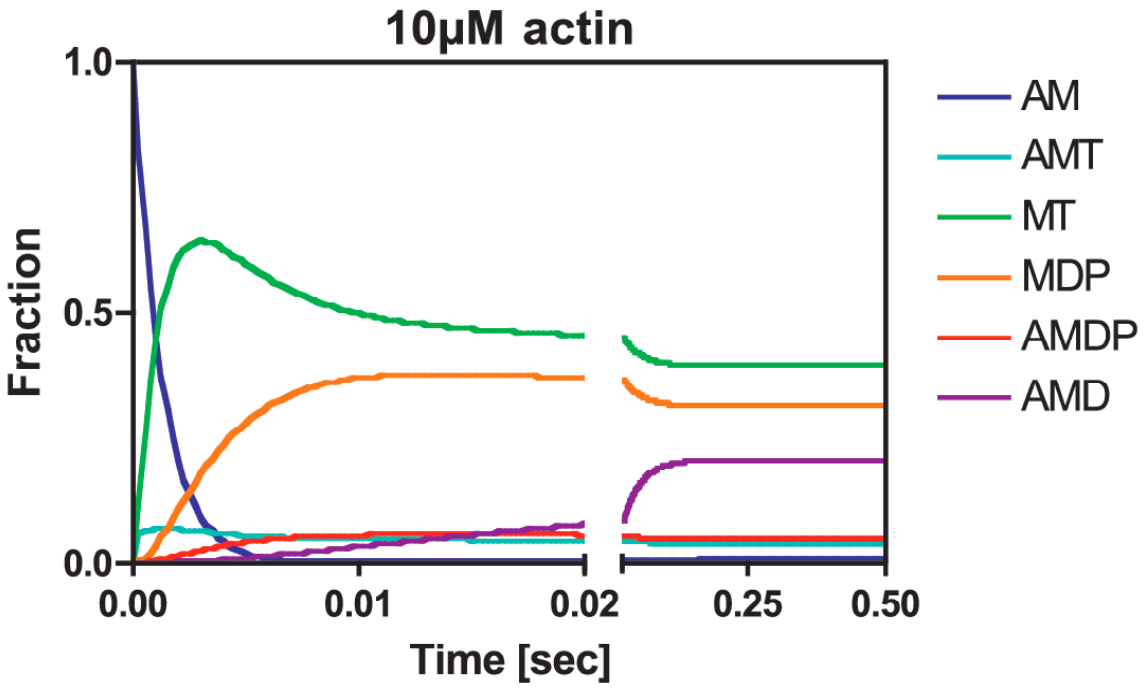

Figure III-13. Computer simulation of the ATPase reaction of M10IQ1 at 10 µM actin. The initial values, rates and equilibrium constants employed in the simulation were as follow. $[AM]_0$ = 1µM, $[AMT]_0 = [MT]_0 = [MDP]_0 = [AMDP]_0 = [AMD]_0$ = 0µM, $K'_1k'_{+2}[ATP]$= 800 s^{-1}, K_8 = 100 µM (rapid equilibrium), k_{+3} = 184 s^{-1}, k_{-3} = 216 s^{-1} (K_3 = 0.85), K_9 = 65 µM (rapid equilibrium), k'_{+4}/K_9 = 1.54 $\mu M^{-1}s^{-1}$, k'_{+4} = 100 s^{-1}, k'_{+5} = 23 s^{-1}. The simultaneous differential equation was solved by Runge-Kutta 4th approximation with calculation time interval of 50 µsec. Contribution of k_{+4}, [M] and [MD] to the overall ATPase rate was ignored for simplicity of the simulation. See also Appendix D.

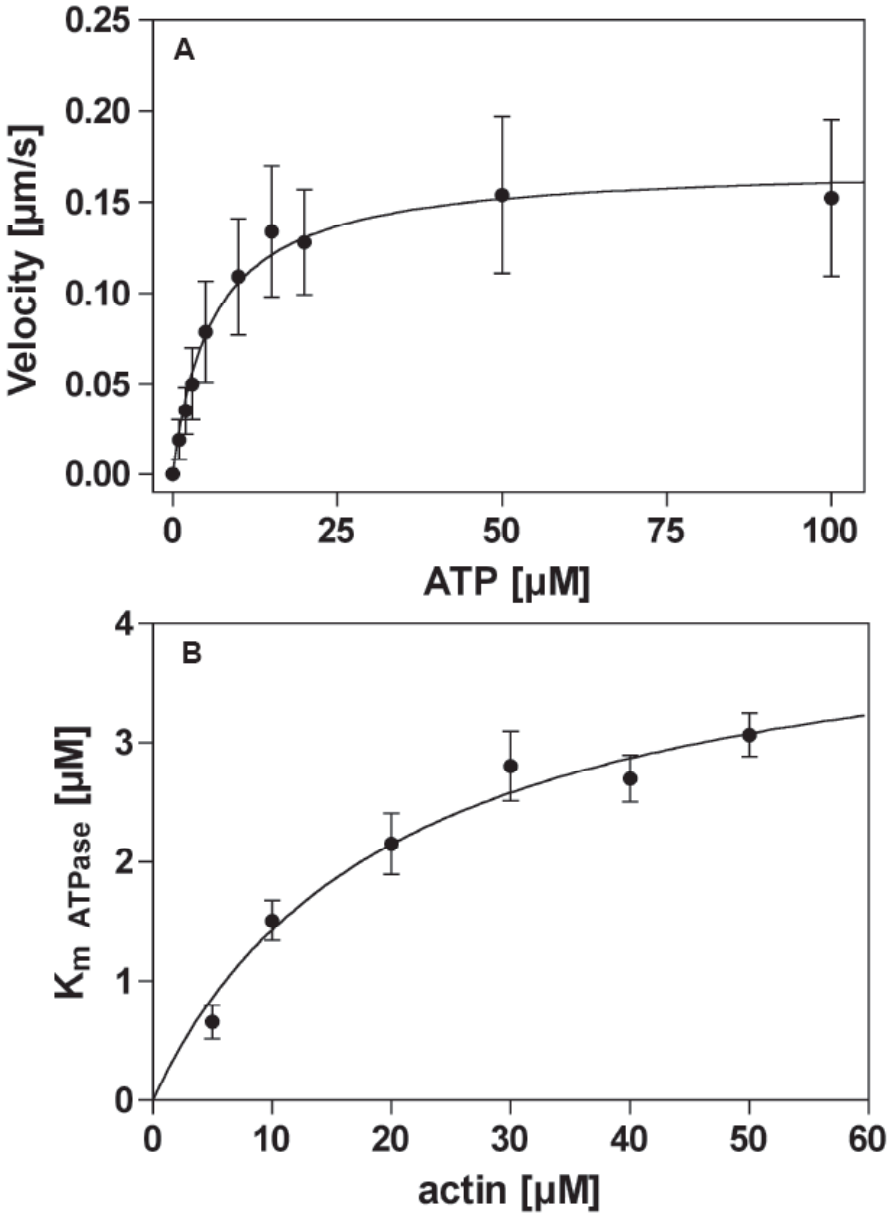

Figure III-14. $K_{m\ motility}$ and $K_{m\ ATPase}$ of M10IQ1. A. ATP-dependence of the actin gliding activity of M10IQ1. Actin translocating velocity of M10IQ1 under various concentrations of ATP was measured and the velocities were plotted against ATP concentrations. $K_{m\ motility}$ value of 6.1 ± 0.7 μM was obtained from hyperbolic analysis. The error bars represent SD (n = 90~150). **B. actin-dependence of $K_{m\ ATPase}$ of M10IQ1.** ATP-dependence of the actin-activated ATPase activity was measured at various actin concentrations and the $K_{m\ ATPase}$ were plotted against actin concentration. The error bars represent standard error from three independent experiments.

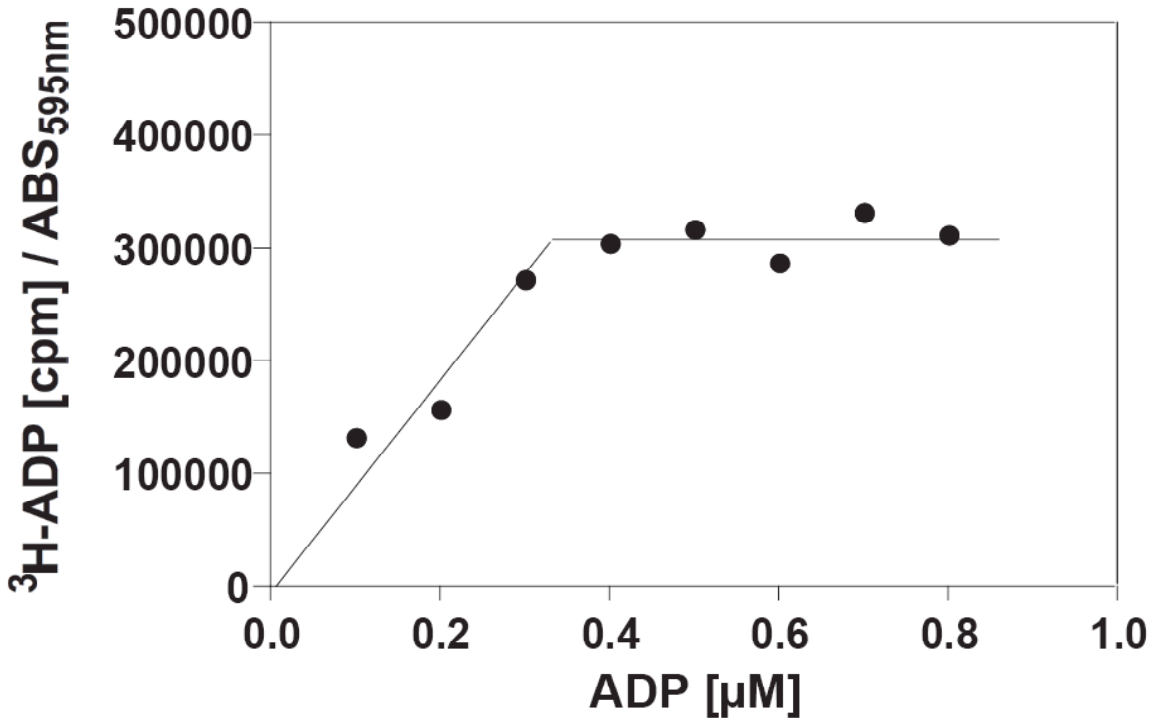

Figure III-15. Active site titration by ADP-Vi. 0.5μM M10IQ1 (determined by Bradford method by taking BSA as a control) was mixed with 1 mM VO_4 and various concentrations of [2,8-^{3}H]ADP (indicated in the x-axis) in buffer B. After 3 hr of incubation at 4^{o}C, the mixture was subjected to G-50 spin-column equilibrated with buffer B. The radioactivity of the elution was determined and normalized by dividing by the apparent protein concentration determined by Bradford method. The normalized value saturated at 0.3μM [2,8-^{3}H]ADP, indicating that the actual concentration of active M10IQ1 was 0.3μM instead of 0.5μM.

CHAPTER IV

PROCESSIVITY OF MYOSIN 10

Introduction

It has been thought that a processive motor, having a high duty ratio, is suitable for cargo transport. In the myosin superfamily, myosin 5a has a high duty ratio (De La Cruz et al., 1999), and it has been shown to be a cargo transporting motor, which moves melanosomes in melanocyte, endoplasmic reticulum in the giant axons of the squid nervous system (Tabb et al., 1998), and synaptic vesicles in brain (Brown et al., 2004; Evans et al., 1998; Prekeris and Terrian, 1997). Biochemical and biophysical studies demonstrated that myosin 5a is a processive motor that travels on an actin filament for a long distance without dissociating from the actin track (Mehta et al., 1999; Sakamoto et al., 2000; Tanaka et al., 2002; Veigel et al., 2002). Myosin 5a exists as a stable homodimer, and its processive movement has been explained by hand-over-hand mechanism using the two heads at a high duty ratio (Warshaw et al., 2005; Yildiz et al., 2003).

Similarly to myosin 5a, recent cell biological studies suggest that myosin 10 transport cargos such as VASP (Tokuo and Ikebe, 2004) and β-integrin (Zhang et al., 2004) inside filopodia. In Chapter III, we found that the duty ratio of myosin 10 is higher

than 50%, suggesting that myosin 10 is a processive motor. These findings strongly suggest that myosin 10 functions as a cargo transporter in a cell.

Unlike myosin 5a, however, the predicted coiled-coil region of myosin 10 does not form a stable coiled-coil, and a recombinant HMM-like myosin 10 (truncated after the predicted coiled-coil region) has been reported to be predominantly monomeric by itself (Knight et al., 2005). Interestingly, the first one-third of the predicted coiled-coil region of myosin 10 is very similar to a part of the predicted coiled-coil region of myosin 6 in terms of the poor hydrophobic seam and high proportion of the charged residues, which prevents the region from forming stable coiled-coil. This highly charged region forms a stable α helix (SAH) instead of coiled-coil (Knight et al., 2005). Myosin 6 has been reported to be a high duty ratio motor with ADP off as the predominant rate-limiting step. Like myosin 10, it is predominantly monomeric by itself (Lister et al., 2004). The monomeric form of myosin 6 is nonprocessive (Lister et al., 2004), however, it becomes processive when dimerized (Nishikawa et al., 2002; Rock et al., 2001). Most of the predicted coiled-coil region of Myosin 7, another high duty ratio motor, is also very similar to the SAH regions of myosin 6 and myosin 10. Like myosin 6, myosin 7 becomes processive when it is dimerized (Yang et al., 2006). Thus, it is very likely that myosin 10 becomes processive when dimerized, thus functions as a transporter. Myosin 10 constructs lacking the coiled-coil region did not localize at the tips of filopodia, and overexpression of the coiled-coil region alone has a dominant negative effect on the intrafilopodial motility of endogenous myosin 10 (Bohil et al., 2006), suggesting that the dimerization of myosin 10 is essential for the function.

To directly test the processivity of myosin 10, we observed single molecule movements of force-dimerized myosin 10 constructs along actin filaments by a total internal reflection microscope (TIRFM).

Materials and methods

Materials - Bovine serum albumin (BSA) was purchased from Sigma (St. Louis, Mo). Alexa Fluor 647 phalloidin and streptavidin were purchased from Invitrogen (Carlsbad,CA). Biotin-maleimide (EZ-link PEO-Maleimide Activated Biotin) was purchased from Pierce (Rockford, IL). For other materials, see "Materials and methods" in Chapter II.

Force-dimerized myosin 10 constructs - An N-terminal tagging vector that introduces a FLAG epitope tag and an eGFP was prepared by modifying the pFastBac vestor. Partial ORFs of bovine myosin 10 (Met1–Ser916, Met1-Lys883, and Met1–Ala939) with 5'-*Sal*I site and 3'-*Hind*III site were ligated into the modified pFastBac vector treated with *Sal*I and *Xba*I together with a partial ORF of mouse myosin 5a (the stable coiled-coil helix region: Leu908 – Glu1090 plus stop codon) with 5'-*Hind*III site and 3'-*Xba*I site. The *Hind*III site inserts two additional amino acids (lysine and leucine) at the junctions of myosin 10 and myosin 5a of these constructs (GFPM10M5cc1, GFPM10M5cc2, and GFPM10M5cc3). Three additional chimeric constructs (GFPM10M5IQcc1, GFPM10M5IQcc2, and GFPM10M5IQcc3) were also produced by the two-step PCR

method (Zarrinpar et al., 2003), and ligated into the modified pFast vector with *Sal*I site and *Xba*I site at 5'-side and 3'-side, respectively.

Baculovirus preparation - See "Materials and methods" in Chapter II.

Protein expression and purification - See "Materials and methods" in Chapter II.

Preparation of biotin-labeled BSA - BSA was dissolved in a buffer containing 100 mM NaCl, and 50 mM Tris-HCl, pH 8.3, and mixed with 10 molar excess of biotin-maleimide for an hour at 23^{o}C. The reaction was terminated by 25 mM DTT, and dialyzed extensively against a dialysis buffer containing 50 mM NaCl, 10 mM Tris-HCl, pH 7.5, and 1 mM DTT at 4^{o}C to eliminate free biotin.

Preparation of biotin-labeled G-actin - G-actin was freshly prepared according to the method by Spudich and Watt (Spudich and Watt, 1971), and the extracted G-actin (180 μM) was mixed with 1.5 molar excess (270 μM) of biotin-maleimide for overnight at 4^{o}C in a buffer containing 2 mM HEPES-KOH, pH 7.8, 0.2 mM ATP, 0.1 mM $CaCl_2$. The reaction was terminated by adding 3 mM DTT. The biotin-G-actin was diluted to 5 μM, and flash-frozen to store at -80 ^{o}C.

Alexa 647 phallodin-labeled F-actin - The biotin-G-actin was premixed with unlabeled-G-actin at various ratios while maintaining the total actin concentration at ~ 1 μM, and

then put into a buffer containing 25 mM KCl, 25 mM HEPES-KOH, pH 7.5, 5 mM $MgCl_2$, 1 mM EGTA, 1 mM DTT, and 40 units/ml Alexa Fluor 647 phalloidin. The solution was kept in the dark for overnight at 4^oC.

In vitro motility assay - See "Materials and methods" in Chapter II.

Total internal reflection microscope (TIRFM) - A prism type total internal reflection microscope was built on an inverted microscope platform (IX71, Olympus). A 473 nm diode laser (DPBL-9040, Photop) and a 635 nm diode laser (Radius 635-25, Coherent) were used to excite GFP and Alexa Fluor 647, respectively. The fluorescence signals from GFP and Alexa Fluo 647 were collected by a high NA objective lens (PlanApo 60X OIL; NA = 1.45, Olympus), and were passed through the W-VIEW apparatus (A-8509, Hamamatsu Photonics) that contained two dichroic mirrors (560DCLP and 600DCSP, Chroma) and two band pass filters (HQ520/40m for GFP and HQ700/75m for Alexa 647 Fluor, Chroma). The fluorescence signals were imaged by a CCD video camera (MC681SPD, Texas Instruments) with an image intensifier (C8600, Hamamatsu Photonics) (Appendix E).

Single molecule experiment - 1 mg/ml biotinylated BSA was applied to a ~20 µl flow chamber made of two coverslips coated with nitrocellulose. After 2 min of incubation at room temperature, unbound biotin-BSA was washed away with buffer M (25 mM KCl, 25 mM HEPES-KOH, pH7.5, 5 mM $MgCl_2$, and 1 mM EGTA). Streptavidin (0.1

mg/ml) was applied to the flow chamber and incubated for 3 min at room temperature. Unbound streptavidin was washed out with buffer M. Biotinylated F-actin labeled with Alexa Fluor 647 phalloidin was applied to the chamber, and incubated for 2 min at room temperature. Finally, a GFP-labeled myosin construct in buffer M containing 0.2 mg/ml calmodulin, 2 mM ATP, 4.5 mg/ml glucose, 36 μg/ml catalase, 216 μg/ml glucose oxidase, 143 mM 2-mercaptoethanol was applied to the flow chamber. GFP and Alexa 647 Fluor fluorescence signals were simultaneously visualized by the TIRF microscope setting described above, and the movement of the GFP signal was monitored at 30 frames / sec.

Results

Generation of force-dimerized myosin 10 constructs using the stable coiled-coil of myosin 5a

The predicted coiled-coil region of myosin 10 consists of ~140 amino acids (Fig. IV-1). The first one-third of the region contains a large number of charged amino acids, and recently this highly charged region has been reported to form a stable alpha helix (SAH), rather than a coiled-coil (Knight et al., 2005). As a result of the SAH formation, the actual length of the neck region of myosin 10 becomes longer than initially predicted (equivalent to 5~6 IQ motifs). The coiled-coil registration in the remaining two-thirds of the predicted coiled-coil region is not clear, and this may explain why myosin 10 is monomeric by itself. At least three possible coiled-coil registrations were found in the

region (Fig. IV-1). Since it was not clear which registration is the authentic one, we generated three different force-dimerized constructs based on these three possible coiled-coil registrations using the stable coiled-coil region of myosin 5a (Fig. IV-2). The N-terminus of each construct was tagged with GFP for single molecule experiments described below. The N-terminal GFP does not interfere with the motor function of myosin molecules (Table II-1). All these constructs were successfully expressed and purified (Fig. IV-3).

We first tested if the force-dimerized GFPM10M5cc constructs retain actin translocating activity by the *in vitro* motility assay (Fig. IV-4). All chimeric constructs showed actin translocating activity, however, the quality and the velocity were different from each other. The actin translocation velocity of GFPM10M5cc1 was ~30% of that of the full-length myosin 10 (0.12 ± 0.04 μm/sec). Many actin filaments dissociated from the myosin-coated glass surface and diffused away, suggesting that the construct is not processive, because processive myosin 5a under a comparable density on the glass surface never shows such actin dissociation. The actin translocation velocity of GFPM10M5cc2 was about two times faster than that of myosin 10 full-length, and the movement of actin filaments was relatively smooth compared to the other chimeric constructs. Dissociation of actin filaments from the glass surface was also observed for this construct. The actin translocation velocity of GFPM10M5cc3 was comparable to that of myosin 10 full-length, however, the movement of actin filaments was rather wiggly as if the construct had problem coordinating the two heads. Apparently, GFPM10M5cc2 seemed to be superior to the other two constructs. However, since all of

the constructs at least retained actin translocating activity and the authenticity of the registration of the coiled-coil cannot be determined simply from this observation, we tested the processivity of all of these GFPM10M5cc constructs in a single molecule experiment.

Single molecule assay

The best way to determine processivity of myosins is to directly observe the successive movement of individual molecules on actin filaments (Sakamoto et al., 2000)(Fig. IV-5). The total internal reflection microscope (TIRFM) was employed to visualize single GFP fluorescence attached to the myosin constructs (Appendix E). By using TIRFM, less than 200 nm from the glass surface is illuminated by the evanescent field, and thus the background noise is highly reduced. As a positive control, GFP-labeled myosin 5a was first tested to evaluate the TIRFM system. As shown in Figure IV-5B, successive movements of GFP-labeled myosin 5a molecules on actin filaments were observed. They were indeed single molecules, because the photobleaching events were either one- or two-step process as observed in our previous study on GFP-labeled dimeric myosin 6 (Nishikawa et al., 2002).

We performed the single molecule assay on the GFP-myosin 10 full-length construct and the GFPM10M5cc constructs under the same condition for GFP-myosin 5a. Unlike GFP-myosin 5a, the GFP-myosin 10 full-length construct did not show processive movement. Interestingly, the clustering of the GFP signals, which is usually observed for GFP-myosin 10 moving inside filopodia, was not observed. The result suggests that

myosin 10 does not cluster by itself. Thus, the apparently nonprocessive nature of the full-length GFP-myosin 10 can be simply explained by the single-headed structure. Contrary to our expectation, none of the GFPM10M5cc constructs showed processive movement on actin filaments. GFP signals frequently appeared on actin filaments, however, those signals did not move successively along the actin filaments, suggesting that the GFPM10M5cc constructs are not processive. However, because the lack of processive movement might be due to the single-headed structure of the constructs, overall structures of the constructs were confirmed by rotary shadowing electron microscopy (Fig. IV-6). As previously reported, the head-neck of myosin 5a is extended, and the Y-shape structure can physically allow the myosin 5a molecule to have 36 nm step size, which is the half pitch of actin filament (Fig. IV-6). All the GFPM10M5cc constructs showed double-headed structure as expected, however, the head-neck region of the constructs did not seem to be extended. Rather, it seemed to be bent over the C-terminal region of the molecules (Fig. IV-6). This kinked head-neck structure of the GFPM10M5cc constructs may explain why they did not show processive movement in the single molecule assay. The result also implies that an additional regulation is required to extend the neck region of myosin 10. In fact, GFP-labeled myosin 10 moves back and forth inside filopodia without changing the overall GFP fluorescence intensity of the moving spots, suggesting that there is an additional regulatory mechanism other than the monomer-dimer transition. Thus, the kinked structure may represent the inactive state of myosin 10 during the retrograde movement of the molecule in the filopodia. In order to bypass this possible regulatory mechanism of myosin 10 to simply evaluate the

processivity of dimerized myosin 10 constructs, additional chimeric constructs were generated (Fig. IV-7 and Fig. IV-8). The converter region and the following neck region are well conserved among myosin 10 and myosin 5a (Fig. IV-7). With three different joining points, the motor domain of myosin 10 was followed by the neck and the coiled-coil of myosin 5a (Fig. IV-8). The resulting GFPM10M5IQcc constructs were successfully purified with reasonable amount of calmodulin (Fig. IV-9), and all showed the typical Y-shape as found in myosin 5a with extended head-neck (Fig. IV-10). Actin translocating activity of these constructs was also examined by *in vitro* motility assay. The actin translocation velocities of those constructs were comparable to that of myosin 10 full-length construct (Fig. IV-11), however, contrary to our expectation, all of the GFPM10M5IQcc constructs showed much worse quality of actin translocating activity than the previous GFPM10M5cc constructs. The movements of the actin filaments were not smooth, and a significant number of actin filaments dissociated from the myosin-coated glass surface. As predicted from this result, neither of the GFPM10M5IQcc constructs showed successive movements on actin filaments in the single molecule assay, suggesting either that myosin 10 is not a processive motor, or that the neck/coiled-coil of myosin 5a is not compatible with the processive movement of myosin 10.

Discussion

It is important to determine the processivity of myosin 10 in order to fully understand the physiological process where the molecule is involved. In this chapter, we

directly tested the processivity of force-dimerized myosin 10 chimeras in single molecule experiments, and unexpectedly, processive movement was not observed. The simplest explanation of the result is that an individual myosin 10 molecule, even if it is dimerized, is not processive. However, this conclusion cannot explain the reason why myosin 10 needs the predicted coiled-coil region for the localization at the tips of filopodia (Berg and Cheney, 2002). It is very likely that myosin 10 needs to be dimerized for processive movement, because other high duty ratio myosins such as myosin 6 and myosin 7, whose predicted coiled-coil regions are very similar to that of myosin 10, become processive when they are dimerized (Nishikawa et al., 2002; Rock et al., 2001; Yang et al., 2006).

Why did the artificially dimerized myosin 10 constructs not show proessive movement? There are several possibilities for the apparent nonprocessive nature of the dimerized myosin 10 constructs in the present study. The first possibility is that the head in the rigor state (AM) or in the ADP-bound form (AMD) dissociates spontaneously from actin due to the high actomyosin dissociation rates. As described in Chapter III, the dissociation rates of myosin 10 from actin in the presence and the absence of ADP were ~2 sec^{-1} and ~1 sec^{-1}, respectively, which are 100~1000-fold faster than those of myosin 5a and myosin 6. Thus, it is possible that dimeric myosin 10 is mechanistically processive (it may take a few steps), but it does not proceed for a long distance because of the extremely fast actomyosin dissociation rates. The second possibility is that there is an additional regulatory mechanism for making myosin 10 processive after being dimerized. The identity of the light chain(s) that actually binds to the neck of myosin 10 in a cell has not been completely clarified. This yet to be identified light chain may be essential for

the additional regulation of the processive when it is dimerized. In fact, the actin translocating activities of some myosins are tightly regulated by light chain phosphorylation or direct binding of calcium ion to the light chain (Sellers, 2000). The third possibility is that even if dimeric myosin 10 is processive, the molecular mechanism of the processive movement may not be the same as that of myosin 5a. For processive movement along actin filaments by hand-over-hand mechanism, the two heads have to be coordinated so that the lead head remains on the actin track while the trail head seeks the forward binding site, otherwise both heads would dissociate from the actin track before proceeding for a long distance even if the motor has a high duty ratio. Recently, this coordination of the two heads has been examined on myosin 5a (Purcell et al., 2005; Veigel et al., 2005). When both heads strongly bind to an actin filament, several picoNewtons of the intramolecular strain is posed onto both heads. The pulling force reduces the ADP release rate from the leading head thus prolonging the actin strong-bound state, whereas the pushing force does not change or even increases the ADP release rate from the trailing head. This increases the probability of the trailing head detaching before the detachment of the leading head, thus decreasing the probability of both heads simultaneously dissociating from the actin filament before stepping for a long distance. The intramolecular strain mechanism of myosin 10, if any, could be different from that of myosin 5a, and this could explain why the qualities of actin filaments movement by the M10M5IQcc chimeras in the *in vitro* motility were much worse than those by the M10M5cc chimeras. It is possible that the motor characteristic and the apparently kinked neck structure of myosin 10 are highly specialized for the unique

intramolecular strain mechanism for moving processively along the tightly bundled actin filaments found in filopodia, but not for single actin filaments found in the cytoplasm. Dimeric myosin 10 might processively move inside filopodia by using more than one actin filaments of the bundled actin.

If myosin 10 is simply not as processive as a typical transporter myosin such as myosin 5a, how does myosin 10 move cargos for a significant distance in cells? One possibility is that dimeric myosin 10 does not have to be highly processive unlike other processive myosins, because the dissociation of myosin 10 from the actin filament does not significantly facilitate the diffusion of the cargo-myosin 10 complex away from the actin filament. It is proposed that myosin 10 carries β-integrin, a trans-membrane molecule, and it is anticipated that the lateral diffusion of the trans-membrane molecules is much slower than the diffusion of cytosolic proteins. Furthermore, it is known that β-integrin forms a large multi-molecule complex with a molecular mass much greater than 1 MDa. Based upon the present results, the time myosin 10 dissociates from actin is less than 30 msec (1/13.5 – 1/20 = 24 msec), and it is plausible that the lateral diffusion of the molecular complex of greater than 1 MDa within this time is less than the head-neck length of myosin 10. Therefore, it is possible that the cargo does not move away from the actin cable during the myosin 10 cross-bridge cycles even if individual myosin 10 molecules are less processive, thus allowing myosin 10 to transport the membrane bound cargos.

Future Direction

Although myosin 10 seemed to be nonprocessive in our *in vitro* single molecule experimental condition, it can still be processive in the physiological environment found in filopodia of a living cell. There may be a binding partner(s) of myosin 10 that assists the processive movement of dimeric myosin 10 such as dynactin for cytoplasmic dynein (King and Schroer, 2000). Analyzing the step size of myosin 10 in a living cell can be an alternative way of testing processivity though it gives less direct evidence. In live-cell imaging, GFP-myosin 10 moves smoothly back and forth inside filopodia, and the GFP signals are often very bright, suggesting that a number of myosin 10 molecules are clustered while moving. The strong GFP signals would enable us to trace the movement with high temporal (msec) and spatial resolution (nm) (Watanabe et al., 2007). If successive stepwise movement with roughly constant step size (most likely ~36nm if it moves like myosin 5a) takes place at least locally while moving to the tip of filopodia, then it is likely that individual myosin 10 molecules are actually processive. If it is nonprocessive and thus requires many myosin 10 molecules for the movement towards the tip of filopodia, then the stepwise movement will become indistinct due to numerous simultaneous interactions of myosin molecules with actin.

Figure IV-1. The predicted coiled-coil region of myosin 10. A partial amino acid sequence of bovine myosin 10 (Tyr 808 – Pro 979) that contains the predicted coiled-coil region is shown. Possible coiled-coil registrations were predicted by COILS (www.russell.embl-heidelberg.de/cgi-bin/coils-svr.pl). The result of running COILS three times with windows of 14, 21, and 28 are indicated below the amino acid sequence. 'frame' denotes the predicted position of the heptad repeat for the highest scoring window that overlaps each position. 'prob' gives a single integer value representation of probability (where 0-9 covers the probability 0-1). The stable alpha helix (SAH) and three possible coiled-coil registrations are also shown above the amino acid sequence.

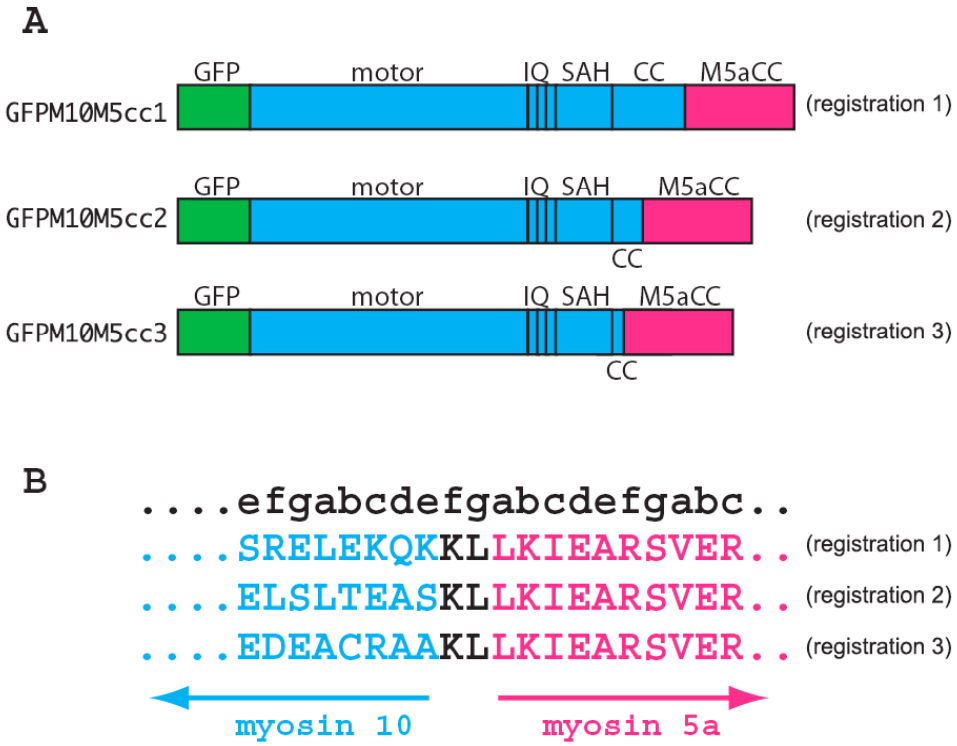

Figure IV-2. GFPM10M5cc constructs. A. Schematic representation of the constructs. The coiled-coil region of mouse myosin 5a was used to force-dimerize bovine myosin 10. Abbreviations are: *SAH*, stable alpha helix; *CC*, the predicted coiled-coil region of myosin 10; *M5aCC*, the stable coiled-coil region (Leu 908 – Glu 1090). A FLAG epitope was attached to the N-terminus of each construct to facilitate purification. **B.** Amino acid sequences at the junctions of the constructs. These constructs were designed not to disrupt the coiled-coil registration at the junction.

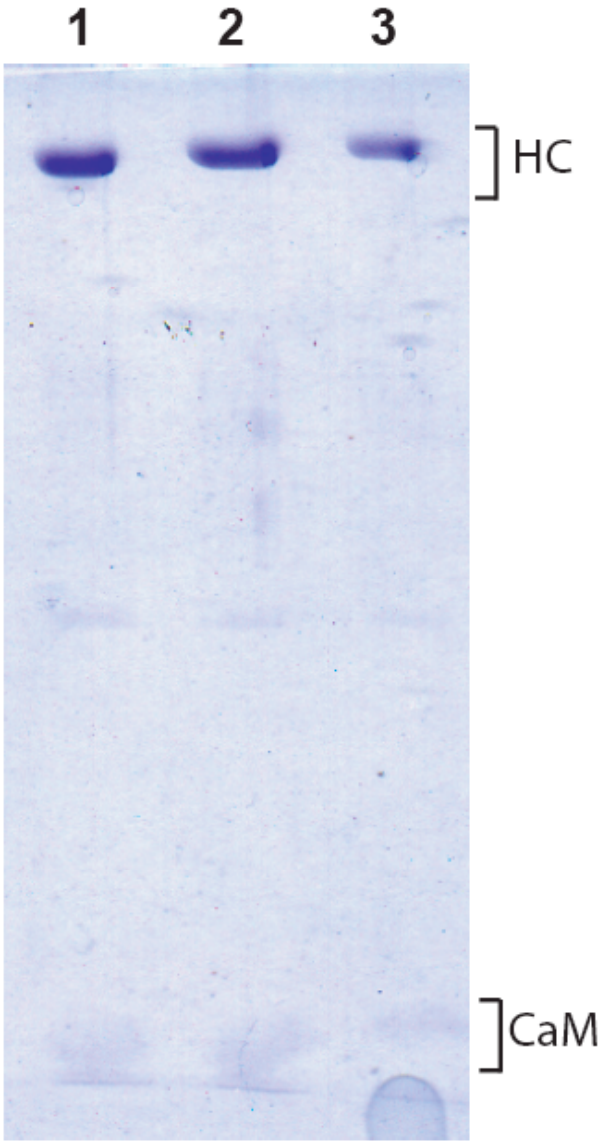

Figure IV-3. Purification of GFPM10M5cc constructs. Each GFPM10M5cc construct was purified by FLAG affinity column, and examined by SDS-PAGE. *Lane 1*, GFPM10M5cc1; *Lane 2*, GFPM10M5cc2; *Lane 3*, GFPM10M5cc3. Abbreviations are: *HC*, heavy chain; *CaM*, calmodulin.

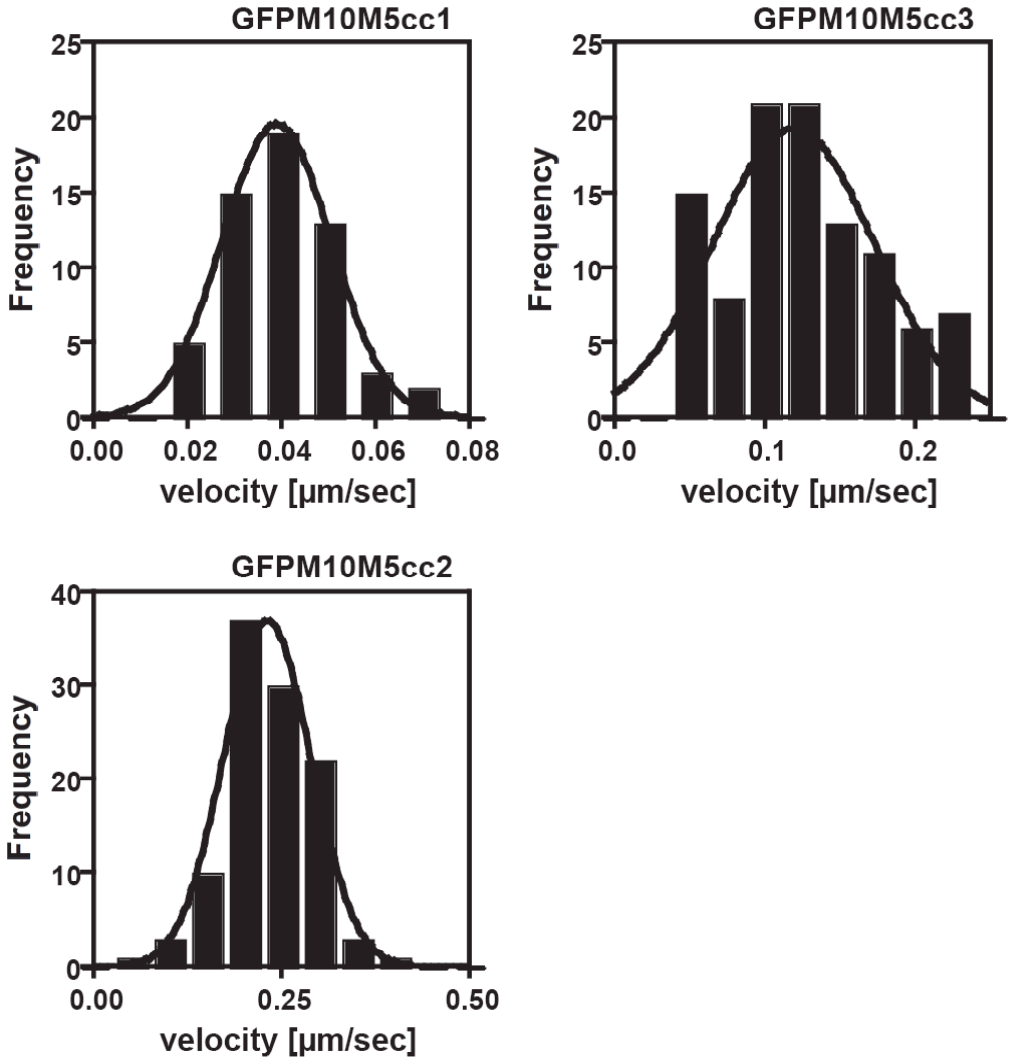

Figure IV-4. ***In vitro*** **actin translocating activity of GFPM10M5cc constructs.** The actin translocating velocities (mean ± s.d.) were 0.039 ± 0.012 μm/sec, 0.23 ± 0.06 μm/sec, and 0.12 ± 0.05 μm/sec for GFPM10M5cc1, GFPM10M5cc2, and GFPM10M5cc3, respectively.

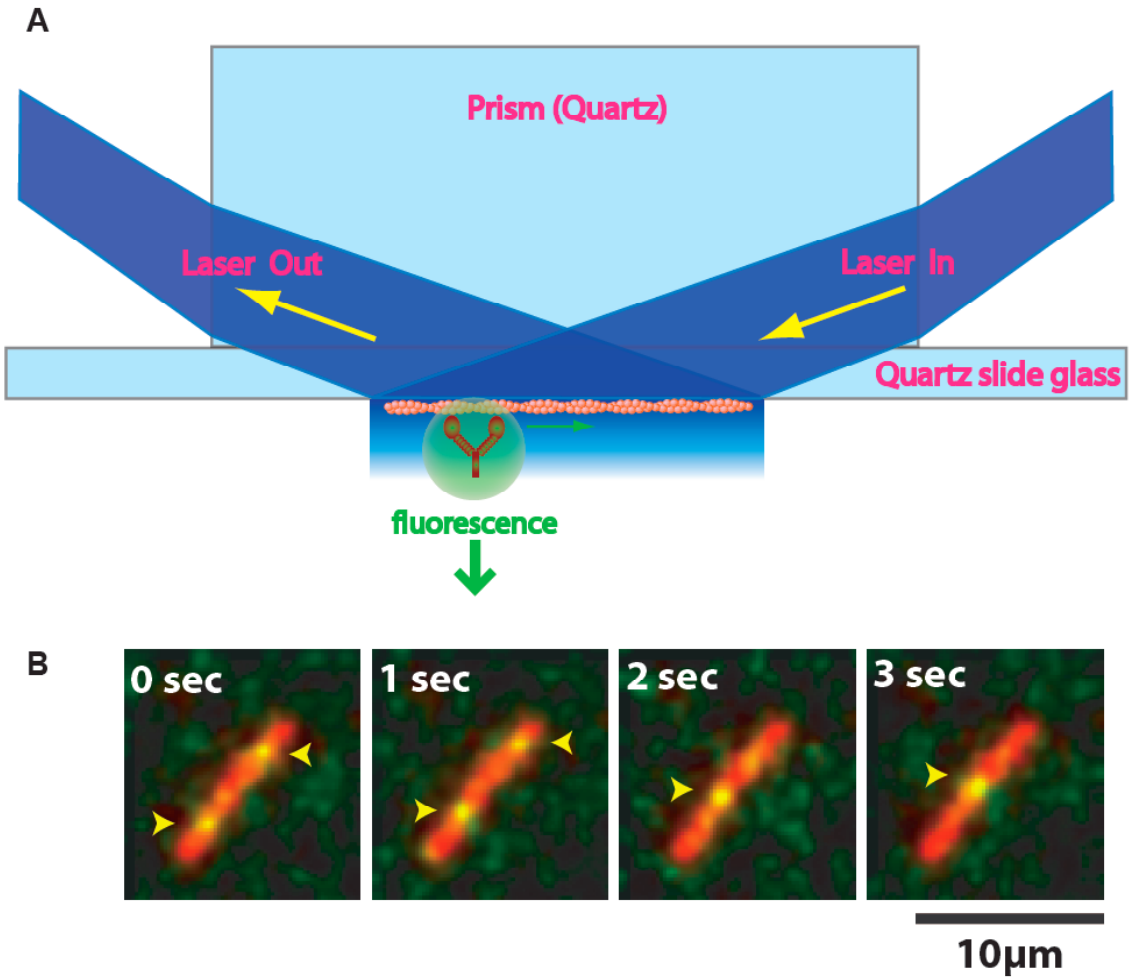

Figure IV-5. Processive movement of single GFP-myosin 5a molecules observed by TIRFM. A. Schematic representation of a GFP-labeled myosin 5a moving along an actin filament processively under the evanescent field (Appendix E). **B.** A typical recording of the processive movement of GFP-myosin 5a molecules. Actin filament was biotinylated and labeled with Alexa Fluo 647 phalloidin to be simultaneously observed with GFP signals (Appendix E). Arrowheads indicate the positions of individual GFP-myosin 5a molecules moving along an actin filament.

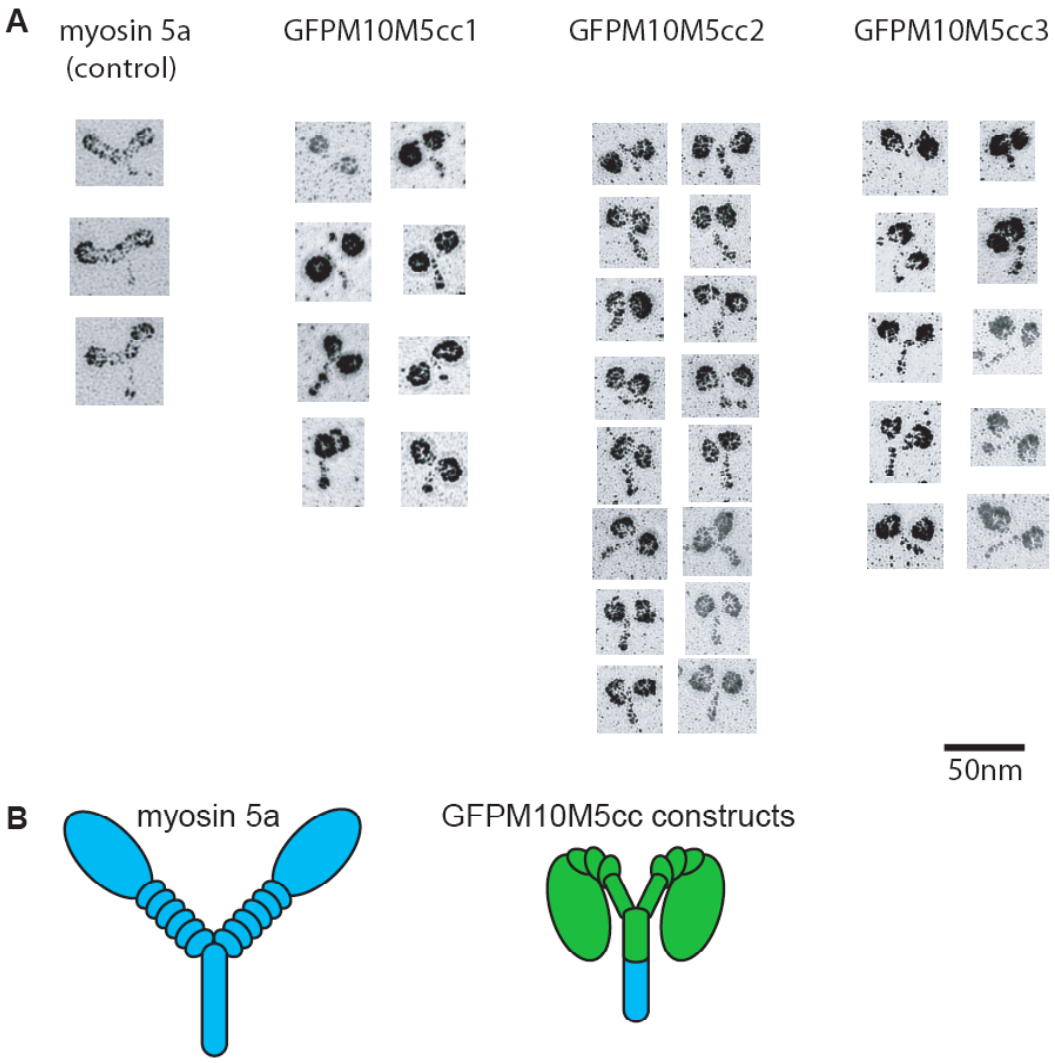

Figure IV-6. Rotary-shadowing electron microscopy of GFPM10M5cc constructs. A. Electron micrographs of the GFPM10M5cc constructs. The Rotary-shadowing electron microscopy was performed by Dr. Katsuhide Mabuchi (Boston Biomedical Research Institute). **B.** Schematic representations of the structures of myosin 5a and the GFPM10M5cc constructs inferred from the electron micrographs. Myosin 5a and myosin 10 are shown in cyan and green, respectively.

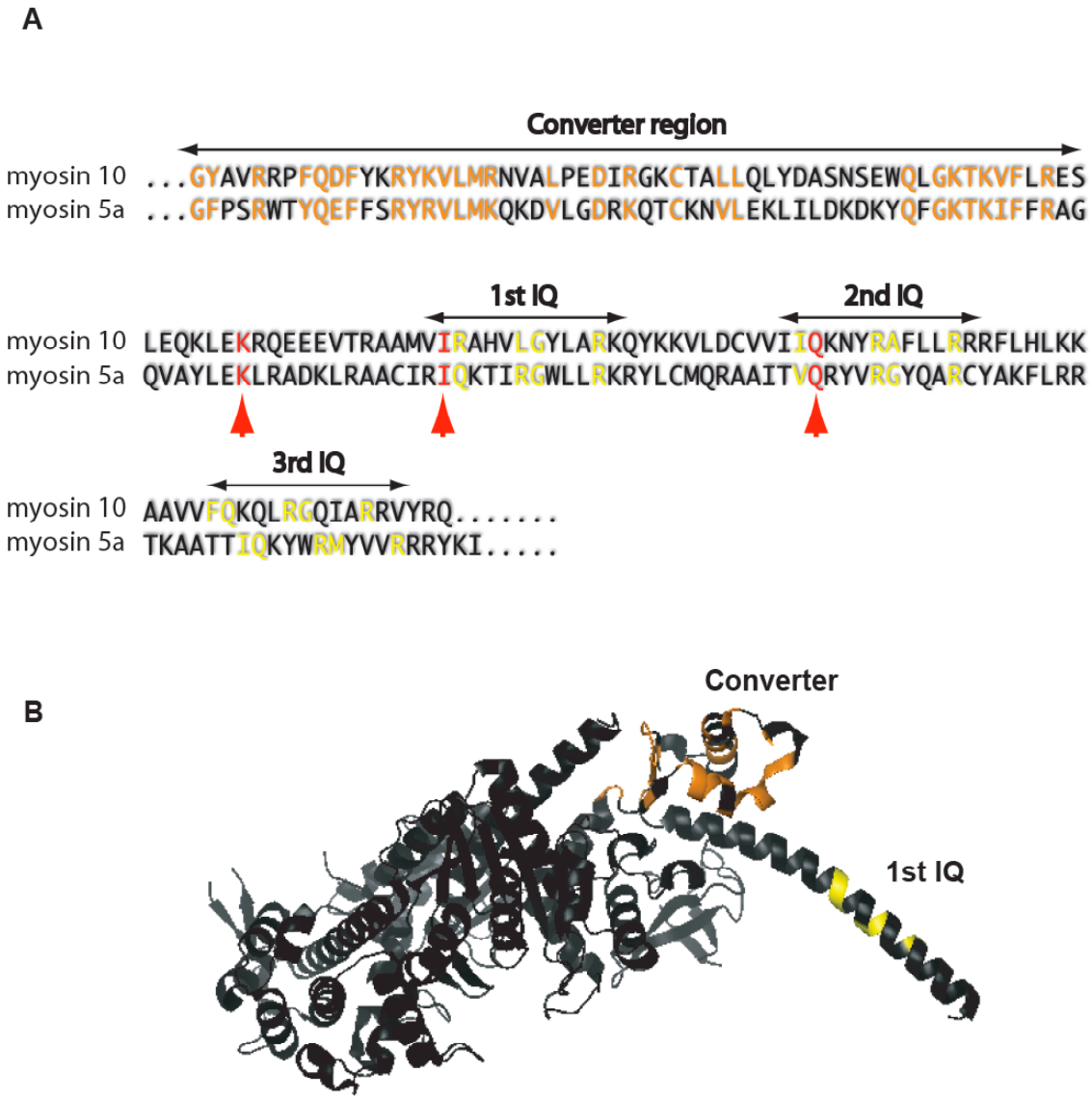

Figure IV-7. Converter-neck region of myosin 10 and myosin 5a. A. Sequence alignment of the converter/neck regions of myosin 10 and myosin 5a is shown. Highly conserved amino acids in the converter regions are colored in orange. Typical amino acids found in the IQ motif are colored in yellow. Red arrowheads indicate the junctions of myosin 10 and myosin 5a in the redesigned hybrid constructs shown in Figure IV-8. Note that the positions of the first IQ and the second IQ of myosin 10 and myosin 5a from their converter regions are the same. **B.** Crystal structure of the motor domain of myosin 5a is shown. The 2nd and the 3rd IQ motifs are not shown in this structure.

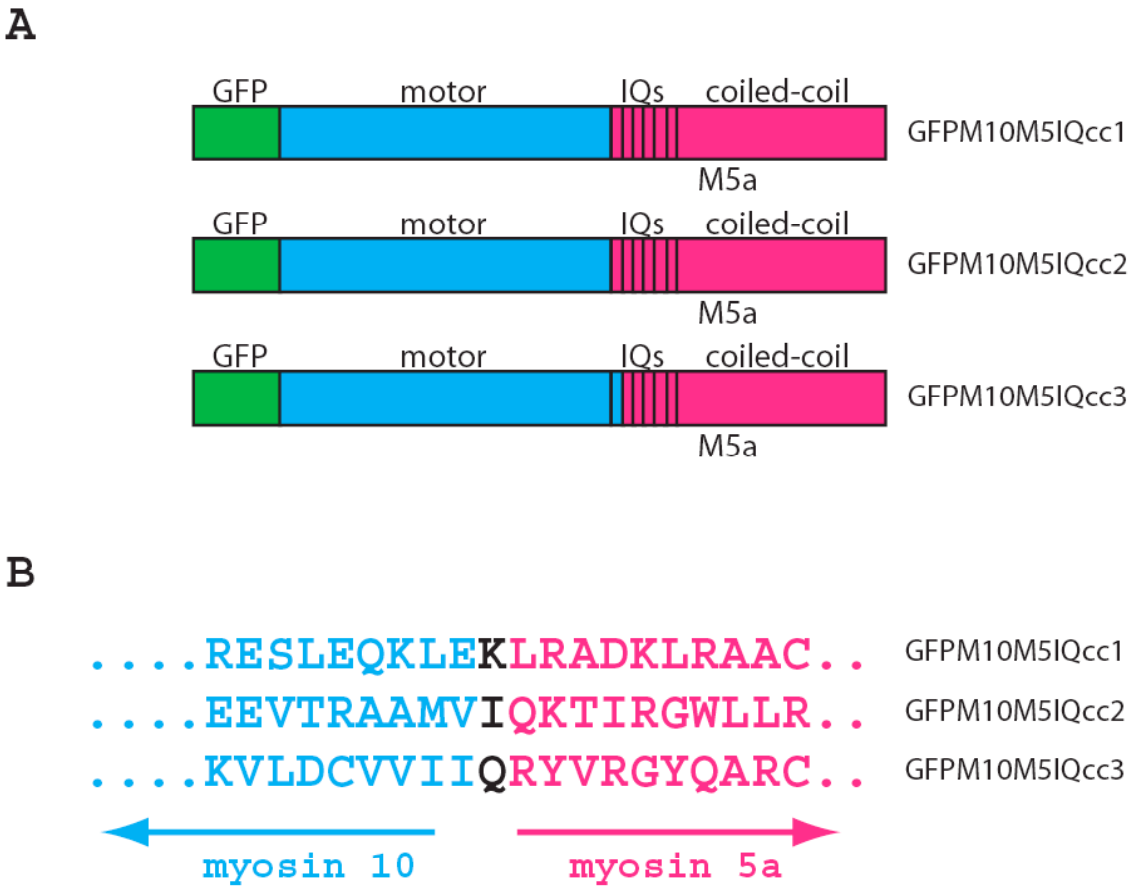

Figure IV-8. GFPM10M5IQcc constructs. A. Schematic representation of the constructs. The globular motor domain of myosin 10 was followed by the IQ motifs and the coiled-coil region of mouse myosin 5a. A FLAG epitope was attached to the N-terminus of each construct to facilitate purification. **B.** Amino acid sequences at the junctions of the constructs. Amino acids at the junction of myosin 10 and myosin 5a of the hybrid constructs are colored in black. See also Figure IV-7.

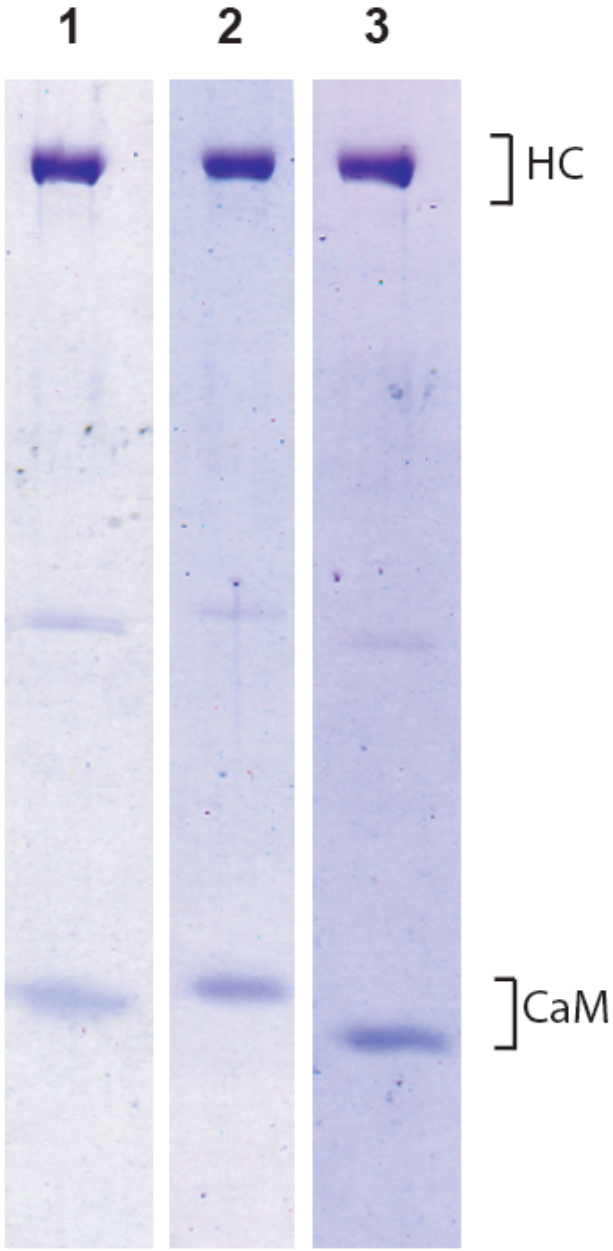

Figure IV-9. Purification of GFPM10M5IQcc constructs. Each GFPM10M5IQcc construct was purified by FLAG affinity column, and examined by SDS-PAGE. *Lane 1*, GFPM10M5IQcc1; *Lane 2*, GFPM10M5IQcc2; *Lane 3*, GFPM10M5IQcc3. Abbreviations are: *HC*, heavy chain; *CaM*, calmodulin.

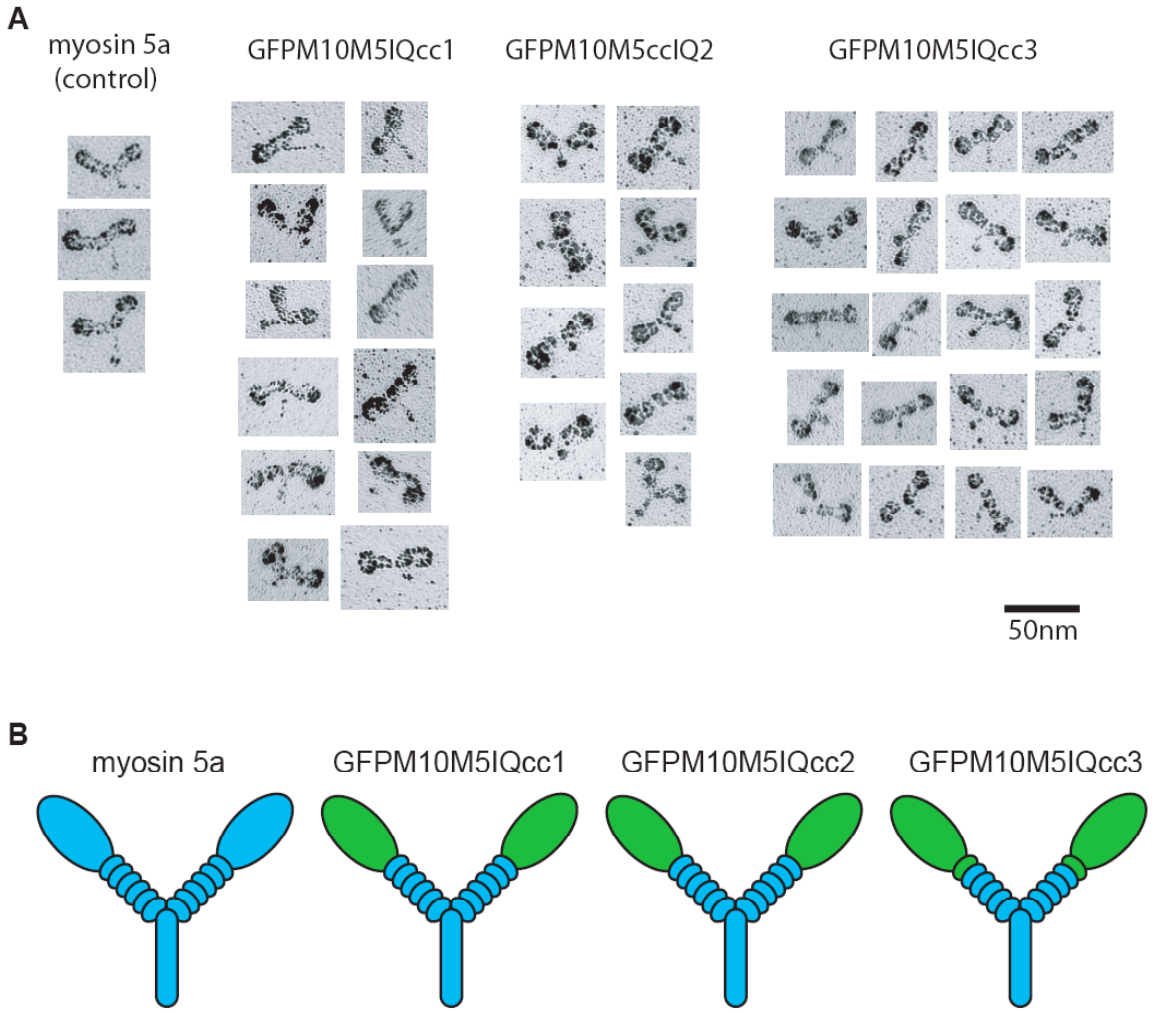

Figure IV-10. Rotary-shadowing electron microscopy of GFPM10M5IQcc constructs. A. Electron micrographs of the GFPM10M5IQcc constructs. The Rotary-shadowing electron microscopy was performed by Dr. Katsuhide Mabuchi (Boston Biomedical Research Institute). **B.** Schematic representations of the structures of myosin 5a and the GFPM10M5IQcc constructs inferred from the electron micrographs. Myosin 5a and myosin 10 are shown in cyan and green, respectively.

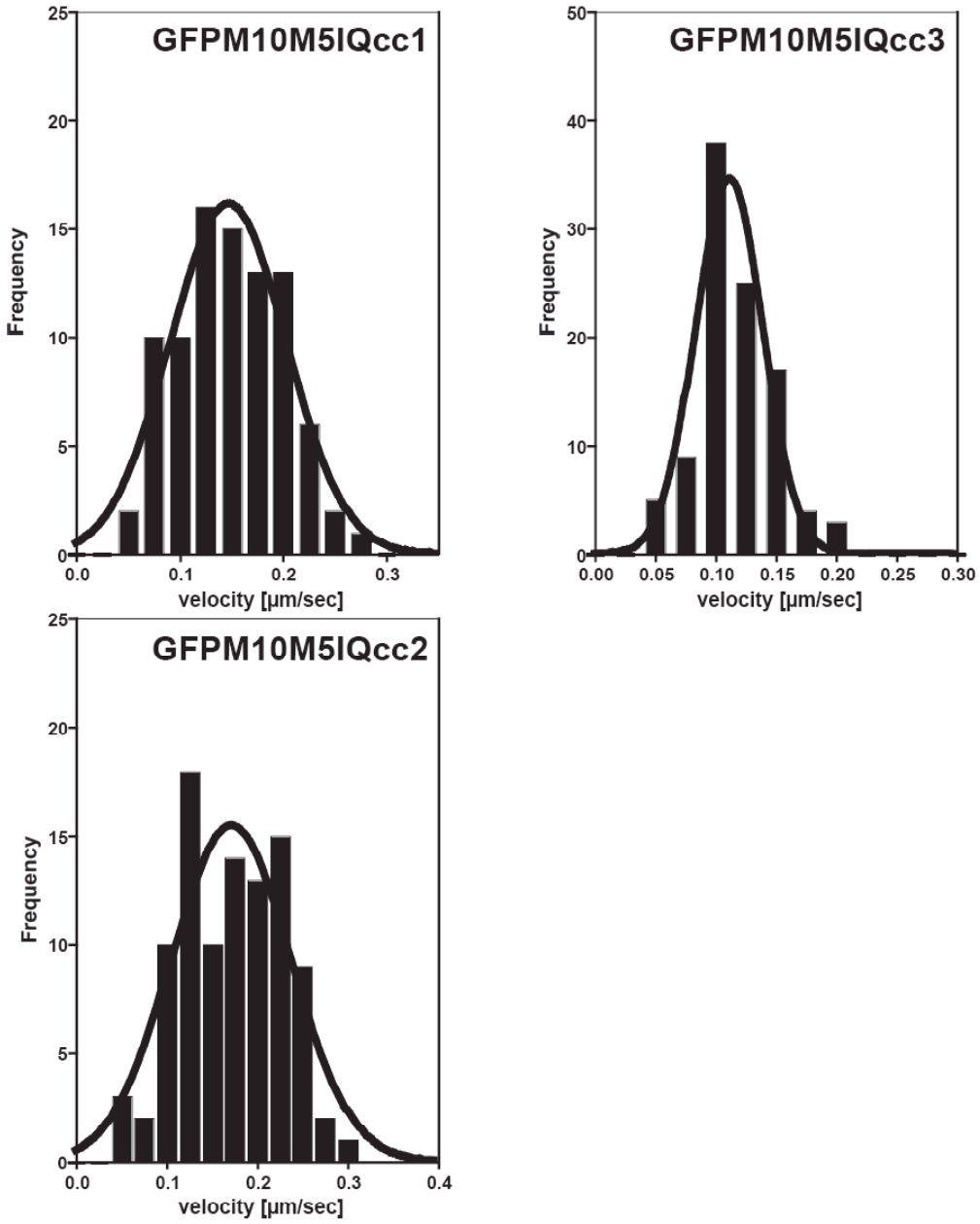

Figure IV-11. *In vitro* actin translocating activity of GFPM10M5IQcc constructs. The actin translocating velocities (mean ± s.d.) were 0.15 ± 0.06 µm/sec, 0.17 ± 0.07 µm/sec, and 0.11 ± 0.03 µm/sec for GFPM10M5IQcc1, GFPM10M5IQcc2, and GFPM10M5IQcc3, respectively.

CHAPTER V

GENERAL DISCUSSION ON THE PHYSIOLOGICAL FUNCTION OF MYOSIN 10

The motor property of myosins - movement directionality and the degree of processivity - is thought to reflect the physiological function of a myosin molecule. Therefore, understanding motor properties of myosin molecules provides insights into the physiological processes where those myosin molecules are involved. As seen in the present study, the plus end-directed movement directionality of myosin 10 is consistent with the suggested physiological function of transporting cargos such as VASP or β-integrin required for the maintenance/elongation of filopodia. The high duty ratio, the long neck (three IQs plus SAH), and the requirement of double-headed structure for the localization at the tip of filopodia all support an idea that myosin 10 functions as a processive cargo transporter like myosin 5a. However, unlike myosin 5a, force-dimerized myosin 10 constructs did not show successive movement along actin filaments in the single molecule experiment. Several possible reasons why we could not observe a processive movement were already discussed in the preceding chapter. Here, assuming that dimeric myosin 10 is not as processive as other processive myosins characterized so far, how myosin 10 functions as an intrafilopodial cargo transporter is discussed.

Muscle myosins are the best examples of nonprocessive myosins with very low duty ratio. The low duty ratio enables muscles to contract very efficiently and quickly with low consumption of ATP. For example, the actin translocating velocity of skeletal

muscle myosin is 5~10 μm/sec, while the maximal actin activated ATPase rate is ~20/sec. This means that skeletal muscle myosins translocates an actin filament 250~500 nm / ATP. *[The distance is far greater than the structural dimension of the protein, and has been a paradox. The concept of duty ratio provides an explanation for the step size paradox. The unitary step size of skeletal muscle myosin is calculated as (5~10 μm/sec) / (~20 /sec) × duty ratio (0.01~0.02) = 2.5~10 nm, which is in the range of the structural dimension of the protein.]* Contrary to those low duty ratio myosins, high duty ratio myosins have small step distances per ATP (e.g. ~20 nm/ATP for myosin 5a), and the ATPase rate needs to be highly increased for attaining an actin translocating velocity comparable to that of muscle myosins. The same calculation gave ~13 nm /ATP for myosin 10 (M10IQ1), which is within the structural dimension of the protein. This is another indirect evidence of myosin 10 as a high duty ratio motor, and strongly suggests that the nonprocessive nature of myosin 10 is qualitatively different from those of other highly nonprocessive muscle myosin motors characterized so far. Therefore, at least the apparent nonprocessive nature of myosin 10 does not seem to attain higher actin translocation efficiency.

Myosin 10 molecules seem to be clustered when they move inside filopodia. A simple explanation is that, because individual myosin 10 molecules are nonprocessive, multiple molecules are required to be able to function as a cargo transporter. If so, is there any advantage in having a nonprocessive motor instead of a processive motor for the cargo transport in filopodia? Myosin 10 has been suggested to transport β-integrin, which associates with the extracellular substrates. Thus, one possibility is that a large

magnitude of force is required for the transport of myosin 10-dependent cargo inside filopodia, and thus multiple myosin 10 molecules are required to work in concert to generate sufficient forces. If myosin 10 is highly processive, and thus binds strongly to actin in the AMD form after translocating along actin, this strong binding itself would interfere with the translocation by other myosin molecules. The extremely low affinity of myosin 10 to actin in the presence and the absence of ADP (AMD and AM forms) may be important for minimizing the resistance while maximizing the number of actomyosin crossbridges for force generation. This is different from typical nonprocessive muscle myosins whose primary advantage are to efficiently and quickly translocate actin filaments by minimizing the number of actomyosin crossbridges. For example, only 3~6 crossbridges out of ~300 crossbridges found in each half of the myosin thick filament maintain contact between the thick filament and thin filament in skeletal muscle because of the low duty ratio (0.01~0.02). Therefore, it is possible that the processivity of myosin 10 is customized for cargo transport that demands strong force.

CHAPTER VI

FINAL REMARKS

- Molecular mechanism behind directionality and processivity -

The ultimate goal of this study is to clarify the molecular mechanism of how myosin motors convert the chemical energy of ATP into mechanical work. Is the fundamental mechanism of biological machines like molecular motors different from that of the manmade machines such as automobiles? If so, how exactly are they different? If not, how well can we describe molecular mechanism with analogies to the manmade machines? It seems intuitive that biological machines and artificial machines are different from each other. The output of artificial machines is usually exactly what we expect. This is because of the large energy input used for operating these machines. The output of biological machines, however, is typically rather stochastic. For example, myosin 5a, a plus end-directed actin-based processive molecular motor, takes variable step sizes (~36 nm on average) while it moves along the actin filament towards the plus end, and, strikingly, it sometimes steps backward (Mehta et al., 1999). This is because of the low energy input for operating molecular motors. Since the free energy released by ATP hydrolysis is just ~20 k_BT under typical physiological conditions, the output of biological machines is easily affected by the thermal energy in the order of k_BT. How can such biological molecular machines maintain life so successfully? Such stochastic

output of individual biological machines may be the key to understanding the underlying logic used in life system as a whole.

Molecular motors such as myosin, kinesin, and dynein are highly accessible simple models from which we can learn the general strategy of biological systems, because the output – the motor activity – is readily measurable by performing the transient kinetics assay, the *in vitro* motility assay, and the single molecule assay, etc. For clarifying the molecular mechanism, it is quite beneficial to compare one molecular motor to the other with a different motor property. Fortunately, there are a number of naturally occurring molecular motors whose motor properties are different from one another. Many of those molecular motors have been thoroughly characterized biochemically and biophysically, and crystal structures of some of them are already available. Further extensive characterization of other yet to be analyzed molecular motors will help us grasping the detailed picture of how these molecular motors work. The present study on myosin 10 provided a unique example of a myosin motor showing nonprocessive nature while retaining a high duty ratio. Combining results obtained in this study with currently available experimental results with other myosin and kinesin molecules, I will discuss the molecular mechanism behind the directionality and the processivity of the myosin motors.

The lever-arm hypothesis

The lever-arm hypothesis has become the textbook norm for explaining how a myosin molecule translocates relative to an actin filament (Fig. VI-1). Briefly, the

hypothesis claims that small conformational changes that take place in the motor core domain associated with the ATP hydrolysis cycle are amplified by the swing of the light chain-bound rigid neck (power stroke) to generate a unitary displacement. The angular change of the neck region associated with the ATPase cycle has been actually observed in muscle (Irving et al., 1995). The swing-like conformational change of the neck has also been supported by cryoelectron microscopic studies (Jontes et al., 1995; Whittaker et al., 1995), and by the X-ray crystallographic studies (Dominguez et al., 1998; Houdusse et al., 2000; Smith and Rayment, 1996).

Movement directionality

The movement directionality of myosins has been explained by the angle of the neck with respect to the motor core domain. The minus end-directed motility of myosin 6 seems to be attributed to its uniquely positioned neck (Appendix Fig. F-1). The facts that modification or truncation of the redirected neck successfully converted the minus end-directed motility into the plus end-directed motility (Bryant et al., 2007; Park et al., 2007)(Appendix F), and that the plus end-directed motility of myosin 1 (MyoE) was reversed simply by rotating the direction of the neck ~180^{o} using protein engineering (Tsiavaliaris et al., 2004) seem to strongly support the hypothesis. To further test if the apparently redirected neck of myosin 6 is responsible for the minus end-directed motility, we generated a number of chimeric myosin constructs comprised of parts from myosin 5a and myosin 6 (Appendix F).

In the case of microtubule-based kinesin motors, the unidirectional processive movement on a microtubule was first explained by the neck linker docking model. In this model, the microtubule-unbound head of dimeric kinesin is pushed towards the plus end direction by the docking of the neck linker to the motor core induced by the conformational change associated with the binding of ATP to the microtubule-bound head of kinesin (Fig. VI-2A) (Rice et al., 1999). The 'neck linker docking' corresponds to the 'power stroke' of myosin, and this model was highly analogous to the lever arm hypothesis of myosin. Rice *et al*. recently measured the free energy released by the neck linker docking of kinesin (Rice et al., 2003), and found that the free energy (1~2 k_BT) was too small to explain the maximal work done by dimeric kinesin, ~14k_BT (~7 pN x 8 nm step size). Although the free energy released by the 'power stroke' of myosins has not been reported on any myosin, it is possible that the free energy released by the 'power stroke' is not sufficient to account for the work done by a myosin molecule (e.g. 16~17k_BT for myosin 5a).

If the translocation is not provided by the 'power stroke', how do motor proteins move unidirectionally? It has been known that a dimeric kinesin molecule moves along microtubule in a hand-over-hand manner with an 8 nm step size towards the plus end, and that an external pulling force on a kinesin molecule against the direction of the movement increases the frequency of backward 8 nm step with ATP consumption (Carter and Cross, 2005). Recently, Taniguchi *et al*. have thoroughly examined the mechanical kinetics and thermodynamics of the movement of dimeric kinesin (Taniguchi et al., 2005). They found that the forward/backward stepping asymmetry of kinesin is generated by ~6 k_BT

of entropic asymmetry, but not enthalpic asymmetry (~0.1 k_BT). This entropic asymmetry is more than three times greater than the free energy released by the neck linker docking (1~2 k_BT). Based on these results, Taniguchi *et al*. proposed that the direction of the movement of kinesin is entropically biased to the plus end direction due to the neck linker docking (1~2 k_BT) and the steric compatibility between the motor domain and microtubule (4~5 k_BT) because of their polar structures (Taniguchi et al., 2005) (Fig. VI-2B). Although similar thermodynamic examination has not been reported on any myosin, it is possible that the unidirectional motility of myosin is also explained by the entropic asymmetry found in kinesin. The apparent swing-like conformational change of the C-terminal neck of a myosin molecule associated with the ATP hydrolysis cycle might be important for generating the entropic asymmetry.

Processivity

The successive movement of double-headed processive myosins has been explained by the hand-over-hand model based on the lever-arm hypothesis (Fig. VI-3), and recent single molecule studies strongly support the model (Asbury et al., 2003; Kaseda et al., 2003; Okten et al., 2004; Warshaw et al., 2005; Yildiz et al., 2003; Yildiz et al., 2004a; Yildiz et al., 2004b). For processive movement by the hand-over-hand mechanism, one of the two heads has to remain on the track until the other head binds to the forward binding site. High duty ratio (>0.5) of the processive motors characterized so far partially explains how the processive movement can be achieved, however, the high duty ratio itself does not explain the long distance processive movement, because the two

heads have to be coordinated. If not coordinated, both heads would simultaneously detach from the track before traveling for a long distance. For kinesins, the coordination between the two heads is achieved by a force between the two heads (5~15 pN) (Rice et al., 2003), which is developed when both heads bind strongly to a microtubule. The intramolecular strain in turn modulates the rates of ATP binding, ADP release, and phosphate release so that the dissociation of the trail head from the microtubule track precedes the ATP binding to the lead head (Cross, 2004; Valentine and Gilbert, 2007). Mutagenesis and chemical crosslinking studies suggest that the neck linker plays an important role for the coordination of the two heads of kinesin motors (Case et al., 2000; Tomishige and Vale, 2000).

The coordination between the two heads by the intramolecular strain-dependent mechanism was also reported in myosin 5a (Purcell et al., 2005; Veigel et al., 2005). Several picoNewtons of the intramolecular force is estimated to be induced when both heads bind to actin. The pulling force on the lead head reduces the ADP release rate, whereas the pushing force on the trail head does not affect or even enhances the ADP release rate. This reduces the probability of simultaneous dissociation of both heads from actin before traveling for a long distance. The apparently nonprocessive nature of the dimerized myosin 10 constructs (Chapter IV) was a surprise. However, this may indicate that the inter-head coordination mechanism found for myosin 5a may not always apply to other processive myosins. A recent study reported that the intramolecular strain-dependent coordination mechanism of myosin 6 is different from that of myosin 5a (Sweeney et al., 2007). Knowing the variations of the inter-head coordination

mechanism is beneficial for better understanding the molecular mechanism behind processivity. Future studies will shed more light on the underlying molecular mechanism of processivity.

Remaining enigma

Myosin 9b - a single-headed processive motor **–** The architecture of the N-terminal motor domain of myosin is highly conserved among the superfamily, suggesting that myosin molecules share a fundamentally similar molecular mechanism. Thus, it is quite natural to assume that the same molecular mechanism is shared among the myosin supterfamily.

The lever-arm hypothesis seems to be successful in explaining the molecular mechanism of directionality and processivity of myosin in general. The processive movement of myosin 5a can be explained by its double-headed structure with hand-over-hand mechanism. Likewise, the processive reversed end-directed motility of myosin 6 can be explained by a hand-over-hand mechanism with redirected necks in its double-headed structure. However, the lever-arm hypothesis cannot explain the molecular mechanism of a single-headed, unidirectional processive myosin – myosin 9b (Inoue et al., 2002; Post et al., 2002). Like other myosins, myosin 9b has an N-terminal globular motor core domain followed by a converter region and a neck region to which four light chains bind. Thus, structurally, myosin 9b is not exceptional when compared to other myosins. However, it can somehow move processively along actin filament unidirectionally without dimerizing or attaching to a scaffold (Nishikawa et al., 2006).

Obviously, the molecular mechanism cannot be explained by the cyclical conformational change of the lever-arm. How does myosin 9b work?

A clue to this question comes from an unconventional kinesin, KIF1A, another example of a single-headed processive motor whose movement mechanism cannot be explained by the conformational change of the distal region such as neck linker docking. The overall structure of the motor domain of KIF1A is very similar to that of conventional kinesin. For the processive movement, the motor domain has to remain associated with the microtubule. The single-headed processive movement of KIF1A has been explained by the lysine-rich microtubule-binding site in the motor core domain termed 'K-loop'. The K-loop is thought to maintain weak binding of the motor core to the microtubule while moving diffusively along the microtubule towards the plus end (Okada and Hirokawa, 2000). A recent study has proposed a molecular mechanism of how a single-headed KIF1A molecule moves towards plus end by diffusional search on the microtubule (Okada et al., 2003).

The loop-2 of myosin 9 contains a significantly large insertion when compared to other classes of myosin. Like K-loop of KIF1A, the loop-2 might play a similar role for maintaining affinity to actin filament during the movement. Although the molecular mechanism of how single-headed myosin 9b moves processively along actin filament towards minus end has not been fully understood, it is less likely that the fundamental molecular mechanism of myosin 9b is completely different from those of other myosins characterized so far. The fact that the monomeric myosin 9b can still function as a processive motor suggests that hand-over-hand with double-headed structure is not

required for a motor to be processive, although it may be advantageous to have a coordinated double-headed structure for processive movement. Further studies on myosin 9 will be beneficial for unraveling the fundamental molecular mechanism of how the movement directionality and the processivity of myosins are determined.

Challenge against the lever-arm hypothesis - The lever-arm hypothesis predicts that the displacement and the velocity of myosin are proportional to the length of the neck domain. Some researchers have shown that the actin translocating velocity is indeed proportional to the length of the neck (lever-arm) (Anson et al., 1996; Uyeda et al., 1996), however, others have shown that the length of the neck does not affect the velocity (Perreault-Micale et al., 2000; Trybus et al., 1999). In the present study on myosin 10, we also found that the actin tranlocating velocity was not affected by the truncation of the neck (Table II-1). In collaboration with the Yanagida laboratory (Osaka, Japan), we further tested if the dimeric structure of myosin 5a with the long neck (23 nm) is essential for the processive movement with the large step size (~36 nm). Surprisingly, a single-headed myosin 5a construct still developed multiple large (~32 nm) steps successively (Watanabe et al., 2004), and the step size was not affected by the truncation of the neck (Tanaka et al., 2002) [(Although the results are still controversial (Sakamoto et al., 2003; Sakamoto et al., 2005)]. The results imply that the molecular mechanism of the processive movement is fundamentally similar among all the processive motors irrespective of their oligomeric states. It seems to be true that the swing-like conformational change of the neck of the myosin molecule associated with the ATP

hydrolysis cycle do occur. However, whether actin translocation is directly powered by the so-called 'power stroke' of the neck (lever-arm) is still very much an open question.

The molecular mechanism of myosin behind directionality and processivity

Lastly, I would like to propose the following regarding the molecular mechanism behind the directionality and processivity of myosin.

The free energy of ATP is used for establishing the actin weak-binding state of the motor core, and for generating entropic asymmetry for the forward step and the backward step – For the diffusional search on actin, the motor core domain has to be in the actin weak-binding state. This requires energy because the motor domain of myosin usually strongly binds to actin in the presence of ADP or in the absence of nucleotides. The entropic asymmetry may be generated by the swing-like conformational change of the neck and/or the steric compatibility between the motor core and actin due to their polar structures. It is important to consider that the entropic asymmetry is generated by using the free energy of the ATP hydrolysis, but not simply by the apparent structural binding compatibility. If the entropic asymmetry is generated merely from the apparent structural factors, the model then calls for 'Maxwell's demon' – the motors move along actin without consuming ATP, which violates the second law of thermodynamics. Even if the dissociation rate of the motor domain from actin is very slow in the absence of ATP, the motor domain can spontaneously detach from actin due to the thermal energy.

Movement directionality can be determined solely by the motor core region - Although lines of evidence now suggest that the positioning of the neck with respect to the head plays a major role in dictating the minus end-directed movement of myosin 6, this cannot explain the minus end-directed motility of myosin 9b. Myosin 9b does not have an insertion in the neck that changes the position of the neck, and even more importantly, it does not have to be dimerized or attached to a scaffold to be processive. In the case of kinesin, disruption of the neck linker does not affect the plus end-directionality (Case et al., 2000), suggesting that the motor core itself is capable of establishing the entropic asymmetry for the forward step and the backward step. In myosin 9b, loop-2 may be involved in determining the movement directionality, and may play a primary role in determining the minus end-directed motility. It is possible that several factors (e.g. loop-2, a redirected neck, etc) concurrently contribute to establishing the entropic asymmetry along actin, and that the balance of those contributions is different among the myosin superfamily.

Processivity is simply determined by the affinity of the motor core region to actin during the actin weak-binding state – The double-headed structure found in many processive myosins may not be fundamentally essential for the successive movement along actin. Having two heads may simply increase the affinity of the motor domain to actin. We actually found that a double-headed myosin 5a with truncated neck and a single-headed myosin 5a are capable of developing multiple large steps successively along actin (Tanaka et al., 2002; Watanabe et al., 2004). It should be emphasized that

most single molecule experiments that demonstrated the hand-over-hand mechanism have been done under low ATP conditions where ATP binding limited the entire ATPase cycle. Under such conditions, one of the two heads is forced to bind actin, thus increasing the chance of observing the hand-over-hand movement. Consistent with this concern, binding of only one of the two heads, but not of both heads, of dimeric myosin 5a to actin was predominantly observed under physiological concentrations of ATP (Walker et al., 2000).

At this point, it is not clear how the globular motor core generates the entropic asymmetry along actin filament by using the free energy of ATP. Additional studies are required for establishing a better model that is capable of explaining the molecular mechanism of directionality and processivity of all myosin motors.

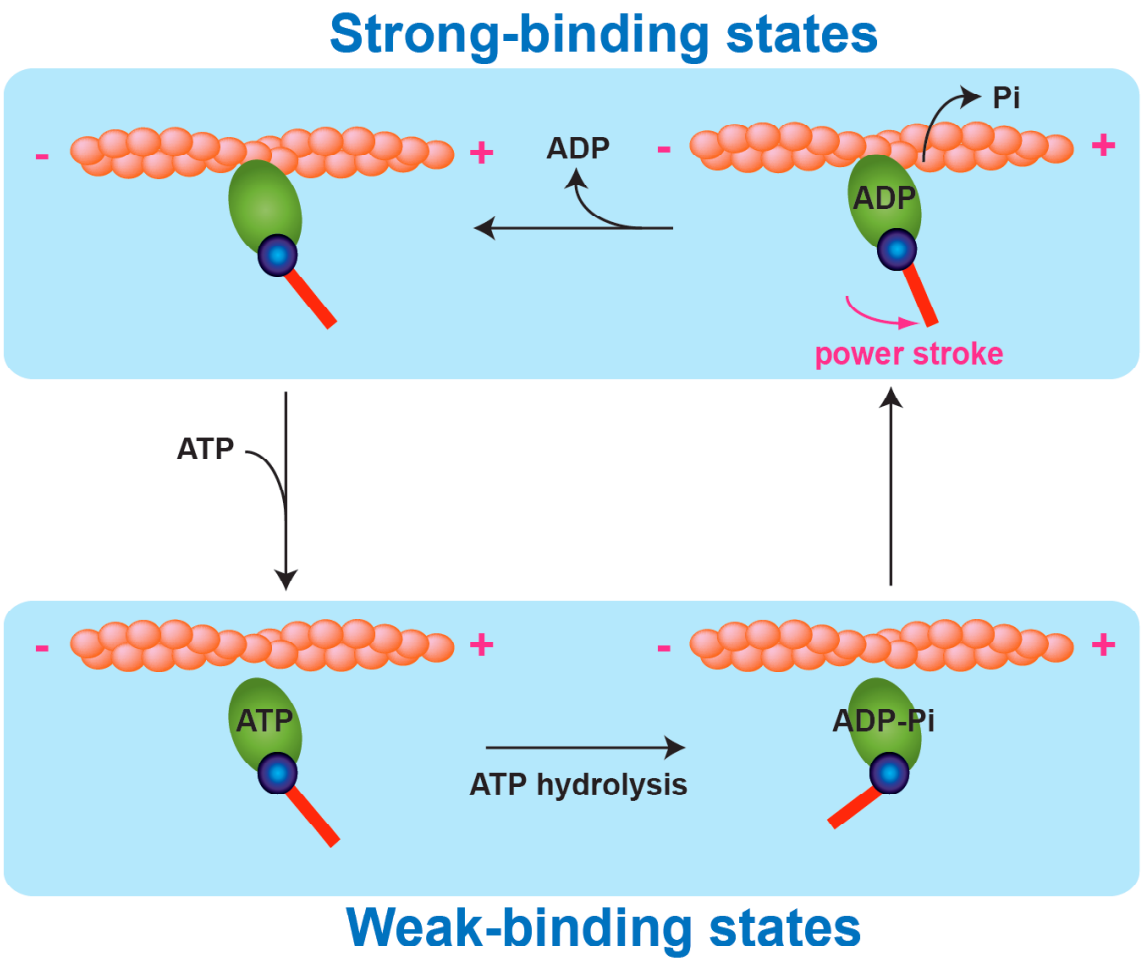

Figure VI-1. The lever-arm hypothesis. The motor domain of myosin, the converter region, and the neck region (lever-arm) are colored in green, blue, and red, respectively. In this hypothesis, small conformational changes in the motor core domain associated with the ATP hydrolysis cycle are thought to be converted into the swing-like motion of the C-terminal neck region (power stroke) to generate a unitary displacement.

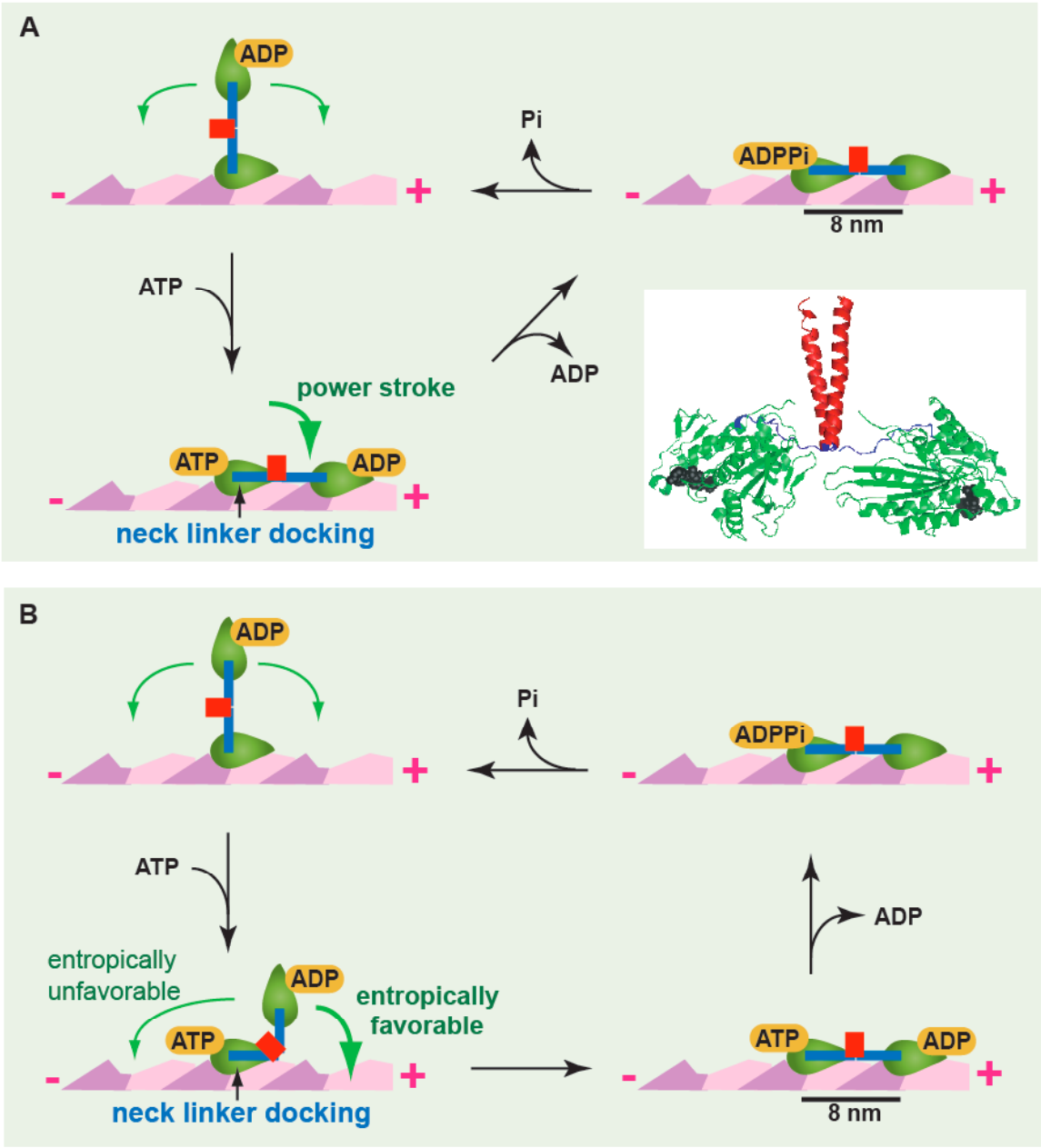

Figure VI-2. Unidirectional processive movement of dimeric kinesin along microtubule. A. Unidirectional processive movement of kinesin along microtubue by neck linker docking mechanism. ***Inset***. The crystal structure of dimeric kinesin (3KIN). The motor core domain (green), neck linker region (blue) and a partial coiled-coil region (red) are shown. **B.** Unidirectional processive movement of kinesin along microtubue driven by entropic asymmetry. The motor core domain, neck linker region, and the coiled-coil region are colored in green, blue, and red, respectively. Microtubule track is shown in pink and purple. ' + ' and '-' indicate the polarity of microtubule.

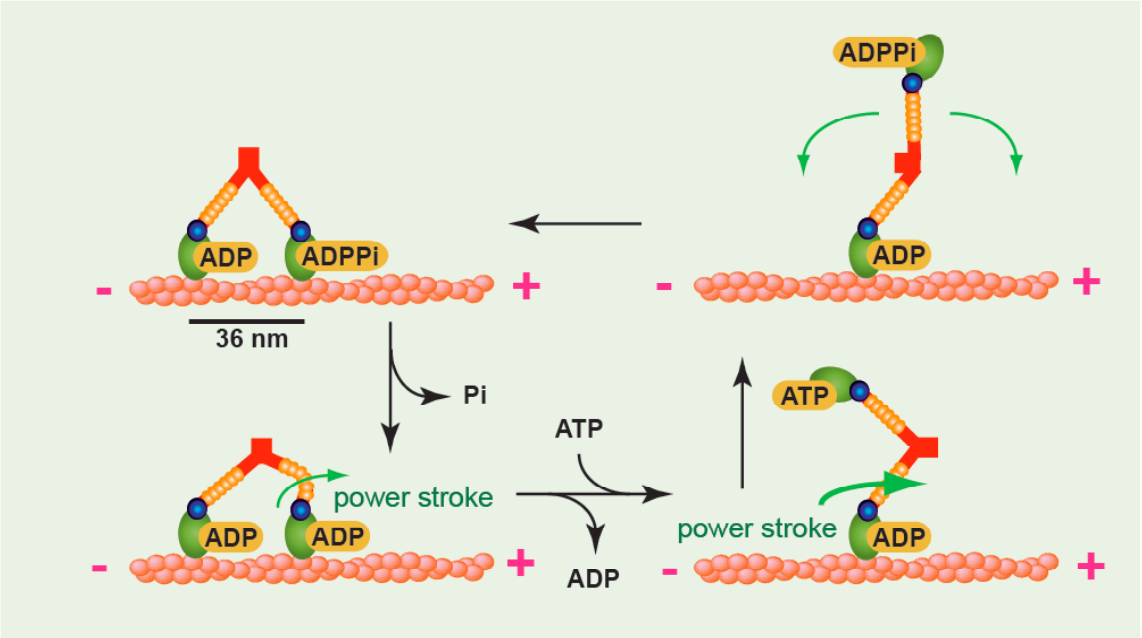

Figure VI-3. Processive movement of myosin 5a by hand-over-hand mechanism. Unidirectional processive movement of myosin 5a along actin driven by hand-over-hand based on the lever-arm hypothesis. The globular motor domain, converter, the neck/coiled-coil region, and calmodulins bound to the neck are colored in green, blue, red, and orange, respectively. Actin track is shown in pale red. ‘ + ’ and ‘ - ’ indicate the polarity of actin.

APPENDIX A

POLARITY-MARKED ACTIN FILAMENT

A simple procedure for preparing polarity-marked actin filaments was developed in the present study (Chapter II). Here, sequential images of the movement of the polarity-marked actin filaments on a myosin 5a-coated glass surface (Fig. A-1) and on a myosin 6-coated glass surface (Fig. A-2) are shown. Myosin 5a and myosin 6 were used as controls for plus end-directed motility and minus end-directed motility, respectively. As expected, almost all the polarity-marked actin filaments moved with the tetramethylrodamine-labeled tips (colored in red) leading the movement on a myosin 5a-coated glass surface, whereas almost all the polarity-marked actin filaments moved with the tetramethylrhodamine-labeled tips trailing the movement on a myosin 6-coated glass surface. Actin filaments without the tetramethylrhodamine cap were also observed. The results confirmed the successful polarity-labeling of actin filaments.

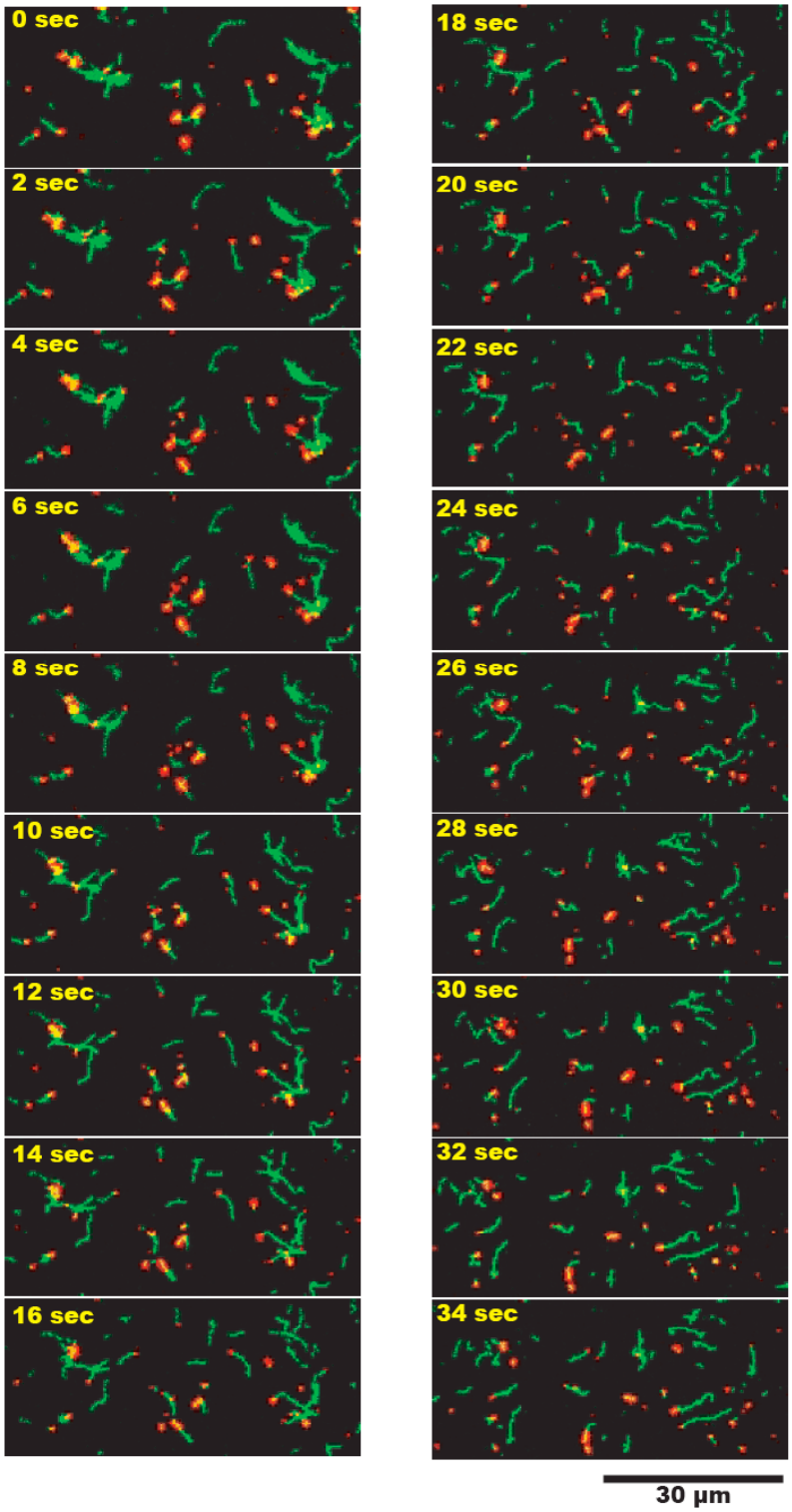

Figure A-1. Sequential images of the polarity-marked actin filaments moving on a myosin 5a-coated glass surface (M5aIQ2).

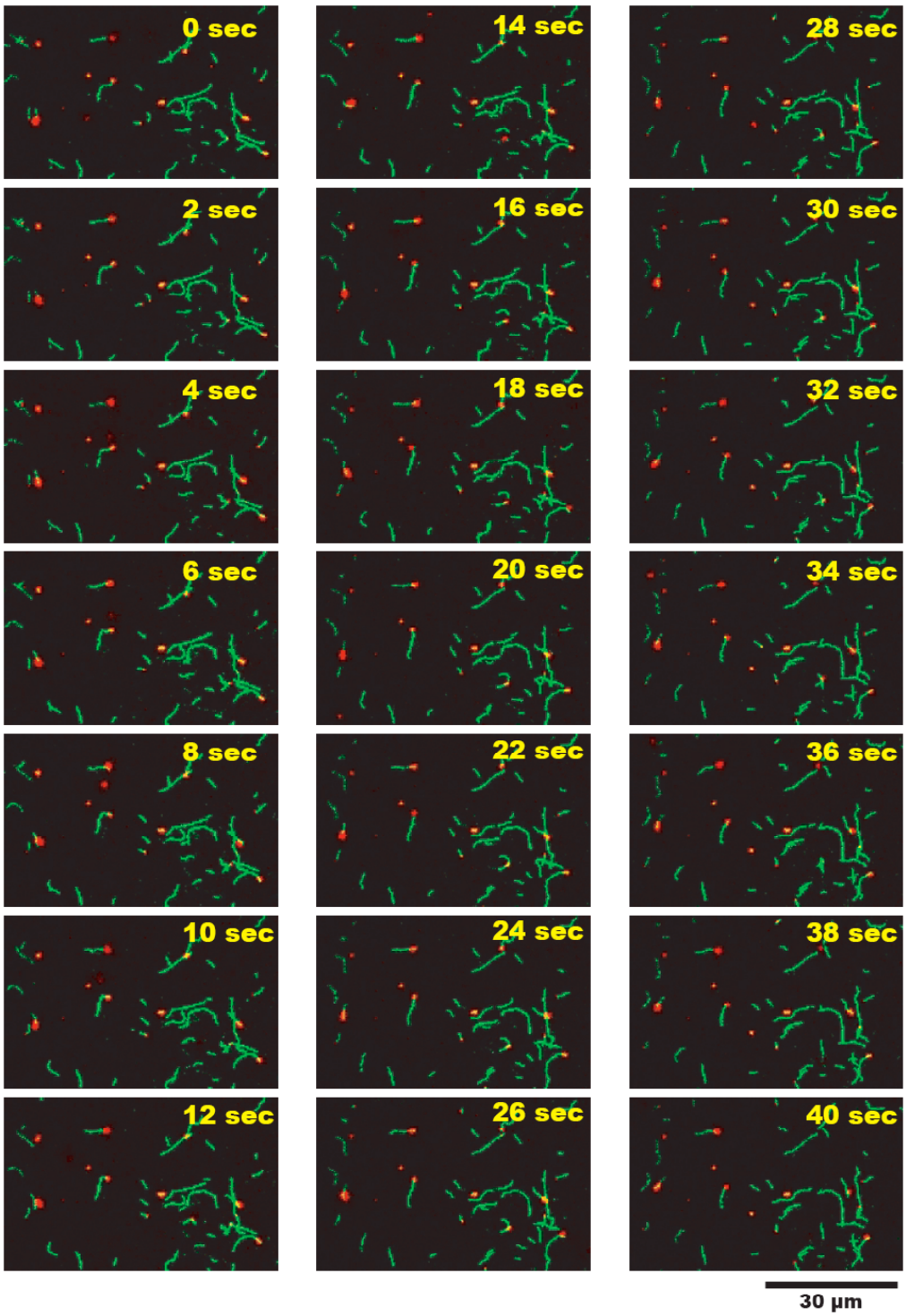

Figure A-2. Sequential images of the polarity-marked actin filaments moving on a myosin 6-coated glass surface (M6IQ1).

APPENDIX B

THE MEANING OF RATE CONSTANTS

Enzymatic reactions are stochastic events. The distribution of the reaction time (time required for the completion of a single reaction) is best explained by a Poisson distribution. This is easily confirmed empirically – a reaction time course always follows an exponential path. Thus, the distribution of the probability of reaction time is described as

$$P(t) = ke^{-kt}dt$$

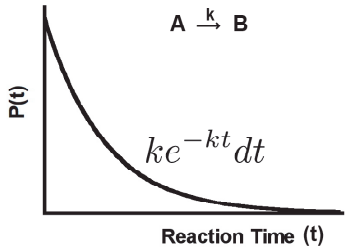

From this probability function, the average reaction time is calculated.

$$\begin{aligned}
\int_0^\infty tP(t) &= k\int_0^\infty te^{-kt}dt \\
&= k\left(\left|t(-\frac{1}{k})e^{-kt}\right|_0^\infty - \int_0^\infty -\frac{1}{k}e^{-kt}dt\right) \\
&= k\left(\left|-\frac{t}{k}e^{-kt}\right|_0^\infty + \frac{1}{k}\left|-\frac{1}{k}e^{-kt}\right|_0^\infty\right) \\
&= k(0 + \frac{1}{k} \times \frac{1}{k}) \\
&= \frac{1}{k}
\end{aligned}$$

For example, the reaction rate of “5/sec” means that it takes 0.2 seconds to complete each reaction on average, or five reactions occurs in a second on average. Since the rate constants depend on an experimental condition, especially on the temperature, care has to be taken for comparison of rate constants obtained from different procedures.

APPENDIX C

ENZYME KINETICS

The kinetic mechanism of myosin ATPase reaction

In general, the reaction scheme of actomyosin ATPase can be described as follow.

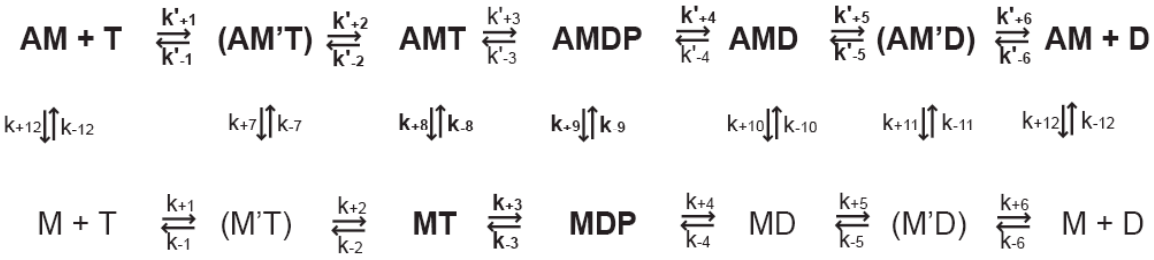

Abbreviations: A, actin; M, myosin; T, ATP; D, ADP; P, phosphate.

Equilibrium constants (K) are defined here as k_+/k_- (ex. $K'_1 \equiv k'_{+1}/k'_{-1}$).

The combination of individual rate constants determines the unique motor property of myosin. Experimental methods for obtaining those rate constants (and the equilibrium constants) with mathematical explanations are described below.

Actin-myosin binding kinetics

The motor domain of myosin tightly binds to actin in the presence of ADP or in the absence of nucleotide. The fraction of the tightly actin-bound reaction intermediate determines the duty ratio of the molecule. The reaction scheme of actin-myosin binding in the absence of nucleotide or in the presence of ADP is described as

$$A + M \underset{k_{+12}}{\overset{k_{-12}}{\rightleftarrows}} AM \qquad A + MD \underset{k_{+10}}{\overset{k_{-10}}{\rightleftarrows}} AMD$$

The fluorescence intensity of pyrene-actin decreases upon binding of myosin. Thus the formation of AM or AMD can be followed by simply monitoring the fluorescence intensity of pyrene. Light scattering measurement is also employed as an alternative method to monitor the binding of myosin to actin – the intensity increases upon binding of myosin to actin. The reaction time course of the AM formation follows a single exponential path, and the apparent rates are explained by

$$k_{obs} = k_{-12}[A] + k_{+12}$$

This is derived from the following calculation.

$$\begin{aligned}
\frac{d[AM]}{dt} &= k_{-12}[A][M] - k_{+12}[AM] \\
&= k_{-12}[A](M_0 - [AM]) - k_{+12}[AM] \qquad M_0 \equiv [M] + [AM] \\
&= k_{-12}[A]M_0 - (k_{-12}[A] + k_{+12})[AM]
\end{aligned}$$

$$\int_0^{AM} \frac{d[AM]}{k_{-12}[A]M_0 - (k_{-12}[A] + k_{+12})[AM]} = \int_0^t dt$$

$$-\frac{1}{k_{-12}[A] + k_{+12}} ln \frac{k_{-12}[A]M_0 - (k_{-12}[A] + k_{+12})[AM]}{k_{-12}[A]M_0} = t$$

$$[AM] = \frac{k_{-12}[A]}{k_{-12}[A] + k_{+12}} M_0 (1 - e^{-(k_{-12}[A] + k_{+12})t})$$

The exponent gives apparent rate constants (k_{obs}) at given actin concentrations. By plotting the apparent rates against the actin concentrations, k_{-12} and k_{+12} are obtained from the slope and from the y-intercept, respectively.

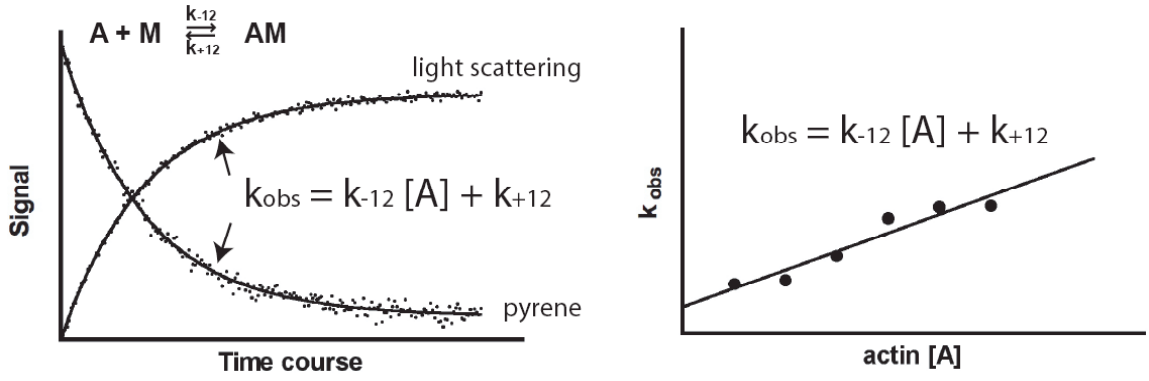

If myosin is premixed with pyrene-actin first and rapidly mixed with excess amount of unlabeled actin, the apparent rate constant of the pyrene fluorescence increment would become k_{+12}. This experiment is often performed for determining k_{+12}, because, for many myosins, k_{+12} (and also k_{+10}) is too small to be determined precisely from the y-intercept. By performing the same experiment described above in the presence of saturating ADP, k_{+10} and k_{-10} will be determined.

Nucleotide binding to myosin

Nucleotide (ATP and ADP) binding to myosin is a two-step process. First, nucleotide quickly binds to (also quickly dissociates from) the active site of myosin and forms a collision complex (shown in parentheses in the reaction scheme). This first step is thought to be in a rapid equilibrium, followed by the second, a relatively slow

isomerization step. The nucleotide binding process is visualized by using fluorescently labeled nucleotide analogs such as mant-ATP (or ADP). The fluorescence intensity of those nucleotide analogs increases several-fold due to isomerization of the motor domain upon binding to the nucleotide. The reaction schemes of the nucleotide binding are as follows. Mathematically, they are all treated in the same way.

For mathematically describing the ATP binding to myosin in the absence of actin, the followings are first defined.

$$K_1 \equiv \frac{k_{+1}}{k_{-1}} = \frac{[M'T]}{[M][T]} \qquad M_0 \equiv [M] + [M'T] + [MT]$$

$$[M] = \frac{M_0 - [MT]}{1 + K_1[T]}$$

By these definitions, the rate of MT formation can be written as

$$\begin{aligned}\frac{d[MT]}{dt} &= k_{+2}[M'T] - k_{-2}[MT] \\ &= K_1 k_{+2}[M][T] - k_{-2}[MT] \\ &= K_1 k_{+2}[T]\frac{M_0 - [MT]}{1 + K_1[T]} - k_{-2}[MT] \\ &= \frac{K_1 k_{+2}[T]M_0}{1 + K_1[T]} - \left(\frac{K_1 k_{+2}[T]}{1 + K_1[T]} + k_{-2}\right)[MT]\end{aligned}$$

By solving this differential equation, we obtain the time-dependent function of MT.

$$\int_0^{MT} \frac{d[MT]}{\frac{K_1 k_{+2}[T] M_0}{1+K_1[T]} - (\frac{K_1 k_{+2}[T]}{1+K_1[T]} + k_{-2})[MT]} = \int_0^t dt$$

$$-\frac{1}{\frac{K_1 k_{+2}[T]}{1+K_1[T]} + k_{-2}} ln \frac{\frac{K_1 k_{+2}[T] M_0}{1+K_1[T]} - (\frac{K_1 k_{+2}[T]}{1+K_1[T]} + k_{-2})[MT]}{\frac{K_1 k_{+2}[T] M_0}{1+K_1[T]}} = t$$

$$[MT] = \frac{\frac{K_1 k_{+2}[T]}{1+K_1[T]} M_0}{\frac{K_1 k_{+2}[T]}{1+K_1[T]} + k_{-2}} (1 - e^{-(\frac{K_1 k_{+2}[T]}{1+K_1[T]} + k_{-2})t})$$

The exponent is an apparent rate constant (k_{obs}) that will be obtained in an actual experiment. The k_{obs} is ATP dependent and is reminiscent of the Michaelis-Menten equation.

$$k_{obs} = \frac{K_1 k_{+2}[T]}{1 + K_1[T]} + k_{-2} = \frac{k_{+2}[T]}{1/K_1 + [T]} + k_{-2}$$

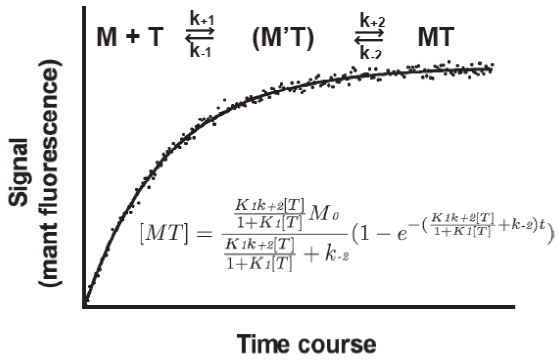

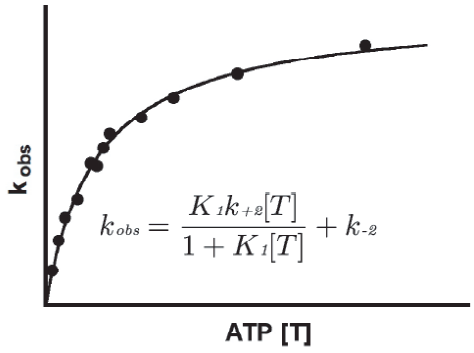

If $1/K_1 >> [T]$,

$$\frac{k_{+2}[T]}{1/K_1 + [T]} + k_{-2} \cong \frac{k_{+2}[T]}{1/K_1} + k_{-2} = K_1 k_{+2}[T] + k_{-2}$$

This explains the initial slope of the ATP-dependent k_{obs} curve. Pyrene-labeled actin is also used for monitoring AMT formation. Actin binds weakly to myosin at the AMT state, and the fluorescence intensity of pyrene increases during the formation of this weakly-bound actomyosin state.

Light scattering measurement is performed for monitoring ATP-induced actomyosin dissociation. For most myosins characterized so far, ATP-induced actomyosin dissociation (k_{+8}) is a quick process, and thus the ATP-dependent k_{obs} curve is indistinguishable from that obtained by pyrene-actin. This was also the case for myosin 10 (see Chapter III). If $k'_{+2} > k_{+8}$, however, the maximum k_{obs} value obtained from light scattering experiment represents $k_{+8} + k_{-8}[A]$, instead of $k'_{+2} + k'_{-2}$.

ATP hydrolysis

In general, the ATP hydrolysis step of myosin is a relatively quick, reversible process as if myosin is chewing up ATP. This step is simply described as

$$\mathrm{MT} \underset{k_{-3}}{\overset{k_{+3}}{\rightleftarrows}} \mathrm{MDP} \qquad \mathrm{AMT} \underset{k'_{-3}}{\overset{k'_{+3}}{\rightleftarrows}} \mathrm{AMDP}$$

The ratio of k_{+3} to k_{-3} (or k'_{+3} to k'_{-3}) determines the fraction of apparently hydrolyzed ATP at this step. It is called the burst size (B).

$$B \equiv \frac{k_{+3}}{k_{+3} + k_{-3}}$$

The burst size can be directly determined by using [γ^{32}P]ATP. After mixing myosin with substoichiometric concentration of [γ^{32}P]ATP, the mixture is quickly mixed with strong acid to inactivate myosin at various time, and the released γ^{32}P is titrated. If the hydrolysis rate (k_{+3}) and the ATP binding rate under the experimental condition (K_1k_{+2}[T]) are faster than the phosphate release rate (k_{+4}), the time-dependent ATP hydrolysis profile is explained by two-phase exponential kinetics. The first phase represents the rate of ATP binding, and the second phase represents phosphate release. The fraction of the amplitude of the fast phase represents the burst size. Due to the use of substoichiometric concentrations of ATP, ATP binding cannot be regarded as a pseudo first order reaction. However, for a practical purpose, this can be ignored for determining the burst size.

The sum of the forward rate and the backward rate ($k_{+3} + k_{-3}$) is determined from the maximum apparent ATP hydrolysis rate under saturating ATP condition if $k_{+2} > (k_{+3} + k_{-3})$. However, this is not practical in general, because the signal to noise ratio plummets with higher concentrations of [γ^{32}P]ATP. Using higher concentration of myosin would compensate the effect, however, this is not practical for determining the maximum k_{obs}, either. There is a relatively conserved tryptophan residue at the tip of the relay helix of myosin head (Fig. F-8), and the fluorescence intensity of this tryptophan increased at the post hydrolysis state. Thus, measurement of the tryptophan fluorescence intensity has

been an alternative way of monitoring the formation of the MDP state. Under low concentrations of ATP ($K_1k_{+2}[T] << (k_{+3} + k_{-3})$), the apparent ATP-dependent k_{obs} curve follows $K_1k_{+2}[T]$ because the rate is limited by ATP binding. If the rate of ATP binding well exceeds the ATP hydrolysis rate under saturating ATP, $k_{+2} > (k_{+3} + k_{-3})$, we can ignore the ATP binding step as if the whole reaction just starts from the MT state. Thus the differential equation describing the formation of MDP can be simplified as follows, and the solution will be

$$\begin{aligned}\frac{d[MDP]}{dt} &= k_{+3}[MT] - k_{-3}[MDP] \\ &= k_{+3}(MT_0 - [MDP]) - k_{-3}[MDP] \qquad MT_0 \equiv [MT] + [MDP] \\ &= k_{+3}MT_0 - (k_{+3} + k_{-3})[MDP]\end{aligned}$$

$$\int_0^{MDP} \frac{d[MDP]}{k_{+3}MT_0 - (k_{+3} + k_{-3})[MDP]} = \int_0^t dt$$

$$-\frac{1}{k_{+3} + k_{-3}} ln \frac{k_{+3}MT_0 - (k_{+3} + k_{-3})[MDP]}{k_{+3}MT_0} = t$$

$$[MDP] = \frac{k_{+3}}{k_{+3} + k_{-3}} MT_0(1 - e^{-(k_{+3}+k_{-3})t})$$

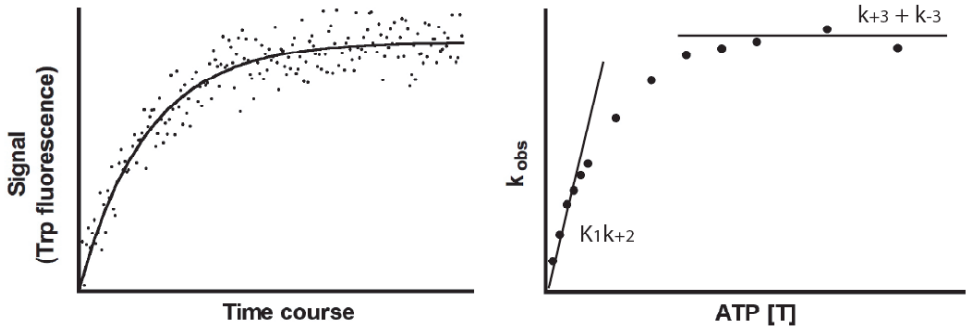

At intermediate concentrations of ATP where $K_1k_{+2}[T]$ is comparable to $(k_{+3} + k_{-3})$, the reaction cannot be simplified as a single step reaction. The whole reaction should be described as a sequential reaction (M ↔ MT ↔ MDP), and the formation of MDP should

not be explained by single exponential kinetics. However, single exponential fittings are usually performed to obtain the k_{obs} values at intermediate ATP conditions, and the maximum k_{osb} (k_{+3} + k_{-3}) is practically estimated by curve fiting using the Michaelis-Menten equation, although these are theoretically not correct. By knowing the burst size, the k_{+3} and k_{-3} values are determined individually.

Inorganic phosphate release

Phosphate release from the active site of myosin is directly monitored by using coumarin-labeled phosphate binding protein (MDCC-PBP). Phosphate binding to MDCC-PBP is very quick (136 $\mu M^{-1}sec^{-1}$) and the fluorescence intensity of coumarin increases ~5-fold upon phosphate binding. For measuring the phosphate release rate, myosin and ATP are first mixed and aged for ensuring the complete ATP binding. This time duration is determined by the ATP binding rate under the experimental condition employed. Then the MT–MDP mixture is quickly mixed with MDCC-PBP with or without actin. The rate of the phosphate release is determined by monitoring the rate of fluorescence intensity increase of MDCC-PBP. The phosphate re-binding rates (k_{-4} and k'_{-4}) are often ignored because they are very small compared to the release rates. This fact is easily confirmed by measuring the steady-state ATPase activity of myosin in the presence of excess amount of phosphate – the ATPase activity is barely inhibited by 1~2 mM of phosphate.

In the absence of actin, the phosphate release step is described as follows, and thus the release of phosphate is explained by a simple exponential kinetics.

$$MDP \xrightarrow{k_{+4}} MD + P$$

$$[MD] = [P] = MDP_0(1 - e^{-(k_{+4})t})$$

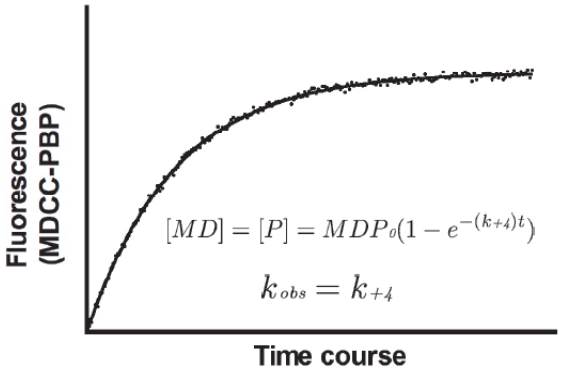

k_{+4} is directly determined by the apparent rate of the phosphate release in a single experiment. (k_{+4} is also determined from the apparent rate of the second exponential in the burst size determination experiment described above.)

In the presence of actin, the reaction scheme is described as a parallel reaction.

$$\begin{array}{ccccc} A + MDP & \underset{k_{+9}}{\overset{k_{-9}}{\rightleftarrows}} & AMDP & \xrightarrow{k'_{+4}} & AMD + P \\ \downarrow{\scriptstyle k_{+4}} & & & & \\ MD + P & & & & \end{array}$$

The description of the rate of the actin-dependent phosphate release process is analogous to that of nucleotide binding rates. (Caution: the reverse rate (k'_{-4}) is ignored, and the K_9 is defined as k_{+9}/k_{-9}.)

$$k_{obs} = \frac{k'_{+4}[A]}{K_9 + [A]}$$

Thus, the overall phosphate release rate is described as follow (see below for a parallel reaction).

$$k_{obs} = \frac{k'_{+4}[A]}{K_9 + [A]} + k_{+4}$$

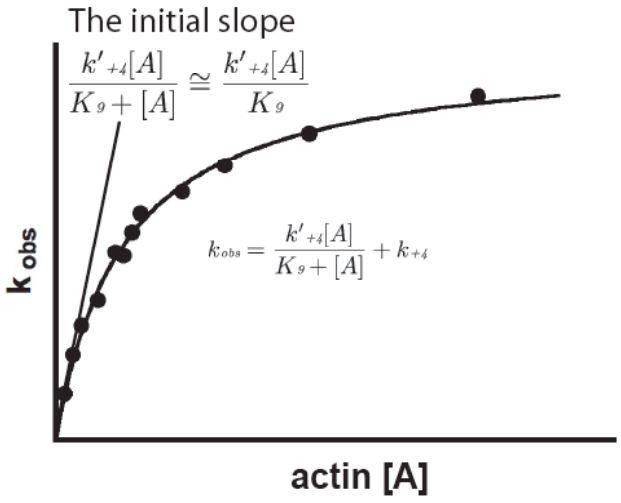

As in the case of nucleotide bindings, under low concentration of actin ([A]<<K_9), the slope can be simply described as k'_{+4} / K_9, which is analogous to "K_1k_{+2}" for the ATP binding kinetics. K_9 and K_8 are usually regarded as rapid equilibrium constants.

Parallel reaction

The time-dependent function of the formation of "b" is derived as follow.

$$\xleftarrow{k_a} a \xrightarrow{k_b} b$$

$$\frac{d[a]}{dt} = -(k_a + k_b)[a]$$

$$[a] = a_0 e^{-(k_a+k_b)t}$$

$$\frac{d[b]}{dt} = k_b[a]$$

$$= k_b a_0 e^{-(k_a+k_b)t}$$

$$[b] = k_b a_0 \int_0^t e^{-(k_a+k_b)t} dt$$

$$= \frac{k_b a_0}{k_a + k_b}(1 - e^{-(k_a+k_b)t})$$

The apparent rate of the formation of "b" becomes ($k_a + k_b$).

APPENDIX D

KINETICS SIMULATION

The objective of performing enzyme kinetic analysis of myosin 10 is to estimate the duty ratio – the fraction of strongly actin-bound intermediates (AMD and AM). Based on the rate constants and equilibrium constants obtained in the current study, the fractions of the reaction intermediates were estimated by computer simulation described below. The fraction of AMDP at steady-state determines the steady-state ATPase activity. Under the saturating ATP condition, the ATP binding rate reaches the maximum rate (k'_{+2} ~ 800 sec^{-1}). The ATP regeneration system (pyruvate kinase + phosphoenolpyruvate) eliminates free ADP, thus the ADP re-binding process can be ignored. In the presence of actin, the ATPase reaction scheme of myosin 10 can be simplified as bellow.

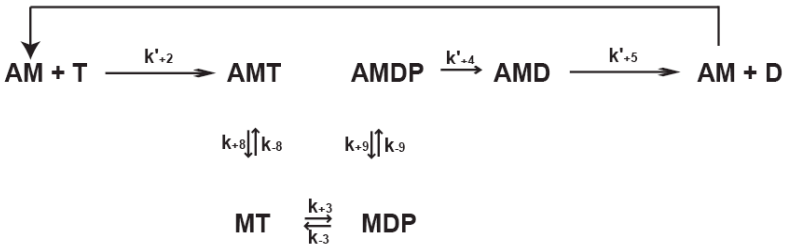

This reaction scheme is expressed as follows in STELLA v8.1.1 software (iseesystems, Lebanon, NH). The simulation was performed by Runge-Kutta 4th approximation with

calculation time interval of 50 μsec. Halving and doubling the calculation time interval did not affect the result.

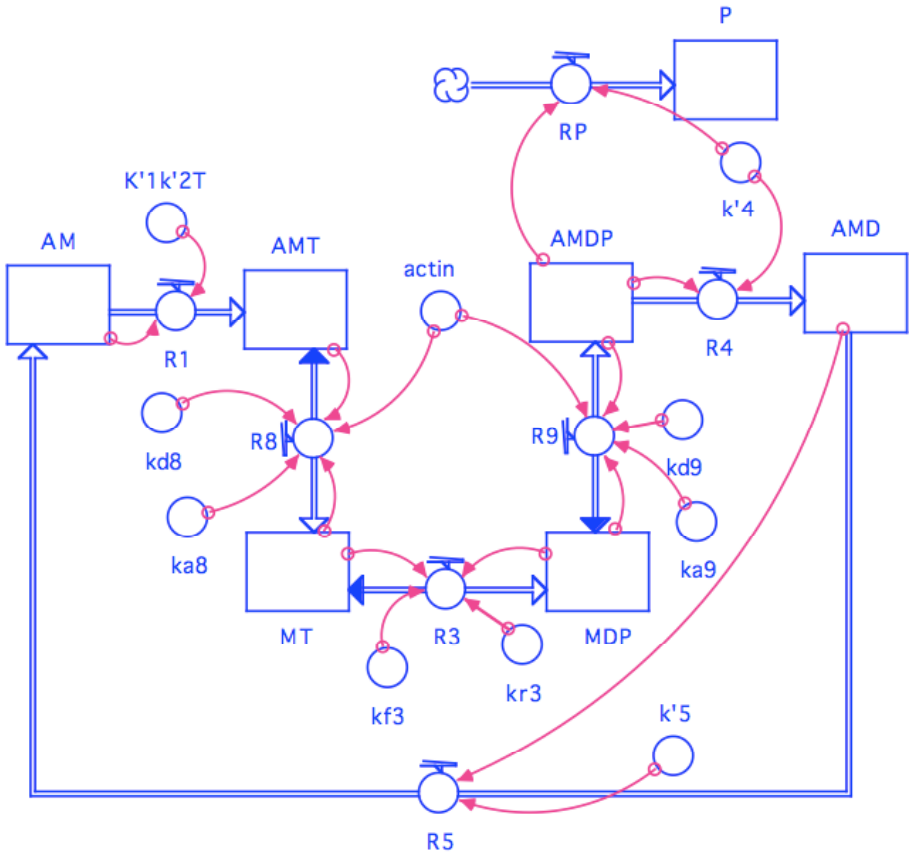

AM(t) = AM(t - dt) + (R5 - R1) * dt

INIT AM = 1

INFLOWS:

R5 = k'5*AMD

OUTFLOWS:

R1 = K'1k'2T*AM

AMD(t) = AMD(t - dt) + (R4 - R5) * dt

INIT AMD = 0

INFLOWS:

R4 = k'4*AMDP

OUTFLOWS:

R5 = k'5*AMD

AMDP(t) = AMDP(t - dt) + (R9 - R4) * dt

INIT AMDP = 0

INFLOWS:

R9 = ka9*actin*MDP-kd9*AMDP

OUTFLOWS:

R4 = k'4*AMDP

AMT(t) = AMT(t - dt) + (R1 - R8) * dt

INIT AMT = 0

INFLOWS:

R1 = K'1k'2T*AM

OUTFLOWS:

R8 = kd8*AMT-ka8*actin*MT

MDP(t) = MDP(t - dt) + (R3 - R9) * dt

INIT MDP = 0

INFLOWS:

R3 = kf3*MT-kr3*MDP

OUTFLOWS:

R9 = ka9*actin*MDP-kd9*AMDP

MT(t) = MT(t - dt) + (R8 - R3) * dt

INIT MT = 0

INFLOWS:

R8 = kd8*AMT-ka8*actin*MT

OUTFLOWS:

R3 = kf3*MT-kr3*MDP

P(t) = P(t - dt) + (RP) * dt

INIT P = 0

INFLOWS:

RP = k'4*AMDP

actin = 10

K'1k'2T = 800

k'4 = 100

k'5 = 23

ka8 = 100

ka9 = 154

kd8 = 10000

kd9 = 10000

kf3 = 184

kr3 = 216

APPENDIX E

TOTAL INTERNAL REFLECTION MICROSCOPE (TIRFM)

The prism-type total internal reflection microscope was built and used in the current study. The advantage of the prism-type TIRFM is its wider observation area with lower background. The disadvantage is the limitation of the thickness of the samples (the sample thickness must be smaller than the working distance of the objective lens). For the *in vitro* single molecule experiment described in Chapter IV, the thickness limitation does not pose any problem. The schematic representation of the TIRFM setup employed in this study is shown below.

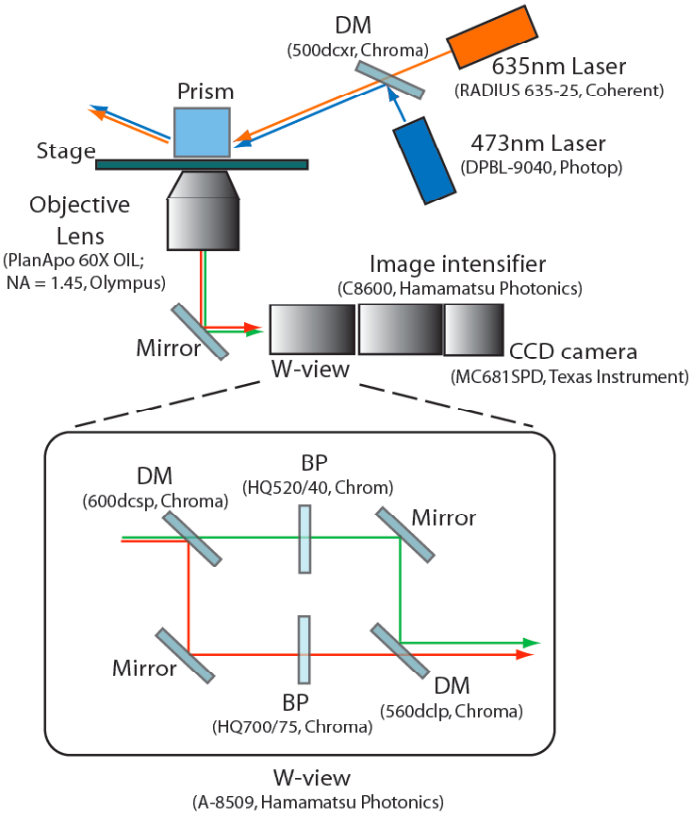

The evanescent field

The total internal reflection microscope (TIRFM) utilizes the evanescent field for illuminating fluorescent samples. The evanescent field is easily obtained by letting the incident light totally reflect on the glass–solution interface. Since its intensity exponentially decays from the glass surface, the evanescent field typically illuminates only 50 ~ 200 nm from the glass surface. Therefore, individual fluorescent sources near the glass surface are visualized with a very high signal-to-noise ratio.

Why does the evanescent field "leak" into the solution, although the incident light totally reflects on the glass-solution interface? Why does it illuminate such a shallow depth from the interface?

Light is described as an electromagnetic wave. When the incident light reflects on the glass-solution interface, two electromagnetic fields – one for the incident light and the other for the reflected light - exist in the glass side. The electromagnetic fields are not vanished suddenly on the solution side. Thus the energy of the electromagnetic fields leaks, but it no longer propagates through the solution side because the energy of the evanescent field does not flow perpendicular to the reflection surface. This leak of the energy of the electromagnetic fields is called evanescent field.

The intensity of the evanescent field exponentially decays with perpendicular distance (z) from the reflection interface:

$$I(z) = I_0 e^{-z/d}$$

where

$$d = \frac{\lambda}{4\pi\sqrt{n_g{}^2 sin^2\theta - n_s{}^2}}$$

Parameter λ is the wavelength of the incident light in vacuum. n_g and n_s are the reflective indexes of the glass and the solution, respectively. θ is the incident angle (measured from the normal to the interface).

APPENDIX F

MOLECULAR MECHANISM OF THE DETERMINATION OF MYOSIN DIRECTIONALITY

Although the results described in this section are worth mentioning in the main body of this thesis, they are treated as an appendix because the contents are not directly related to the study on myosin 10. The results provide important insights into how the movement directionality of myosin is determined.

Introduction

Movement directionality of motor proteins is one of the most important characteristics that define their distinct physiological functions in a cell. As mentioned in Chapter II, the plus end-directed movement directionality of myosin 10 suggests the possible physiological function as a plus end-directed transporter inside filopodia.

What determines the movement directionality of myosins? Myosin 6 was the first myosin identified as a minus end-directed myosin, and it is proposed that the unique 53-amino acid insertion in the neck region of the molecule is responsible for the minus end-directed movement by acting as a reversed lever (Wells et al., 1999). The hypothesis was convincing because only class 6 myosins retain the unique insertion in the neck, and it

was the sole myosin identified as a minus end-directed myosin when it was first characterized. The neck region of myosin 6 turned out to be actually redirected by ~120^{o} relative to plus end-directed myosins (Fig. F-1), (Menetrey et al., 2005). Tsiavaliaris *et al*. have successfully converted the plus end-directed movement of myosin 1 (MyoE) into the opposite direction by attaching protein motifs at the C-terminal end of the neck so that the direction of the C-terminal tip is redirected ~180^{o} (Tsiavaliaris et al., 2004). The result strongly supports the lever-arm hypothesis in which the movement directionality and the step size of a myosin molecule are determined by the direction and the length of the neck. However, it is important to confirm if the minus end-directed movement of myosin 6 is simply achieved by the apparently redirected neck. Identification of myosin 9b, which does not have such a unique insertion in the neck region, as another minus end-directed myosin (Inoue et al., 2002) argued against the reversed lever hypothesis, although the minus end-directed movement directionality of myosin 9b is controversial (O'Connell and Mooseker, 2003).

In this chapter, a series of chimeric myosin constructs using parts from myosin 5a (plus end-directed) and myosin 6 (minu edn-directed) were generated to identify the site(s) in a myosin molecule that is responsible for determining the movement directionality.

Materials and methods

Materials - Nickel-nitrilotriacetic acid agarose (Ni-NTA) was purchased from Qiagen (Hilden, Germany). For other materials, see "Materials and methods" in Chapter II.

Cloning of human myosin 6 - Human kidney total RNA was purchased from Clontech (Mountain View, CA), and cDNA library was obtained by reverse transcription with random oligonucleotides. The entire ORF region of myosin 6 (Met 1 – Lys 1285) was subcloned in pFastBac vector (for baculovirus expression system) with *Eco*RI site and *Mlu*I site at 5'-side and 3'-side, respectively.

Cloning of human myosin 5a - Human brain total RNA was purchased from Clontech (Mountain View, CA), and cDNA library was obtained by reverse transcription with random oligonucleotides. A partial ORF region of myosin 5a (Met 1 – Lys 1189) was subcloned in pFastBac vector (for baculovirus expression system) with *Eco*RI site and *Mlu*I site at 5'-side and 3'-side, respectively.

Construction of myosin 5a–myosin 6 chimera - The myosin consructs were generated by two-step PCR method by using human myosin 5a and human myosin 6. (Zarrinpar et al., 2003)

Baculovirus preparation - See "Materials and methods" in Chapter II.

Protein expression and purification - To express the recombinant myosin 5a, myosin 6, or myosin 5a – myosin 6 chimeric constructs, Sf9 cells (approximately 8 x 10^7 cells) were co-infected with two viruses expressing the myosin heavy chain and calmodulin. The infected cells were harvested after culturing for three days at 28^{o}C, and washed with a buffer containing (150 mM NaCl, 30 mM Tris-HCl, pH 7.5, and 5 mM EGTA). The cells were then lysed by sonication in 4 ml of lysis buffer (100 mM NaCl, 30 mM Tris-HCl, pH 7.5, 2 mM $MgCl_2$, 0.2 mM EGTA, 1 mM ATP, 1 mM phenylmethyl sulfonyl fluoride, 0.1 mg/ml trypsin inhibitor, 10 µg/ml leupeptin, 1 mM 2-mercaptoethanol). After centrifugation at 300,000 ×g for 10 min at 4^{o}C, the supernatant was incubated with 100 µl of Ni-NTA resin in a 5-ml plastic tube on a rotation wheel for 15~20 min at 4^{o}C. The resin suspension was then loaded in a column (1 x 10 cm) and washed with 5 ml of a wash buffer (300 mM NaCl, 20 mM Tris-HCl, pH 7.5, 10 mM Imidazole-HCl, pH 7.5, 0.1 mM EGTA, 10 µg/ml leupeptin, and 1 mM 2-mercaptoethanol). Protein was eluted with a buffer containing 100 mM NaCl, 200 mM Imidazole-HCl, pH 7.5, 0.1 mM EGTA, 5 µg/ml leupeptin, and 1mM 2-mercaptoethanol. Freshly prepared DTT (1 mM final concentration) was added to the eluted fraction, and stored on ice.

Polarity-marked actin filaments - See "Materials and methods" in Chapter II.

In vitro motility assay - See "Materials and methods" in Chapter II.

Results

Myosin 5a and myosin 6 were used for generating chimeric myosin constructs to identify the region(s) responsible for directionality determination because of their similarity in motor property and opposite movement directionalities. By having ADP release step as the predominant rate-limiting step during the ATPase cycle (De La Cruz et al., 2001; De La Cruz et al., 1999), both of them are highly processive motors that move along actin filaments as dimers in a hand-over-hand mechanism. The crystal structures of the motor domain are now available for both myosin 5a (Coureux et al., 2004) and myosin 6 (Menetrey et al., 2005) (Fig. F-1), which enable us to carefully design chimeric constructs.

The unique insertion in the neck of myosin 6

Before the crystal structures of myosin 5a and myosin 6 became available, we examined the effect of the unique insertion only found in the neck of myosin 6 by generating myosin 5a-myosin6 hybrids. The result is summarized in Figure F-2 and Table F-1. Contrary to the general expectation, we found that the swapping of the neck did not reverse the inherent movement directionality of each myosin, although the actin translocating activity was significantly reduced. Thus, we concluded that the globular core domain of myosin determines the movement directionality.

After the crystal structures of myosin 5a and myosin 6 became available, our result on M6M5HMM was reexamined by Park *et al*. by generating similar chimera using

different joining point (Park et al., 2007). They have successfully converted the minus end-directed motility of myosin 6 into plus end-directed motility by replacing the neck region with that of myosin 5a. Since the converter domain and the beginning of the neck region reside at the close proximity, replacement of the whole neck region of myosin 6 with that of myosin 5a may have disrupted an intramolecular interaction of the converter-neck in our M6M5HMM construct (Fig. F-3). In order to further examine this issue, we generated additional chimeras based on the recently available information from the crystal structures. (Fig. F-4). M6M5conv has the globular motor domain of myosin 6 followed by the converter and the neck of myosin 5a. M6M5dPro has the globular motor domain and the converter domain of myosin 6 followed by the neck of myosin 5a after Asp 773 of myosin 6. Since the neck of myosin 6 is bent at the proline 774, the elimination of the proline residue was expected to extend the neck of M6M5dPro (Fig. F-3). Both chimeric constructs showed plus end-directed motility (Table F-2), suggesting that the minus end-directed movement of myosin 6 is determined by the reorientated neck as proposed.

If the orientation of the neck is the sole determinant of movement directionality, the plus end-directed motility of myosin 5a should be converted into the opposite direction by introducing the reorientated neck of myosin 6. However, conversion of the plus end-directionality of myosin by using myosin parts has not succeeded yet. As shown in Figure F-2, replacement of the whole converter-neck region of myosin 5a with that of myosin 6 did not change the plus end-directionality, implying that the apparently

reorientated neck itself is not the sole determinant of the minus end-directed motility of myosin 6.

The N-terminal variable region

The N-terminal region of myosin resides at close proximity of the converter-neck region (Fig. F-1), and is highly variable among the superfamily (Fig. F-5). The lever arm hypothesis claims that the conformational change inside the globular motor domain induced by the hydrolysis of ATP changes the conformation of the converter domain, which allows the lever arm to swing. Since the neck of myosin 6 is reorientated by ~120^{o} relative to plus end-directed myosins, the N-terminal region of myosin 6 might have coevolved with the converter-neck region to facilitate the opposite swing of the neck. The effect of the N-terminal region on the movement directionality was tested by using chimeras shown in Figure F-6, and the result was summarized in Table F-2. Although the actin translocating velocities were reduced, the original movement directionalities of myosin 5a and myosin 6 were not affected by the deletion of the N-terminal variable regions themselves (dM5 and dM6).

Removal of the N-terminal variable region of myosin 5a (dM5M6) or replacement of the variable region with that of myosin 6 (M6M5M6) did not improve the result of the M5M6HMM chimera used in our previous study (Fig. F-2 and Table F-1), rather, those chimeras lost actin translocating activity. Removal of the N-terminal variable region of myosin 6 (dM6M5) or replacement with that of myosin 5a (M5M6M5) did not change

the result on M6M5conv, suggesting that the N-terminal variable region of myosin has little effect on the determination of the movement directionality.

The contribution of the N-terminal region to movement directionality was further examined by using additional chimeras shown in Figure F-7. Although the M5M6M5LP chimeras showed comparable actin translocating velocities to M6M5conv chimeras, M6M5M6LP did not show any motility (Table F-2).

Altogether, the results suggest that the N-terminal region of myosin is not important for deciding the movement directionality. The effect of the N-terminal region of myosin was not pursued further.

The relay helix

The relay helix translocates in response to the conformational change inside the core of the motor domain induced by ATP hydrolysis (Fig. F-8). This conformational change is responsible for the increase in the fluorescence of the relatively conserved tryptophan residue at the tip of the relay helix. It has been proposed that this translocation of the relay helix changes the conformation of the converter domain, thus allowing the neck to swing (Fig. F-8). The primary structure of the relay helix and the converter region are relatively conserved among myosins, and the apparent positioning of those regions in the crystal structure of myosin 6 looks similar to other myosins (Fig. F-1). However, it may be possible that a subtle difference in the relay helix-converter interaction is essential for the reorientated lever arm to swing backward. To test this possibility, we generated a series of chimeric myosin constructs shown in Figure F-9.

Although the actin translocating velocities of M5relay and M6relay were reduced, replacement of the relay helix itself did not affect the plus end-directed motility of myosin 5a and the minus end-directed motility of myosin6 (Table F-2). Replacement of the relay helix region of M5M6conv with that of myosin 6 (M5M6relay) did not confer minus end-directed motility to the construct, either. Likewise, replacement of the relay helix region of M6M5conv with that of myosin 5a (M6M5relay) did not rescue the slow, plus end-directed actin translocation of the M6M5conv construct. These results suggest that the relay helix-converter interaction of myosin 6 is not uniquely adjusted for the minus end-directed motility.

The small insertion in the motor domain

Besides the insertion in the neck, myosin 6 has another small insertion at the vicinity of the ATP binding site (Fig. F-5 and Fig. F-10). The small insertion is responsible for the very slow second-order ATP binding rate of myosin 6 (Menetrey et al., 2005). The deletion of the insertion not only increases the second-order ATP binding rate, but also increases the maximum ATPase activity of myosin 6 by increasing the ADP release rate ~3-fold (Menetrey et al., 2005). Recently, this small insertion has been found to be important for coordination of the two heads of myosin 6 for the processive movement – deletion of the insert abolishes the processibly of myosin 6 (Sweeney et al., 2007). We generated a myosin 6 construct in which small insertion region was replaced with the comparable region of myosin 5a (Fig. F-10). This chimera (M6ins5) showed ~3-fold increase in actin translocating velocity that is consistent with the ~3-fold increment

of the ATPase activity reported previously (Menetrey et al., 2005). However, the movement directionality did not change. Similarly, introducing the small insertion of myosin 6 to M5M6conv did not confer minus end-directed motility on the construct (Fig. F-10B and Table F-2). These results suggest that the small insertion in the motor domain of myosin 6 is not essential for the minus end-directed motility.

Discussion

In this chapter, a number of hybrid myosin constructs were generated and their movement directionalities were tested to identify the region(s) inside the myosin molecule that is responsible for determining the movement directionality. Because we were not able to identify the exact region(s) responsible for determining the directionality, a possible molecular mechanism behind the directionality is discussed by referring to some advanced studies on kinesin motors.

Kinesin and its related protein, non-claret disjunctional (Ncd) protein, are microtubule-based molecular motors that move along a microtubule towards plus end and minus end, respectively. Kinesin and Ncd have very similar motor core structures to those of myosins (Fig. F-11), implying that they share similar ATP-driven motor mechanism. The motor core domain of Ncd directly interacts with the distal end of the stalk, and the motor core region is relatively immobilized against the stalk (Sablin et al., 1998). Unlike Ncd, the motor core domain of kinesin does not directly interact with the stalk because of a linker region that joins the motor core and the stalk. This so-called

'neck linker' region comprised of ~15 amino acids was proposed to be important for the efficient unidirectional processive movement of kinesin. The neck regions of kinesin and Ncd have been identified to be responsible for dictating the movement directionality. Fusing the neck and stalk of kinesin (plus end-directed) to the motor core of Ncd (minus end-directed) generated a plus end-directed motor (Case et al., 1997; Henningsen and Schliwa, 1997), whereas fusing the neck and stalk from Ncd to the motor core of kinesin generated a minus end-directed motor (Endow and Waligora, 1998). These neck regions of kinesin and Ncd roughly correspond to the converter region of myosins (Fig. F-11), and the neck linker region of kinesin is often compared to the lever arm of myosin. Remarkably, however, disruption of the structure of the neck linker did not affect the plus end-directed motility of kinesin (Case et al., 2000; Inoue et al., 1997; Sablin et al., 1998). Also interestingly, the minus end-directed motility of Ncd is easily reversed by a single or double point mutation in the neck without swapping the whole neck/stalk region (Endow and Higuchi, 2000; Endow and Waligora, 1998). These results suggest that the neck region is not required for defining the plus end-directed motility, and that the plus end-directed motility is an intrinsic nature of the motor core domain of kinesin and Ncd.

The directionality of myosin is reminiscent of the directionality of kinesin and Ncd - the minus end-directed motility of myosin 6 was easily reversed, implying that the motor core of myosin inherently has plus end-directed motility. The minus end-directed motility of myosin 6 has been successfully converted into the plus end-directed motility by swapping the redirected neck with the straight neck of myosin 5a or replacing the whole converter-neck region with that of myosin 5a. Likewise, the plus end-directed

motility of myosin 1 (MyoE) has been successfully converted into minus end-directed movement by attaching artificial protein motifs at the C-terminal end of the neck so that the direction of the C-terminal tip is redirected ~180^{o} (Tsiavaliaris et al., 2004). These results seem to strongly support the idea that the ~120^{o} redirected neck of myosin 6 is responsible for the reversed directionality by changing the direction of the swing of the lever arm. Although the idea seems to be reasonable based on the lever arm hypothesis, there are at least two inexplicable issues. First, it cannot explain the minus end-directed motility of myosin 9b. The neck region of myosin 9b does not seem to be bent because it does not contain an insertion found in the neck region of myosin 6 (Fig F-5). Second, the plus end-directed motility of myosin 5a failed to be converted by introducing the converter-neck region of myosin 6 (M5M6, M5M6conv, M5M6SH, dM5M6, M6M5M6, M6M5M6LP). The apparent negative results can be simply explained by the disruption of the proper intramolecular interactions by force-connecting different myosin parts. However, this is less likely for some chimeras (M5M6conv, dM5M6, M6M5M6, M6M5M6LP) because their complementary chimeric constructs (M6M5conv, dM6M5, M5M6M5, M5M6M5LP) all showed reproducible plus end-directed motility despite their slower actin translocation rates.

The globular motor cores of myosin 6 and myosin 5a are similar, and dimeric myosin 6 and myosin 5a have similar average step size when they move along actin filaments (~36nm). However, the step size distribution of myosin 6 is much wider than that of myosin 5a. Since the predicted coiled-coil region of myosin 6 does not form stable coiled-coil, the broad step size distribution has been thought to be a result of zip-

unzip transition of the coiled-coil. However, Park *et al.* reported recently that even if the neck and the coiled-coil of myosin 6 were replaced with the neck and the stable coiled-coil of myosin 5a, the broad step size distribution was not affected (Park et al., 2007). This result strongly suggests that the intrinsic motor property of myosin 6 is evidently different from that of myosin 5a.

We propose that there is an alternative or an additional structural element(s) in the globular motor domain that defines the minus end-directed motility of myosin 6. Unfortunately, we were unable to identify the region in the current study. At least, the N-terminal variable region, the relay helix, and the small insertion in the vicinity of the ATP binding site of myosin 6 are not essential for defining the minus end-directed motility. The other possible region not tested at this point is the loop 2 region. Loop 2 is involved in one of the actin binding sites of myosin, and is highly variable among the myosin superfamily (Fig. F-5). As mentioned in Chapter VI, myosin 9 contains an extremely large insertion in this loop, and its movement directionality cannot be explained by the apparent structure of the neck region. It would be interesting to see if the loop-2 region is essential for deciding the movement directionality of myosin motors.

Table F-1. Directionality and velocity of the movement of myosin constructs

Construct	Directionality	Velocity ($\mu m\ s^{-1}$)
M5HMM	Plus	0.32 ± 0.08 (n = 112)
M6HMM	Minus	0.29 ± 0.11 (n = 80)
M5M6HMM	Plus	0.13 ± 0.06 (n = 125)
M6M5HMM	Minus	0.05 ± 0.02 (n = 101)
M5M6CVHMM	Plus	0.06 ± 0.03 (n = 98)
M5M6SHCVHMM	Plus	0.05 ± 0.02 (n = 91)

Actin filament motility was observed in 25 mM KCl, 5 mM $MgCl_2$, 25 mM Imidazole-HCl, pH 7.5, 1 mM EGTA, 0.5% methylcellulose; 4.5 mg ml^{-1} glucose, 216 $\mu g\ ml^{-1}$ glucose oxidase, 36 $\mu g\ ml^{-1}$ catalase and 5 mM ATP at 25 °C. All values of velocity are mean velocity ± s.d.

Table F-2. Directionality and velocity of the movement of myosin constructs

Construct	Directionality	Velocity [μm/sec]
M5	plus	0.272 ± 0.086
M5IQ2	plus	0.267 ± 0.064
M6	minus	0.185 ± 0.066
M6IQ1	minus	0.142 ± 0.030
M6M5conv (1)	plus	0.021 ± 0.005
M6M5conv (2)	plus	0.024 ± 0.008
M6M5dPro	plus	0.018 ± 0.005
dM5	plus	0.021 ± 0.011
dM6M5	plus	0.027 ± 0.014
M5M6M5	plus	0.025 ± 0.009
dM6	minus	0.120 ± 0.050
dM5M6	N.D.	N.D.
M6M5M6	N.D.	N.D.
M5M6M5LP (1)	plus	0.022 ± 0.005
M5M6M5LP (2)	plus	0.017 ± 0.004
M6M5M6LP (1)	N.D.	N.D.
M6M5M6LP (2)	N.D.	N.D.
M5relay	plus	0.010 ± 0.004
M6relay	minus	0.016 ± 0.006
M5M6relay	N.D.	N.D.
M6M5relay	plus	0.004 ± 0.002
M6ins5	minus	0.463 ± 0.127
M5M6ins6	N.D.	N.D.

N.D., The movement of actin filaments could not be detected.

Abbreviations not mentioned in the text are: M5, human myosin 5a (Met 1- Lys 1189); M5IQ2, human myosin 5a (Met 1 - Lys 823); M6, human myosin 6 (Met 1 - Lys 1285); M6IQ1, human myosin 6 (Met 1 - Thr 845). A myc epitope tag and an octahistidine tag were attached at the C-terminal end of each construct.

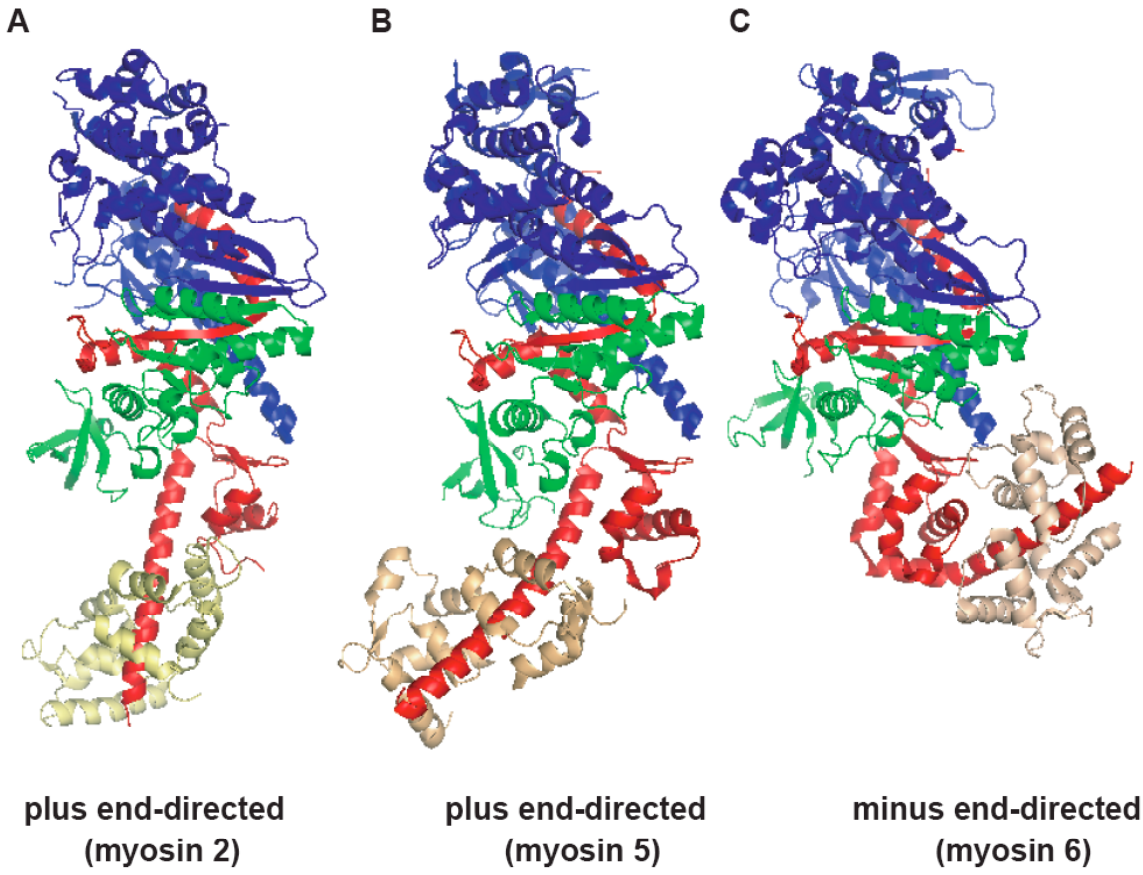

Figure F-1. Myosin crystal structures. Only the motor domains and their first light chains (colored in pale yellow or light orange) are shown. The heavy chains are colored in green, blue, and red, from the N-terminus to the C-terminus. **A**, Class 2 myosin (1DFK). **B**, Class 5 myosin (1OE9), **C**, Class 6 myosin (2BKH).

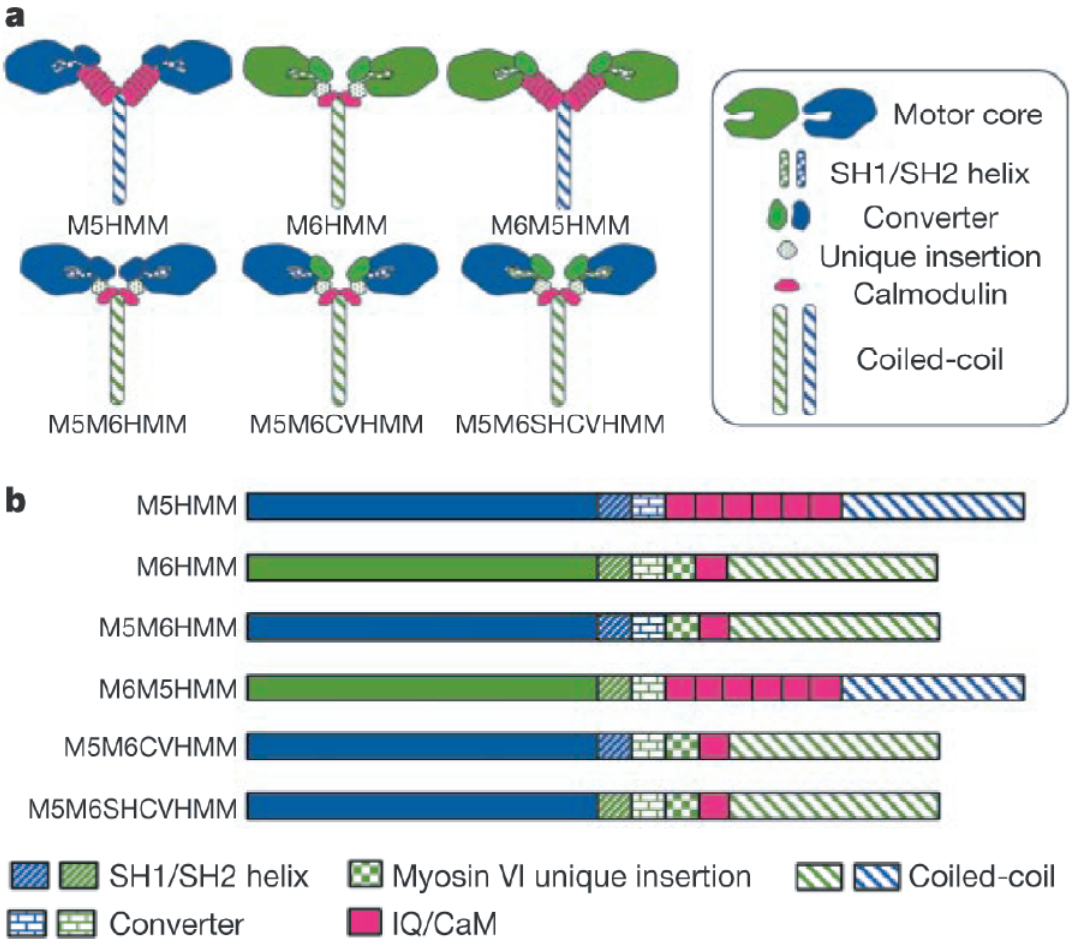

Figure F-2. Structure of the hybrid myosin constructs. a, Schematic representation of indicated myosin constructs. M5HMM consists of the two complete heads of myosin 5a (motor domain + six IQ motifs) plus the entire coiled-coil domain of myosin 5a. M6HMM consists of the two complete heads of myosin 6 (motor domain + myosin 6-specific large insert + one IQ motif) plus the entire coiled-coil domain of myosin 6. M5M6HMM is composed of two heads (containing the motor domain and converter domain of myosin 5a and the myosin 6 specific large insert + myosin 6 IQ motif) plus the entire coiled-coil domain of myosin 6. M5M6CVHMM substitutes the converter domain of M5M6HMM with the myosin 6 converter domain. M5M6SHCVHMM substitutes the SH1/SH2 helix and converter domain of M5M6HMM with its myosin 6 counterpart. M6M5HMM is composed of two heads (containing the motor domain and converter domain of myosin 6 connected with the six myosin 5a IQ motifs, but without the large myosin 6-specific insert) plus the entire coiled-coil domain of myosin 5a. **b**, Primary structure of various myosin constructs. Myosin 5a (blue) and myosin 6 (green) sequences are indicated. Red box, IQ motif; checkered box, myosin 6-specific large insertion between the converter and IQ domain; solid bar, the motor core.

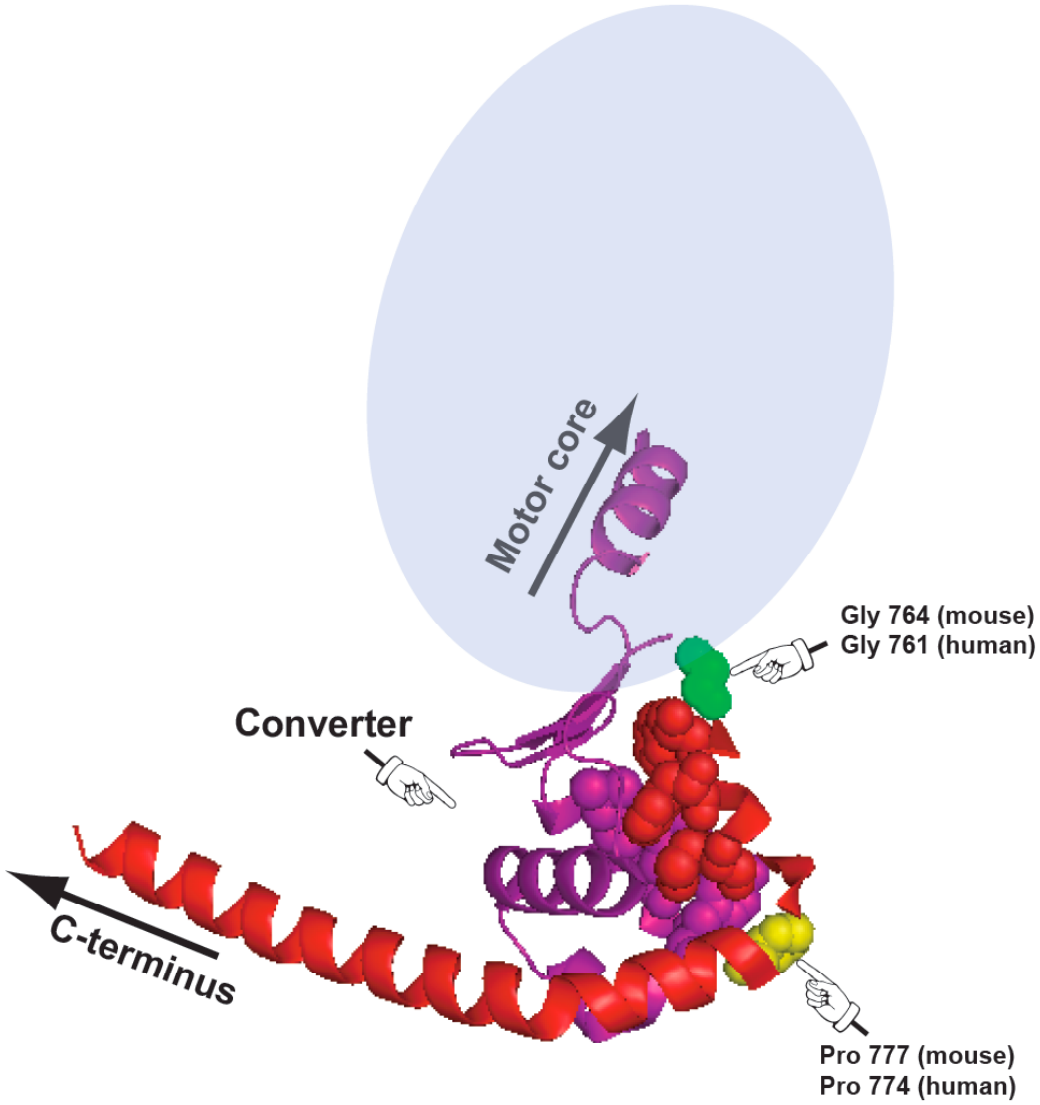

Figure F-3. The converter-neck region of myosin 6. The SH helix and the converter domain are shown in purple, and the neck is shown in red. Amino acid residues at the interface of the converter and the root of the neck are shown with spheres. The green sphere indicates the conserved glycine residue that was used as the joining point of myosin 5a and myosin 6 in our previous study (M5M6HMM and M6M5HMM in Figure F-2). The yellow sphere indicates the proline residue, which seems to be important for redirecting the neck.

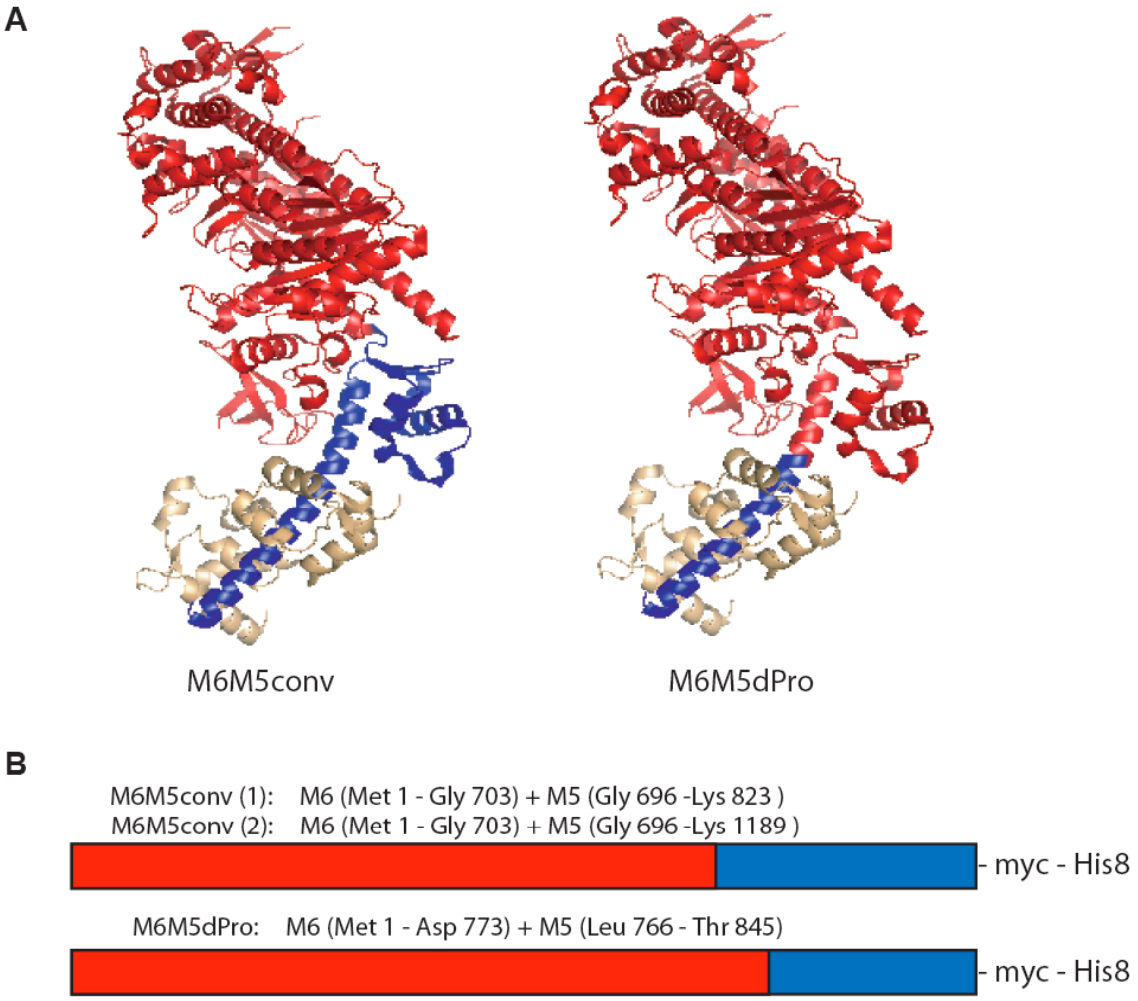

Figure F-4. M6M5conv and M6M5dPro chimeras. A, The expected overall structures of the motor domain of the chimeras are shown using the crystal structure of myosin 5a. Red and blue colors indicate contribution from myosin 6 and myosin 5a, respectively. The light chain is shown in light orange. **B**, Schematic representation of M6M5conv and M6M5dPro constructs. Human myosin 6 and myosin 5a are used for generating these chimeras. A myc epitope tag and an octahistidine tag were attached at the C-terminal end of each construct for facilitating protein purification and the following ensemble *in vitro* motility assay.

Figure F-5. Sequence alignment of myosins from class 1, 2, 3, 5, 6, 7, 9, and 10. The amino acid sequences of the N-terminal motor domain and the neck are shown. Highly conserved amino acids are shown in magenta.

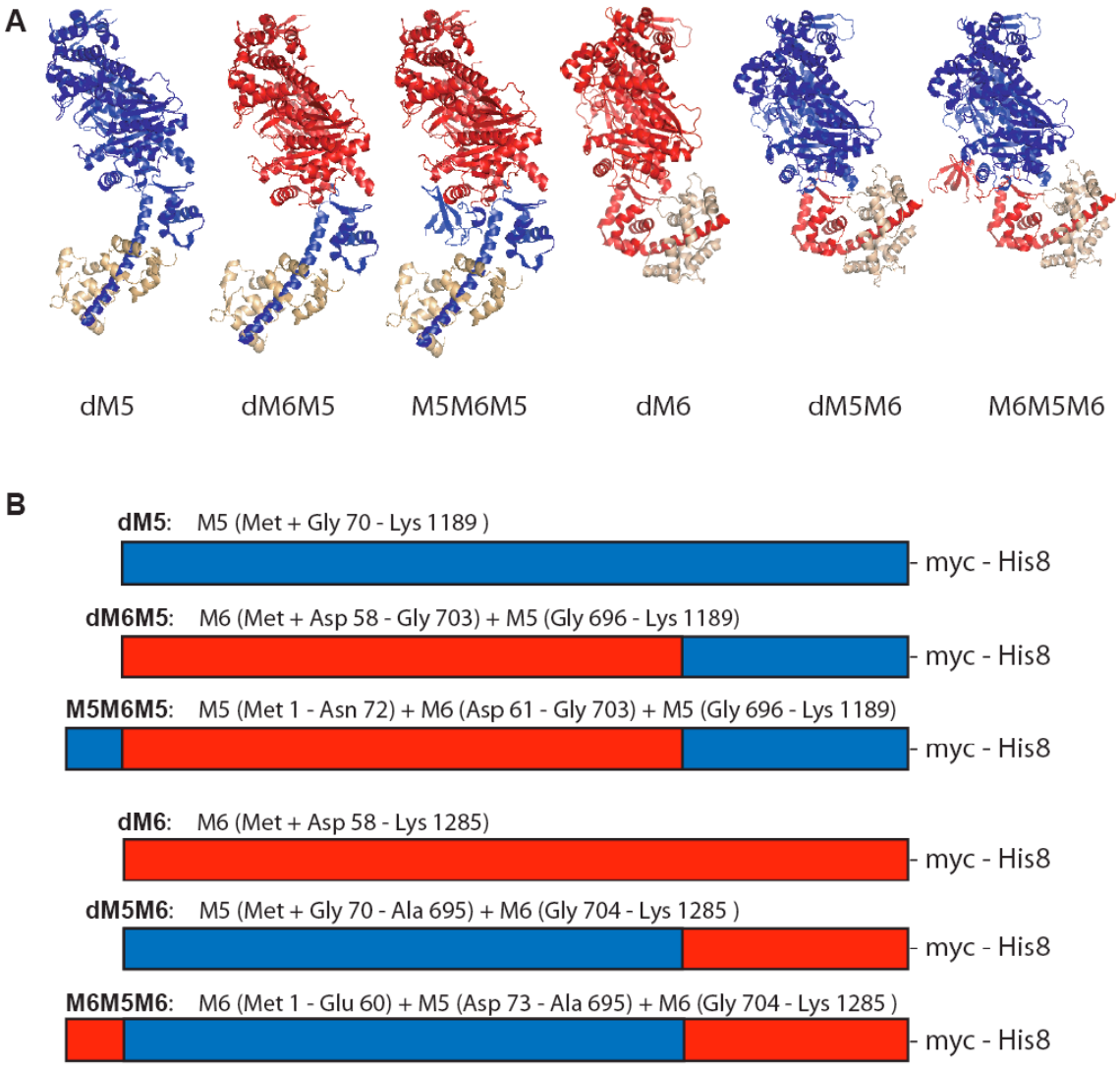

Figure F-6. dM5, dM6M5, M5M6M5, dM6, dM5M6, and M6M5M6 chimeras. A, The expected overall structures of the motor domain of the chimeras are shown using the crystal structure of myosin 6 and myosin 5a. Red and blue colors indicate contribution from myosin 6 and myosin 5a, respectively. The light chain is shown in light orange. **B**, Schematic representation of dM5, dM6M5, M5M6M5, dM6, dM5M6, and M6M5M6 constructs. Human myosin 6 and myosin 5a are used for generating these chimeras. A myc epitope tag and an octahistidine tag were attached at the C-terminal end of each construct for facilitating protein purification.

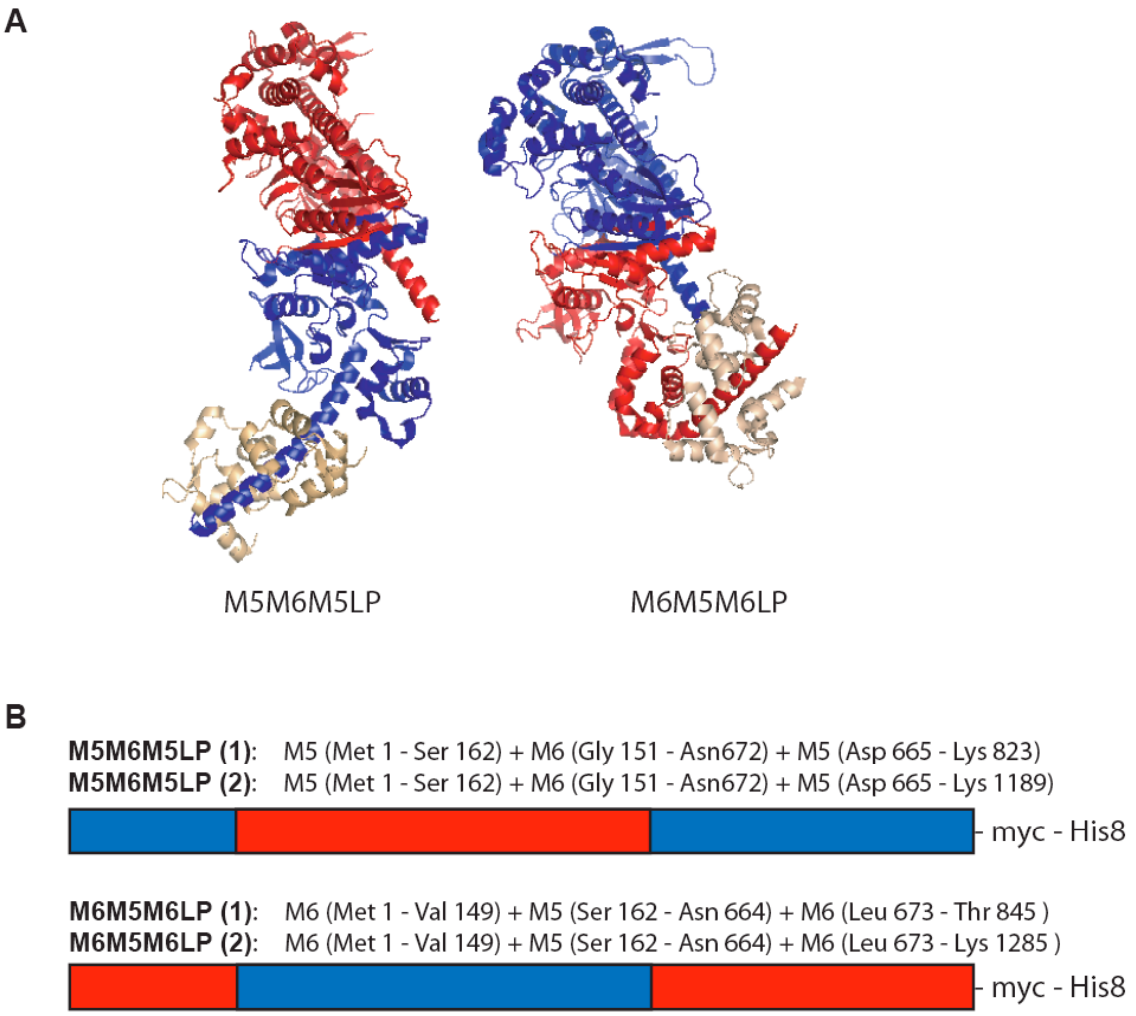

Figure F-7. M5M6M5LP and M6M5M6LP chimeras. A, The expected overall structures of the motor domain of the chimeras are shown using the crystal structure of myosin 6 and myosin 5a. Red and blue colors indicate contribution from myosin 6 and myosin 5a, respectively. The light chain is shown in light orange. **B**, Schematic representation of M5M6M5LP and M6M5M6LP constructs. Human myosin 6 and myosin 5a are used for generating these chimeras. A myc epitope tag and an octahistidine tag were attached at the C-terminal end of each construct for facilitating protein purification.

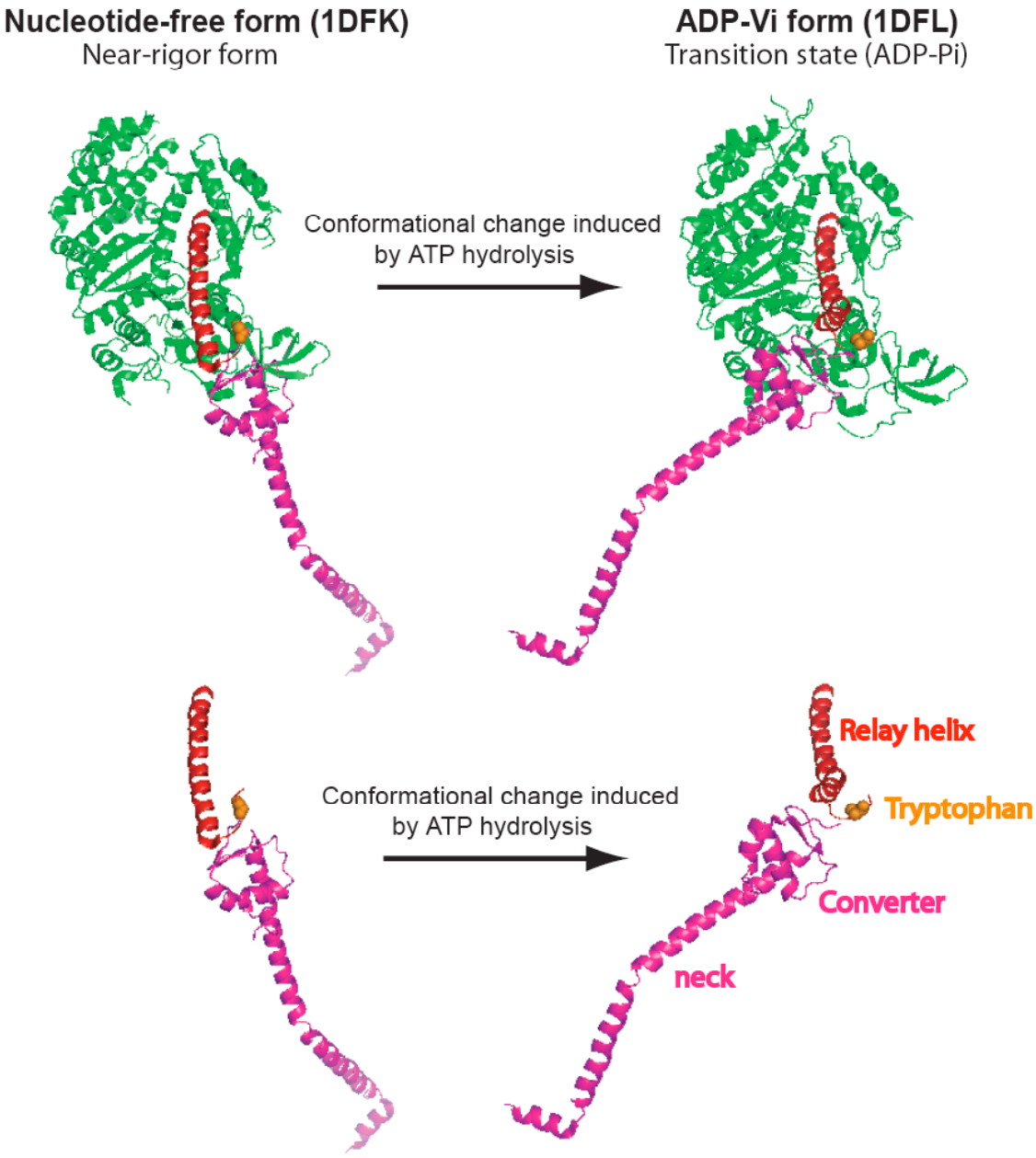

Figure F-8. Conformational change of myosin induced by the ATP hydrolysis. Two crystal structures of scallop myosin 2 (Houdusse et al., 2000) are shown. The relay helix is colored in red. The converter and the neck region are colored in magenta. The relatively conserved tryptophan residue at the tip of the relay helix is shown in orange with sphere. The apparent swing-like conformation change of the neck seems to be linked to the translocation of the relay helix induced by the hydrolysis of ATP.

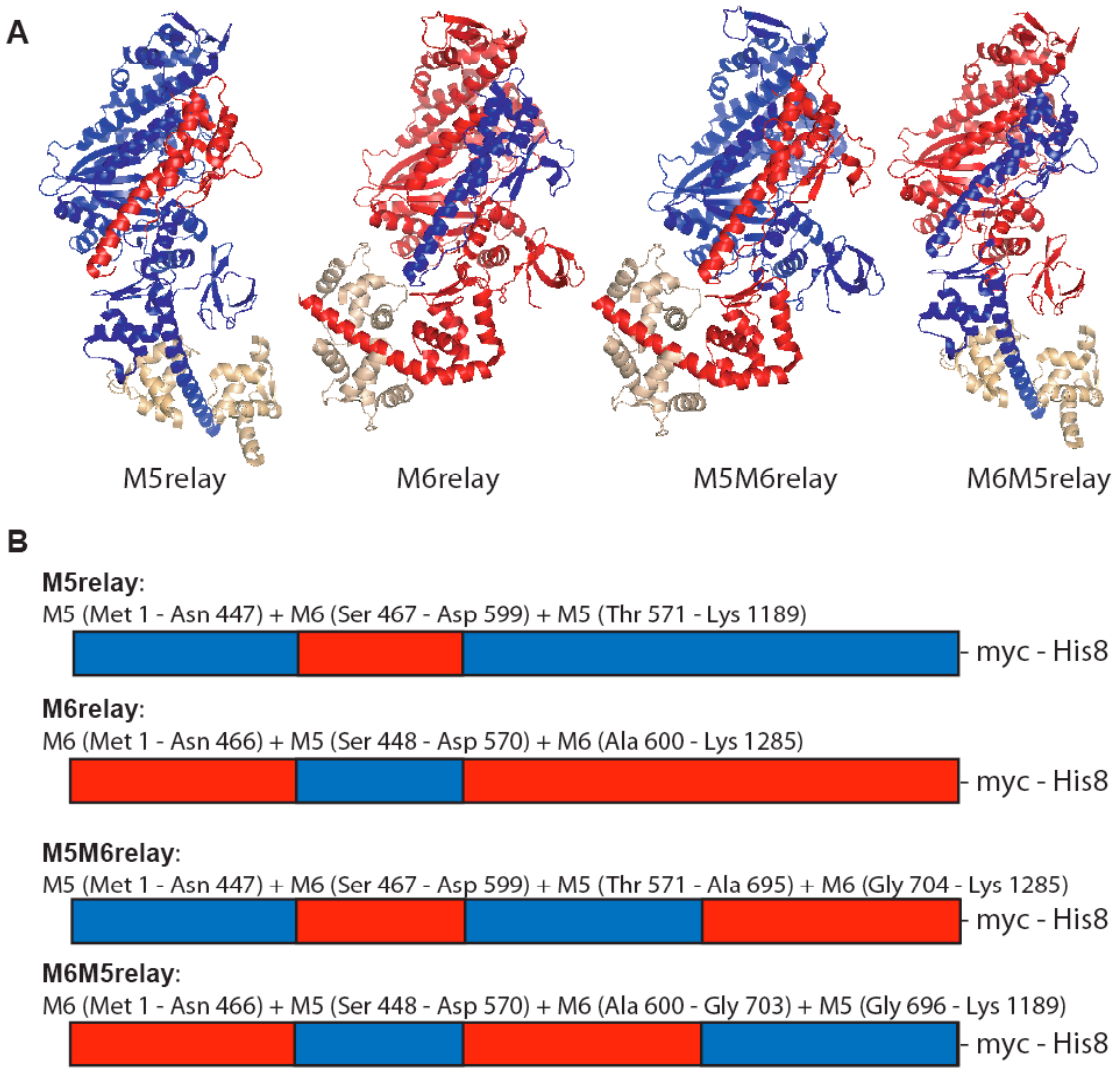

Figure F-9. M5relay, M6relay, M5M6relay, and M6M5relay chimeras. A, The expected overall structures of the motor domain of the chimeras are shown using the crystal structure of myosin 6 and myosin 5a. Red and blue colors indicate contribution from myosin 6 and myosin 5a, respectively. The light chain is shown in light orange. **B**, Schematic representation of M5relay, M6relay, M5M6relay, and M6M5relay constructs. Human myosin 6 and myosin 5a are used for generating these chimeras. A myc epitope tag and an octahistidine tag were attached at the C-terminal end of each construct for facilitating protein purification.

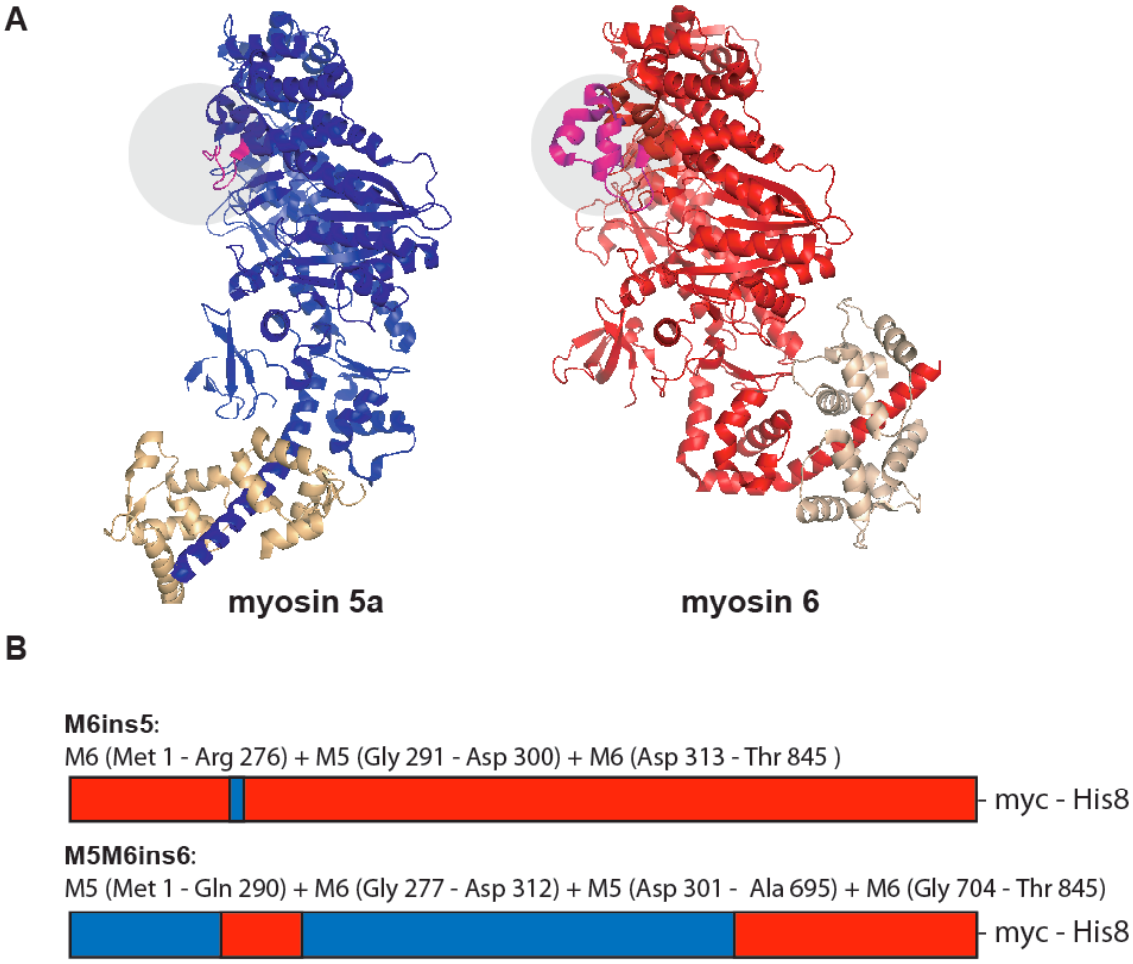

Figure F-10. The small insertion in the vicinity of the ATP binding site of myosin 6. **A,** The crystal structures of the motor domain of myosin 5a and myosin 6 are shown. The heavy chains of myosin 5a and myosin 6 are colored in blue and red, respectively. Their light chains are shown in light orange. The unique small insertion of myosin 6 and the corresponding site in myosin 5a are highlighted in magenta. **B**, Schematic representation of M6ins5 and M5M6ins6 constructs. Red and blue colors indicate contribution from myosin 6 and myosin 5a, respectively. Human myosin 6 and myosin 5a are used for generating these chimeras. A myc epitope tag and an octahistidine tag were attached at the C-terminal end of each construct for facilitating protein purification and the following ensemble *in vitro* motility assay.

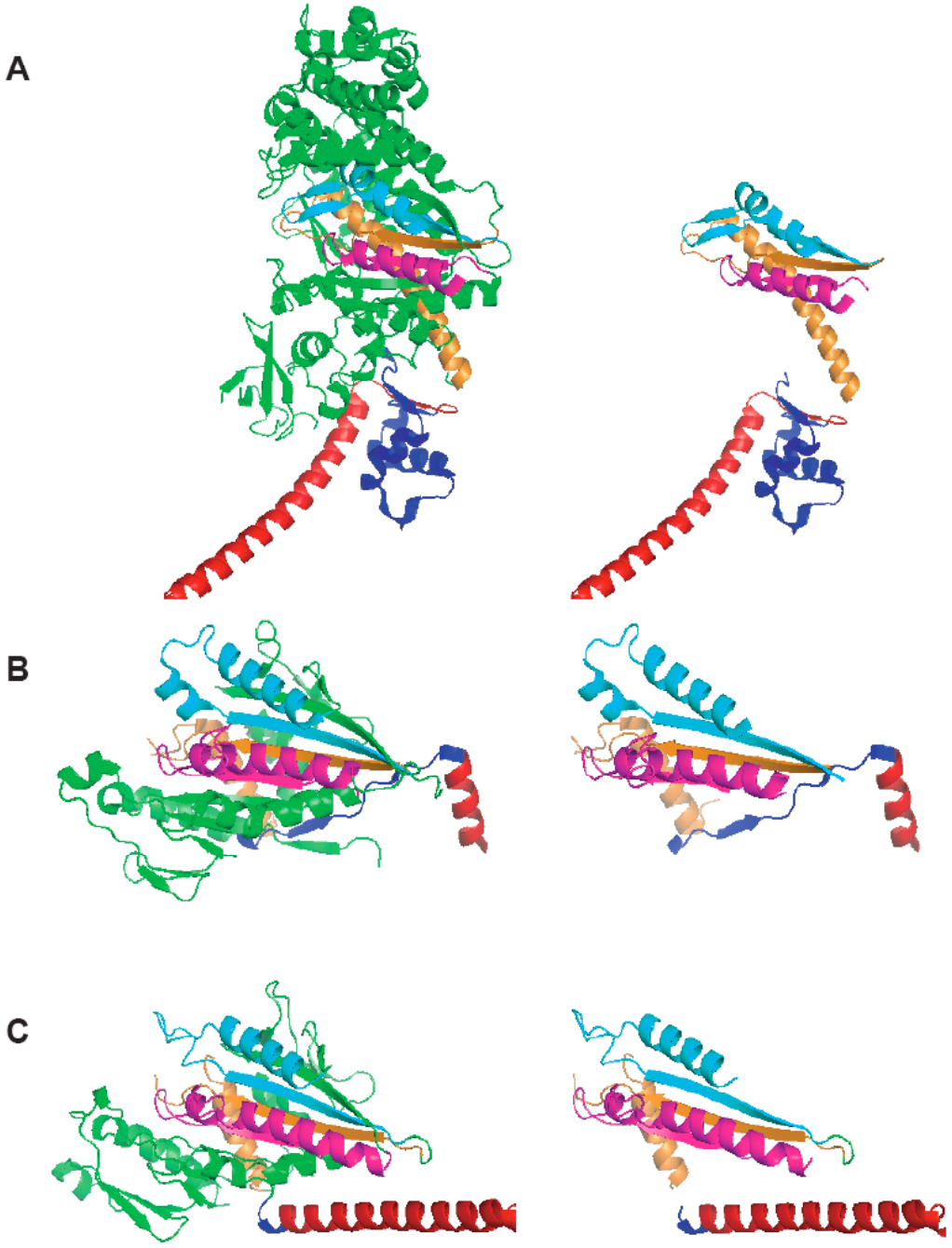

Figure F-11. The crystal structures of myosin 5a, kinesin, and Ncd. The regions containing P-loop, switch I, and switch II/relay helix are colored in magenta, cyan, and orange, respectively. The converter region and the neck linker region are colored in blue. The neck regions are colored in red. **A,** The crystal structure of myosin 5a (1OE9). **B**, The crystal structure of kinesin (1MKJ). **C,** The crystal structure of Ncd (2NCD).

REFERENCES

Altman, D., H.L. Sweeney, and J.A. Spudich. 2004. The mechanism of myosin VI translocation and its load-induced anchoring. *Cell*. 116:737-49.

Anson, M., M.A. Geeves, S.E. Kurzawa, and D.J. Manstein. 1996. Myosin motors with artificial lever arms. *Embo J*. 15:6069-74.

Asbury, C.L., A.N. Fehr, and S.M. Block. 2003. Kinesin moves by an asymmetric hand-over-hand mechanism. *Science*. 302:2130-4.

Aschenbrenner, L., S.N. Naccache, and T. Hasson. 2004. Uncoated endocytic vesicles require the unconventional myosin, Myo6, for rapid transport through actin barriers. *Mol Biol Cell*. 15:2253-63.

Bear, J.E., T.M. Svitkina, M. Krause, D.A. Schafer, J.J. Loureiro, G.A. Strasser, I.V. Maly, O.Y. Chaga, J.A. Cooper, G.G. Borisy, and F.B. Gertler. 2002. Antagonism between Ena/VASP proteins and actin filament capping regulates fibroblast motility. *Cell*. 109:509-21.

Berg, J.S., and R.E. Cheney. 2002. Myosin-X is an unconventional myosin that undergoes intrafilopodial motility. *Nat Cell Biol*. 4:246-50.

Berg, J.S., B.H. Derfler, C.M. Pennisi, D.P. Corey, and R.E. Cheney. 2000. Myosin-X, a novel myosin with pleckstrin homology domains, associates with regions of dynamic actin. *J Cell Sci*. 113 Pt 19:3439-51.

Bohil, A.B., B.W. Robertson, and R.E. Cheney. 2006. Myosin-X is a molecular motor that functions in filopodia formation. *Proc Natl Acad Sci U S A*. 103:12411-6.

Bridgman, P.C., S. Dave, C.F. Asnes, A.N. Tullio, and R.S. Adelstein. 2001. Myosin IIB is required for growth cone motility. *J Neurosci*. 21:6159-69.

Brown, J.R., P. Stafford, and G.M. Langford. 2004. Short-range axonal/dendritic transport by myosin-V: A model for vesicle delivery to the synapse. *J Neurobiol*. 58:175-88.

Brune, M., J.L. Hunter, J.E. Corrie, and M.R. Webb. 1994. Direct, real-time measurement of rapid inorganic phosphate release using a novel fluorescent probe and its application to actomyosin subfragment 1 ATPase. *Biochemistry*. 33:8262-71.

Bryant, Z., D. Altman, and J.A. Spudich. 2007. The power stroke of myosin VI and the basis of reverse directionality. *Proc Natl Acad Sci U S A*. 104:772-7.

Buss, F., S.D. Arden, M. Lindsay, J.P. Luzio, and J. Kendrick-Jones. 2001. Myosin VI isoform localized to clathrin-coated vesicles with a role in clathrin-mediated endocytosis. *Embo J*. 20:3676-84.

Carter, N.J., and R.A. Cross. 2005. Mechanics of the kinesin step. *Nature*. 435:308-12.

Case, R.B., D.W. Pierce, N. Hom-Booher, C.L. Hart, and R.D. Vale. 1997. The directional preference of kinesin motors is specified by an element outside of the motor catalytic domain. *Cell*. 90:959-66.

Case, R.B., S. Rice, C.L. Hart, B. Ly, and R.D. Vale. 2000. Role of the kinesin neck linker and catalytic core in microtubule-based motility. *Curr Biol*. 10:157-60.

Chen, Y., F. Ding, H. Nie, A.W. Serohijos, S. Sharma, K.C. Wilcox, S. Yin, and N.V. Dokholyan. 2007. Protein folding: Then and now. *Arch Biochem Biophys*.

Cheney, R.E., M.K. O'Shea, J.E. Heuser, M.V. Coelho, J.S. Wolenski, E.M. Espreafico, P. Forscher, R.E. Larson, and M.S. Mooseker. 1993. Brain myosin-V is a two-headed unconventional myosin with motor activity. *Cell*. 75:13-23.

Coureux, P.D., H.L. Sweeney, and A. Houdusse. 2004. Three myosin V structures delineate essential features of chemo-mechanical transduction. *Embo J*. 23:4527-37.

Cox, D., J.S. Berg, M. Cammer, J.O. Chinegwundoh, B.M. Dale, R.E. Cheney, and S. Greenberg. 2002. Myosin X is a downstream effector of PI(3)K during phagocytosis. *Nat Cell Biol*. 4:469-77.

Cross, R.A. 2004. The kinetic mechanism of kinesin. *Trends Biochem Sci*. 29:301-9.

Davenport, R.W., P. Dou, V. Rehder, and S.B. Kater. 1993. A sensory role for neuronal growth cone filopodia. *Nature*. 361:721-4.

De La Cruz, E.M., E.M. Ostap, and H.L. Sweeney. 2001. Kinetic mechanism and regulation of myosin VI. *J Biol Chem*. 276:32373-81.

De La Cruz, E.M., A.L. Wells, S.S. Rosenfeld, E.M. Ostap, and H.L. Sweeney. 1999. The kinetic mechanism of myosin V. *Proc Natl Acad Sci U S A*. 96:13726-31.

De La Cruz, E.M., A.L. Wells, H.L. Sweeney, and E.M. Ostap. 2000. Actin and light chain isoform dependence of myosin V kinetics. *Biochemistry*. 39:14196-202.

deCastro, M.J., C.H. Ho, and R.J. Stewart. 1999. Motility of dimeric ncd on a metal-chelating surfactant: evidence that ncd is not processive. *Biochemistry*. 38:5076-81.

Dominguez, R., Y. Freyzon, K.M. Trybus, and C. Cohen. 1998. Crystal structure of a vertebrate smooth muscle myosin motor domain and its complex with the essential light chain: visualization of the pre-power stroke state. *Cell*. 94:559-71.

El Mezgueldi, M., N. Tang, S.S. Rosenfeld, and E.M. Ostap. 2002. The kinetic mechanism of Myo1e (human myosin-IC). *J Biol Chem*. 277:21514-21.

Endow, S.A., and H. Higuchi. 2000. A mutant of the motor protein kinesin that moves in both directions on microtubules. *Nature*. 406:913-6.

Endow, S.A., and K.W. Waligora. 1998. Determinants of kinesin motor polarity. *Science*. 281:1200-2.

Evans, L.L., A.J. Lee, P.C. Bridgman, and M.S. Mooseker. 1998. Vesicle-associated brain myosin-V can be activated to catalyze actin-based transport. *J Cell Sci*. 111 (Pt 14):2055-66.

Foth, B.J., M.C. Goedecke, and D. Soldati. 2006. New insights into myosin evolution and classification. *Proc Natl Acad Sci U S A*. 103:3681-6.

Frank, D.J., T. Noguchi, and K.G. Miller. 2004. Myosin VI: a structural role in actin organization important for protein and organelle localization and trafficking. *Curr Opin Cell Biol*. 16:189-94.

Gerhardt, H., M. Golding, M. Fruttiger, C. Ruhrberg, A. Lundkvist, A. Abramsson, M. Jeltsch, C. Mitchell, K. Alitalo, D. Shima, and C. Betsholtz. 2003. VEGF guides angiogenic sprouting utilizing endothelial tip cell filopodia. *J Cell Biol*. 161:1163-77.

Hasson, T. 2003. Myosin VI: two distinct roles in endocytosis. *J Cell Sci*. 116:3453-61.

Henningsen, U., and M. Schliwa. 1997. Reversal in the direction of movement of a molecular motor. *Nature*. 389:93-6.

Herm-Gotz, A., S. Weiss, R. Stratmann, S. Fujita-Becker, C. Ruff, E. Meyhofer, T. Soldati, D.J. Manstein, M.A. Geeves, and D. Soldati. 2002. Toxoplasma gondii myosin A and its light chain: a fast, single-headed, plus-end-directed motor. *Embo J*. 21:2149-58.

Homma, K., J. Saito, R. Ikebe, and M. Ikebe. 2001. Motor function and regulation of myosin X. *J Biol Chem*. 276:34348-54.

Houdusse, A., V.N. Kalabokis, D. Himmel, A.G. Szent-Gyorgyi, and C. Cohen. 1999. Atomic structure of scallop myosin subfragment S1 complexed with MgADP: a novel conformation of the myosin head. *Cell*. 97:459-70.

Houdusse, A., A.G. Szent-Gyorgyi, and C. Cohen. 2000. Three conformational states of scallop myosin S1. *Proc Natl Acad Sci U S A*. 97:11238-43.

Howard, J. 2001. Mechanics of motor proteins and the cytoskeleton. Sinauer Associates, Publishers, Sunderland, Mass. xvi, 367 p. pp.

Ikebe, M., T. Kambara, W.F. Stafford, M. Sata, E. Katayama, and R. Ikebe. 1998. A hinge at the central helix of the regulatory light chain of myosin is critical for phosphorylation-dependent regulation of smooth muscle myosin motor activity. *J Biol Chem*. 273:17702-7.

Inoue, A., J. Saito, R. Ikebe, and M. Ikebe. 2002. Myosin IXb is a single-headed minus-end-directed processive motor. *Nat Cell Biol*. 4:302-6.

Inoue, Y., Y.Y. Toyoshima, A.H. Iwane, S. Morimoto, H. Higuchi, and T. Yanagida. 1997. Movements of truncated kinesin fragments with a short or an artificial flexible neck. *Proc Natl Acad Sci U S A*. 94:7275-80.

Irving, M., T. St Claire Allen, C. Sabido-David, J.S. Craik, B. Brandmeier, J. Kendrick-Jones, J.E. Corrie, D.R. Trentham, and Y.E. Goldman. 1995. Tilting of the light-chain region of myosin during step length changes and active force generation in skeletal muscle. *Nature*. 375:688-91.

Isakoff, S.J., T. Cardozo, J. Andreev, Z. Li, K.M. Ferguson, R. Abagyan, M.A. Lemmon, A. Aronheim, and E.Y. Skolnik. 1998. Identification and analysis of PH domain-containing targets of phosphatidylinositol 3-kinase using a novel in vivo assay in yeast. *Embo J*. 17:5374-87.

Jontes, J.D., E.M. Wilson-Kubalek, and R.A. Milligan. 1995. A 32 degree tail swing in brush border myosin I on ADP release. *Nature*. 378:751-3.

Kalhammer, G., and M. Bahler. 2000. Unconventional myosins. *Essays Biochem*. 35:33-42.

Kambara, T., T.E. Rhodes, R. Ikebe, M. Yamada, H.D. White, and M. Ikebe. 1999. Functional significance of the conserved residues in the flexible hinge region of the myosin motor domain. *J Biol Chem*. 274:16400-6.

Kaseda, K., H. Higuchi, and K. Hirose. 2003. Alternate fast and slow stepping of a heterodimeric kinesin molecule. *Nat Cell Biol*. 5:1079-82.

King, S.J., and T.A. Schroer. 2000. Dynactin increases the processivity of the cytoplasmic dynein motor. *Nat Cell Biol*. 2:20-4.

Knight, P.J., K. Thirumurugan, Y. Xu, F. Wang, A.P. Kalverda, W.F. Stafford, 3rd, J.R. Sellers, and M. Peckham. 2005. The predicted coiled-coil domain of myosin 10 forms a novel elongated domain that lengthens the head. *J Biol Chem*. 280:34702-8.

Kouyama, T., and K. Mihashi. 1981. Fluorimetry study of N-(1-pyrenyl)iodoacetamide-labelled F-actin. Local structural change of actin protomer both on polymerization and on binding of heavy meromyosin. *Eur J Biochem*. 114:33-8.

Kovacs, M., F. Wang, and J.R. Sellers. 2005. Mechanism of action of myosin X, a membrane-associated molecular motor. *J Biol Chem*. 280:15071-83

Kron, S.J., and J.A. Spudich. 1986. Fluorescent actin filaments move on myosin fixed to a glass surface. *Proc Natl Acad Sci U S A*. 83:6272-6.

Lister, I., S. Schmitz, M. Walker, J. Trinick, F. Buss, C. Veigel, and J. Kendrick-Jones. 2004. A monomeric myosin VI with a large working stroke. *Embo J*. 23:1729-38.

Mallavarapu, A., and T. Mitchison. 1999. Regulated actin cytoskeleton assembly at filopodium tips controls their extension and retraction. *J Cell Biol*. 146:1097-106.

Mashanov, G.I., D. Tacon, M. Peckham, and J.E. Molloy. 2004. The spatial and temporal dynamics of pleckstrin homology domain binding at the plasma membrane measured by imaging single molecules in live mouse myoblasts. *J Biol Chem*. 279:15274-80.

Mehta, A.D., R.S. Rock, M. Rief, J.A. Spudich, M.S. Mooseker, and R.E. Cheney. 1999. Myosin-V is a processive actin-based motor. *Nature*. 400:590-3.

Menetrey, J., A. Bahloul, A.L. Wells, C.M. Yengo, C.A. Morris, H.L. Sweeney, and A. Houdusse. 2005. The structure of the myosin VI motor reveals the mechanism of directionality reversal. *Nature*. 435:779-85.

Nishikawa, M., S. Nishikawa, A. Inoue, A.H. Iwane, T. Yanagida, and M. Ikebe. 2006. A unique mechanism for the processive movement of single-headed myosin-IX. *Biochem Biophys Res Commun*. 343:1159-64.

Nishikawa, S., K. Homma, Y. Komori, M. Iwaki, T. Wazawa, A. Hikikoshi Iwane, J. Saito, R. Ikebe, E. Katayama, T. Yanagida, and M. Ikebe. 2002. Class VI myosin moves processively along actin filaments backward with large steps. *Biochem Biophys Res Commun*. 290:311-7.

O'Connell, C.B., and M.S. Mooseker. 2003. Native Myosin-IXb is a plus-, not a minus-end-directed motor. *Nat Cell Biol*. 5:171-2.

Okada, Y., H. Higuchi, and N. Hirokawa. 2003. Processivity of the single-headed kinesin KIF1A through biased binding to tubulin. *Nature*. 424:574-7.

Okada, Y., and N. Hirokawa. 2000. Mechanism of the single-headed processivity: diffusional anchoring between the K-loop of kinesin and the C terminus of tubulin. *Proc Natl Acad Sci U S A*. 97:640-5.

Okten, Z., L.S. Churchman, R.S. Rock, and J.A. Spudich. 2004. Myosin VI walks hand-over-hand along actin. *Nat Struct Mol Biol*. 11:884-7.

Park, H., A. Li, L.Q. Chen, A. Houdusse, P.R. Selvin, and H.L. Sweeney. 2007. The unique insert at the end of the myosin VI motor is the sole determinant of directionality. *Proc Natl Acad Sci U S A*. 104:778-83.

Perreault-Micale, C., A.D. Shushan, and L.M. Coluccio. 2000. Truncation of a mammalian myosin I results in loss of Ca2+-sensitive motility. *J Biol Chem*. 275:21618-23.

Post, P.L., M.J. Tyska, C.B. O'Connell, K. Johung, A. Hayward, and M.S. Mooseker. 2002. Myosin-IXb is a single-headed and processive motor. *J Biol Chem*. 277:11679-83.

Prekeris, R., and D.M. Terrian. 1997. Brain myosin V is a synaptic vesicle-associated motor protein: evidence for a Ca2+-dependent interaction with the synaptobrevin-synaptophysin complex. *J Cell Biol*. 137:1589-601.

Purcell, T.J., H.L. Sweeney, and J.A. Spudich. 2005. A force-dependent state controls the coordination of processive myosin V. *Proc Natl Acad Sci U S A*. 102:13873-8.

Rayment, I., W.R. Rypniewski, K. Schmidt-Base, R. Smith, D.R. Tomchick, M.M. Benning, D.A. Winkelmann, G. Wesenberg, and H.M. Holden. 1993. Three-dimensional structure of myosin subfragment-1: a molecular motor. *Science*. 261:50-8.

Reynard, A.M., L.F. Hass, D.D. Jacobsen, and P.D. Boyer. 1961. The correlation of reaction kinetics and substrate binding with the mechanism of pyruvate kinase. *J Biol Chem*. 236:2277-83.

Rice, S., Y. Cui, C. Sindelar, N. Naber, M. Matuska, R. Vale, and R. Cooke. 2003. Thermodynamic properties of the kinesin neck-region docking to the catalytic core. *Biophys J*. 84:1844-54.

Rice, S., A.W. Lin, D. Safer, C.L. Hart, N. Naber, B.O. Carragher, S.M. Cain, E. Pechatnikova, E.M. Wilson-Kubalek, M. Whittaker, E. Pate, R. Cooke, E.W.

Taylor, R.A. Milligan, and R.D. Vale. 1999. A structural change in the kinesin motor protein that drives motility. *Nature*. 402:778-84.

Rock, R.S., S.E. Rice, A.L. Wells, T.J. Purcell, J.A. Spudich, and H.L. Sweeney. 2001. Myosin VI is a processive motor with a large step size. *Proc Natl Acad Sci U S A*. 98:13655-9.

Rogers, M.S., and E.E. Strehler. 2001. The tumor-sensitive calmodulin-like protein is a specific light chain of human unconventional myosin X. *J Biol Chem*. 276:12182-9.

Rorth, P. 2003. Communication by touch: role of cellular extensions in complex animals. *Cell*. 112:595-8.

Ross, M.E., X. Zhou, G. Song, S.A. Shurtleff, K. Girtman, W.K. Williams, H.C. Liu, R. Mahfouz, S.C. Raimondi, N. Lenny, A. Patel, and J.R. Downing. 2003. Classification of pediatric acute lymphoblastic leukemia by gene expression profiling. *Blood*. 102:2951-9.

Sablin, E.P., R.B. Case, S.C. Dai, C.L. Hart, A. Ruby, R.D. Vale, and R.J. Fletterick. 1998. Direction determination in the minus-end-directed kinesin motor ncd. *Nature*. 395:813-6.

Sakamoto, T., I. Amitani, E. Yokota, and T. Ando. 2000. Direct observation of processive movement by individual myosin V molecules. *Biochem Biophys Res Commun*. 272:586-90.

Sakamoto, T., F. Wang, S. Schmitz, Y. Xu, Q. Xu, J.E. Molloy, C. Veigel, and J.R. Sellers. 2003. Neck length and processivity of myosin V. *J Biol Chem*. 278:29201-7.

Sakamoto, T., A. Yildez, P.R. Selvin, and J.R. Sellers. 2005. Step-size is determined by neck length in myosin V. *Biochemistry*. 44:16203-10.

Self, T., T. Sobe, N.G. Copeland, N.A. Jenkins, K.B. Avraham, and K.P. Steel. 1999. Role of myosin VI in the differentiation of cochlear hair cells. *Dev Biol*. 214:331-41.

Sellers, J.R. 2000. Myosins: a diverse superfamily. *Biochim Biophys Acta*. 1496:3-22.

Sheetz, M.P., and J.A. Spudich. 1983. Movement of myosin-coated fluorescent beads on actin cables in vitro. *Nature*. 303:31-5.

Smith, C.A., and I. Rayment. 1996. X-ray structure of the magnesium(II).ADP.vanadate complex of the Dictyostelium discoideum myosin motor domain to 1.9 A resolution. *Biochemistry*. 35:5404-17.

Spudich, J.A., and S. Watt. 1971. The regulation of rabbit skeletal muscle contraction. I. Biochemical studies of the interaction of the tropomyosin-troponin complex with actin and the proteolytic fragments of myosin. *J Biol Chem*. 246:4866-71.

Svitkina, T.M., E.A. Bulanova, O.Y. Chaga, D.M. Vignjevic, S. Kojima, J.M. Vasiliev, and G.G. Borisy. 2003. Mechanism of filopodia initiation by reorganization of a dendritic network. *J Cell Biol*. 160:409-21.

Sweeney, H.L., H. Park, A.B. Zong, Z. Yang, P.R. Selvin, and S.S. Rosenfeld. 2007. How myosin VI coordinates its heads during processive movement. *Embo J*. 26:2682-92.

Tabb, J.S., B.J. Molyneaux, D.L. Cohen, S.A. Kuznetsov, and G.M. Langford. 1998. Transport of ER vesicles on actin filaments in neurons by myosin V. *J Cell Sci*. 111 (Pt 21):3221-34.

Tanabe, K., I. Bonilla, J.A. Winkles, and S.M. Strittmatter. 2003. Fibroblast growth factor-inducible-14 is induced in axotomized neurons and promotes neurite outgrowth. *J Neurosci*. 23:9675-86.

Tanaka, H., K. Homma, A.H. Iwane, E. Katayama, R. Ikebe, J. Saito, T. Yanagida, and M. Ikebe. 2002. The motor domain determines the large step of myosin-V. *Nature*. 415:192-5.

Taniguchi, Y., M. Nishiyama, Y. Ishii, and T. Yanagida. 2005. Entropy rectifies the Brownian steps of kinesin. *Nat Chem Biol*. 1:342-7.

Tokuo, H., and M. Ikebe. 2004. Myosin X transports Mena/VASP to the tip of filopodia. *Biochem Biophys Res Commun*. 319:214-20.

Tominaga, M., H. Kojima, E. Yokota, H. Orii, R. Nakamori, E. Katayama, M. Anson, T. Shimmen, and K. Oiwa. 2003. Higher plant myosin XI moves processively on actin with 35 nm steps at high velocity. *Embo J*. 22:1263-72.

Tomishige, M., and R.D. Vale. 2000. Controlling kinesin by reversible disulfide cross-linking. Identifying the motility-producing conformational change. *J Cell Biol*. 151:1081-92.

Trybus, K.M., E. Krementsova, and Y. Freyzon. 1999. Kinetic characterization of a monomeric unconventional myosin V construct. *J Biol Chem*. 274:27448-56.

Tsiavaliaris, G., S. Fujita-Becker, and D.J. Manstein. 2004. Molecular engineering of a backwards-moving myosin motor. *Nature*. 427:558-61.

Tsui, H.C., K.L. Lankford, and W.L. Klein. 1985. Differentiation of neuronal growth cones: specialization of filopodial tips for adhesive interactions. *Proc Natl Acad Sci U S A*. 82:8256-60.

Uyeda, T.Q., P.D. Abramson, and J.A. Spudich. 1996. The neck region of the myosin motor domain acts as a lever arm to generate movement. *Proc Natl Acad Sci U S A*. 93:4459-64.

Valentine, M.T., and S.P. Gilbert. 2007. To step or not to step? How biochemistry and mechanics influence processivity in Kinesin and Eg5. *Curr Opin Cell Biol*. 19:75-81.

Veigel, C., S. Schmitz, F. Wang, and J.R. Sellers. 2005. Load-dependent kinetics of myosin-V can explain its high processivity. *Nat Cell Biol*. 7:861-9.

Veigel, C., F. Wang, M.L. Bartoo, J.R. Sellers, and J.E. Molloy. 2002. The gated gait of the processive molecular motor, myosin V. *Nat Cell Biol*. 4:59-65.

Walker, M.L., S.A. Burgess, J.R. Sellers, F. Wang, J.A. Hammer, 3rd, J. Trinick, and P.J. Knight. 2000. Two-headed binding of a processive myosin to F-actin. *Nature*. 405:804-7.

Walker, R.A., E.D. Salmon, and S.A. Endow. 1990. The Drosophila claret segregation protein is a minus-end directed motor molecule. *Nature*. 347:780-2.

Warshaw, D.M., G.G. Kennedy, S.S. Work, E.B. Krementsova, S. Beck, and K.M. Trybus. 2005. Differential labeling of myosin V heads with quantum dots allows direct visualization of hand-over-hand processivity. *Biophys J*. 88:L30-2.

Watanabe, T.M., T. Sato, K. Gonda, and H. Higuchi. 2007. Three-dimensional nanometry of vesicle transport in living cells using dual-focus imaging optics. *Biochem Biophys Res Commun*. 359:1-7.

Watanabe, T.M., H. Tanaka, A.H. Iwane, S. Maki-Yonekura, K. Homma, A. Inoue, R. Ikebe, T. Yanagida, and M. Ikebe. 2004. A one-headed class V myosin molecule develops multiple large (approximately 32-nm) steps successively. *Proc Natl Acad Sci U S A*. 101:9630-5.

Weber, K.L., A.M. Sokac, J.S. Berg, R.E. Cheney, and W.M. Bement. 2004. A microtubule-binding myosin required for nuclear anchoring and spindle assembly. *Nature*. 431:325-9.

Wells, A.L., A.W. Lin, L.Q. Chen, D. Safer, S.M. Cain, T. Hasson, B.O. Carragher, R.A. Milligan, and H.L. Sweeney. 1999. Myosin VI is an actin-based motor that moves backwards. *Nature*. 401:505-8.

White, H.D., B. Belknap, and M.R. Webb. 1997. Kinetics of nucleoside triphosphate cleavage and phosphate release steps by associated rabbit skeletal actomyosin, measured using a novel fluorescent probe for phosphate. *Biochemistry*. 36:11828-36.

Whittaker, M., E.M. Wilson-Kubalek, J.E. Smith, L. Faust, R.A. Milligan, and H.L. Sweeney. 1995. A 35-A movement of smooth muscle myosin on ADP release. *Nature*. 378:748-51.

Yang, Y., M. Kovacs, T. Sakamoto, F. Zhang, D.P. Kiehart, and J.R. Sellers. 2006. Dimerized Drosophila myosin VIIa: a processive motor. *Proc Natl Acad Sci U S A*. 103:5746-51.

Yildiz, A., J.N. Forkey, S.A. McKinney, T. Ha, Y.E. Goldman, and P.R. Selvin. 2003. Myosin V walks hand-over-hand: single fluorophore imaging with 1.5-nm localization. *Science*. 300:2061-5.

Yildiz, A., H. Park, D. Safer, Z. Yang, L.Q. Chen, P.R. Selvin, and H.L. Sweeney. 2004a. Myosin VI steps via a hand-over-hand mechanism with its lever arm undergoing fluctuations when attached to actin. *J Biol Chem*. 279:37223-6.

Yildiz, A., M. Tomishige, R.D. Vale, and P.R. Selvin. 2004b. Kinesin walks hand-over-hand. *Science*. 303:676-8.

Yonezawa, S., N. Yoshizaki, M. Sano, A. Hanai, S. Masaki, T. Takizawa, T. Kageyama, and A. Moriyama. 2003. Possible involvement of myosin-X in intercellular adhesion: importance of serial pleckstrin homology regions for intracellular localization. *Dev Growth Differ*. 45:175-85.

Zarrinpar, A., S.H. Park, and W.A. Lim. 2003. Optimization of specificity in a cellular protein interaction network by negative selection. *Nature*. 426:676-80.

Zhang, H., J.S. Berg, Z. Li, Y. Wang, P. Lang, A.D. Sousa, A. Bhaskar, R.E. Cheney, and S. Stromblad. 2004. Myosin-X provides a motor-based link between integrins and the cytoskeleton. *Nat Cell Biol*. 6:523-31.

Zhu, X.J., C.Z. Wang, P.G. Dai, Y. Xie, N.N. Song, Y. Liu, Q.S. Du, L. Mei, Y.Q. Ding, and W.C. Xiong. 2007. Myosin X regulates netrin receptors and functions in axonal path-finding. *Nat Cell Biol*. 9:184-92.